Delft University Of Technology

Faculty of Electrical Engineering, Mathematics and Computer Science

Future Hydrogen Town

Designing a PV-Hydrogen-Battery-FC system for a typical neighbourhood in the Netherlands

Author:
Megan Atkins

Delft
August 27, 2020

ACKNOWLEDGEMENTS

Although I did a lot of work within this masters thesis, it would not have been possible without a few key people to help me through it all.

Firstly, thank you to my PhD supervisor Thierry de Vrijer. Without his constant help and willingness to answer all my questions, I wouldn't have been able to get to the final finished product you see here. You were honestly one of the best daily supervisors I could have asked for, always understanding and also critical of the work, making me stop and think clearly about what I was doing before I got stuck down too many rabbit holes. I know sometimes it was strange having a student with which most of the interactions were over Skype but in the end it worked out with no problems! I also want to thank my supervisor Arno Smets for motivating me to take this project. Your way with words had me convinced from the very beginning.

I also want to thank Chaturika Chowdhary Kota for connecting me to this masters thesis topic and keeping me motivated and sane throughout the whole process. And to Huw Jones and my parents, Rebecca Foreman and Graham Atkins, for being hugely supportive of all the work I have done. Your love and motivation helped me to reach this end goal so thank you for everything!

Megan Atkins, Delft, August 2020

ABSTRACT

One of the goals outlined during the Paris Agreement in 2015 aimed at 'holding the increase in global average temperature to well below 2°C above pre-industrial levels and pursuing efforts to limit the temperature increase to 1.5°C' [14]. In conjunction with this, the Klimaatakkord of the Netherlands aims to 'reduce greenhouse gas emissions in the Netherlands by 49% compared to 1990 levels' [112]. To achieve this goal, a rapid decarbonisation of our economy and energy system is needed. Currently, residential usage accounts 20.4% of Dutch energy consumption [66]. To reach these targets, the integration of renewable energy sources in Dutch households will be a needed.

Solar energy is already one of the most affordable renewable energy sources available and is currently being integrated into newly built households across the Netherlands. However, as the renewable capacity of the Netherlands expands, so will the need for energy storage to meet the mismatch between renewable generation and demand. A battery bank is usually adopted to supply this mismatch on a daily basis and the production and consumption of hydrogen the chosen technology for a seasonal one. Thus, future households and neighbourhoods in the Netherlands must incorporate both in order to maximise self sufficiency from the grid. The high costs of these components make it unsuitable for implementation in a single household, but scaling up to provide for an entire neighbourhood is a more feasible approach. This results in a so called grid-connected hybrid PV-Battery-Electrolyser-FC energy system.

This final thesis project models and optimises a grid-connected hybrid PV-Battery-Electrolyser-FC energy system to asses its feasibility, both economically and technologically, for utilisation on a neighbourhood in the Netherlands. The simulation model of the hybrid energy system is designed TRNSYS. The model is optimised to minimise the levelised cost of eletricity (LCOE) and to maintain a self-sufficiency ratio of 1% for the hybrid energy system in TRNOPT. Several scenarios are optimised based on the overall system layout and cases dependant on the electrical, heat and mobility demand. The particle swarm optimisation (PSO) and Hooke-Jeeves optimisation algorithms are used for the optimisation process in GenOpt. In addition, a literature study on the learning curves of different components in the hybrid energy system was performed to predict their costs in 2030. The results of this were used to optimise the system as if it were built in 2030.

The simulated hybrid PV-Battery-Electrolyser-FC energy systems are technically feasible for most scenarios and load profiles for a Dutch neighbourhood. The one exception to this is heat load demand with de-centralised PV generation, which saw an energy deficit at the end of the year. The lowest LCOE of 0.749 €/kWh was found for the centralised scenario implementing smart load management in the load demand. It is found that de-centralising the PV-system to the roofs of houses and the battery storage system each increases of the LCOE of the system due to larger installations costs and a different battery technology. The preliminary results of the future scenarios suggest the results will follow the same trends as was seen in 2020. The LCOE reduces by 21% - 28% compared to the LCOE of 2020. However, more research is needed on this topic to draw conclusive results.

ACRONYMS

Acronyms

AC	Alternating Current
AOI	Angle Of Incidence
BOS	Balance of System
CAGR	Compound Annual Growth Rate
DC	Direct Current
DoD	Depth of Discharge
EV	Electric vehicle
FC	Fuel Cell
GA	Genetic Algorithm
GenOpt	Generic Optimization Program
HOMER	Hybrid Optimization Model for Electric Renewables
IRENA	International Renewable Energy Agency
KNMI	Royal Netherlands Meteorological institute
LCOE	Levelized Cost Of Energy
LLP	Loss of Load Probability
MPPT	Maximum Power Point Tracker
NPV	Net Present Value
OECD	Organisation for Economic Co-operation and Development
PEMFC	Proton Exchange Membrane Fuel Cell
POA	Plane Of Array
PSO	Particle Swarm Optimization
PV	Photovoltaic
PVMD	Photovoltaic Materials and Devices
SLM	Smart Load Management
SoC	State of Charge
SSR	Self Sufficiency Ratio
STC	Standard Test Conditions
TRNOPT	Transient System Simulation Tool Optimisation

TRNSYS	Transient System Simulation Tool
UV	Ultraviolet

Chemical Formula

CO_2	Carbon dioxide
KOH	Potassium hydroxide
NaOH	Sodium hydroxide

Symbols

b_{SSR}	Penalty error for SSR constraint
b_{tank}	Penalty error for hydrogen tank constraint
c_1	Multiplier for the SSR interior penalty function
c_2	Multiplier for the SOC interior penalty function
E_{agen}	Annual electricity generation
$E_{batt_{rated}}$	Rated capacity of the battery
$E_{batt_{max}}$	Maximum capacity of the battery
$E_{batt_{min}}$	Minimum capacity of the battery
$E_{invested}$	Primary energy invested in PV system
$E_{gen-load}$	Generated energy delivered to the load
E_{OM}	Annual primary energy used for OM of PV system
$E_{rated_{batt}}$	Rated energy capacity of battery
E_{sys}	Energy provided to the system
F_C	Fuel costs of system
g	Gravitational acceleration constant
G_{POA}	Plane of array irradiance
G_{beam}	Beam irradiance
$G_{diffuse}$	Diffuse irradiance
G_{ground}	Ground reflected irradiance
h	Height difference in pump
I_C	Investment costs of system
I_{ely}	Electrolyser current
I_{fc}	Fuel cell
I_{SC}	Short circuit voltage
I_{MPP}	Current at maximum power point
M_{C_d}	Maintenance costs of system
N_S	Number of modules facing S

N_{SSE}	Number of modules facing SSE
N_{SWW}	Number of modules facing SWW
P_{AC}	Final AC output power of inverter
P_{AC0}	Maximum AC power rating for inverter at reference conditions
P_{aux}	Auxilliary power
P_{batt}	Instantaneous power to/from battery
P_{DC}	Input DC power to inverter
P_{DC0}	Maximum DC-power input to inverter
P_{ely}	Rated power of electrolyser
P_{exc}	Excess power after power is delivered to battery
P_{from_grid}	Power from grid
P_{from_tank}	Power produced by the fuel cell and delivered to system
p_{gas}	Pressure of gas
P_{load}	Load demand
$P_{max_{Ely}}$	Maximum power electrolyser
$P_{max_{FC}}$	Maximum power fuel cell
P_{MPP}	Power at maximum power point
P_{net}	Net power after PV is delivered to load
P_{pump}	Power delivered to pump
P_{pv}	Power generated from PV
P_{short}	Power shortage after power is taken from battery
P_{sys}	Instantaneous power to the system
P_{to_tank}	Power sent to grid
P_{to_tank}	Power used for producing and storing hydrogen
P_{S0}	DC-power required to start inverter
$Q_{conduction}$	Heat lost through conduction
$Q_{heatdemand}$	Total heat lost in each household
$Q_{internal}$	Internal heat gains from objects that emit heat
$Q_{ventilation}$	Heat lost through ventilation
r	Discount rate
R_C	Replacement costs of system
SOC_{batt}	State of charge of battery

$SOC_{batt_{max}}$	Maximum state of charge of battery
$SOC_{batt_{min}}$	Maximum state of charge of battery
SOC_{tank}	State of charge of hydrogen tank
SSR	Self sufficiency ratio
T_{batt}	Operating temperature of battery
T_{gas}	Temperature of gas
V_{act}	Activation overpotential
$V_{cell_{ely}}$	Voltage in one cell - alkaline electrolyser
$V_{cell_{fc}}$	Voltage in one cell - fuel cell
V_{con}	Concentration overpotential
V_{DC}	Input DC voltage to inverter
V_{DC0}	DC-voltage level for rated AC-power of inverter
V_{ely}	Electrolyser voltage
V_{gas}	Volume of gas
V_{MPP}	Voltage at maximum power point
V_{OC}	Open circuit voltage
V_{ohm}	Ohmic overpotential
V_{rev}	Reversible voltage
V_{tank}	Volume of the hydrogen tank
V_{tn}	Thermoneautral voltage
y	Project lifetime
η_{batt}	Battery round-trip efficiency
η_C	Coulombic efficiency
η_{pump}	Pump efficiency
η_V	Voltaic efficiency
ρ_{H_20}	Density of water
ϕ_{pump}	Volumetric flow into pump

CONTENTS

LIST OF FIGURES

LIST OF TABLES

1 INTRODUCTION

An important outcome of the 2015 Paris Agreement of the United Nations Framework Convention on Climate Change was a commitment for the world to limit a future global warming "to 1.5°C above pre-industrial levels", and by doing so, stay well below 2°C [142]. The societal and ecological impacts of a projected 1.5°C and 2°C warming will likely occur through increased sea level rise, reduction in water availability, reduction in agricultural yields and an increased risk of extreme events [118]. The resulting need to mitigate the effects of human induced climate change are now greater than ever.

One of the main causes of human induced climate change is the production of CO_2 by burning fossil fuels (the primary energy provider in most countries). In 2020, risks related to human induced climate change were the top five of those listed by the World Economic Forum [Hofmeijer]. Not only have catastrophic events events been predicted to occur, and are already starting to occur in some nations, but the current global consumption rate of fossil fuels is higher than the earth can replenish. A switch to using alternative, renewable energy sources must happen as soon as possible if we are to prevent the most damaging effects of the climate crisis and to enable us to live without exhausting our supply of fossil fuels. The energy industry requires radical change and a transition to using more sustainable energy sources.

1.1 RENEWABLE SOLUTIONS

1.1.1 Solar Energy

The largest and most readily available source of renewable energy on the planet is the sun. The sun can reliably provide energy every day, although it is limited by the number of daylight hours, the unpredictability of weather conditions (clouds, rain etc.) and the intensity of the radiation in the given the location. These can result in both daily and seasonal fluctuations in solar power generation. Such fluctuations can be tackled by implementing short-term and long-term storage mechanisms along side the solar energy generation, making solar energy generation a more viable option.

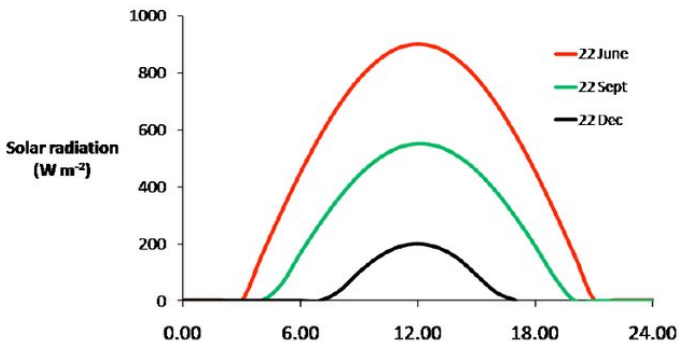

Figure 1.1: The daily fluctuation in solar power generation in different seasons [28].

Most solar energy is harvested with the use of photovoltaic (PV) panels. In the Netherlands, the amount of PV farms has quadrupled in the last five years and is continuing to grow [132]. All new houses built in the Netherlands are usually built with PV installations in the roofs, including the PV panels, charge controller and power electronics. Most PV systems that are installed are connected to the grid, allowing consumers to become 'prosumers' that can sell and transport excess energy generation to the grid.

1.1.2 Energy Storage

One of the oldest and most mature methods of storing electricity in a chemical form is through a battery. The first battery was created by Volta in 1800. Since then, technologies have expanded and been researched extensively, with the lithium-ion battery and lead-acid battery being the most commonly used today in conjunction with solar energy generation. Lithium ion batteries have dominated battery technology in recent years with its high energy density, high round-trip efficiency and relatively low depth of discharge. However, their high costs mean that often the lead-acid battery is still used, especially for smaller PV systems. Lead-acid battery are disadvantaged by their negative impacts on the environment in terms of disposal and their relatively short cycle life. Both battery technologies suffer from self-discharge, which varies at depending on the external temperature. For example, at a temperature of 20°C, the self-discharge of a lead-acid battery is 3-5% per month. However, this increases to 10% at 30°C. This self discharge can decrease the lifetime and the state of charge. The storage capacity of lithium-ion batteries also decreases significantly below temperatures of 5°C and thus must be externally heated in cold climates.

These high self discharge rates also make battery storage unsuitable to combat the seasonal fluctuations in solar energy supply. For long-term storage, electrochemical storage in the form of chemical bonds such as ammonia, hydrogen and hydrocarbons is commonly used. All of these chemical compounds contain at least one hydrogen bond. In ammonia, the hydrogen atom is bonded with a nitrogen atom. In the hydrocarbons, it bonds with a carbon atom. And within a hydrogen molecule, the hydrogen atom bonds to itself to become a pair. Hydrogen is the most abundant chemical element in the universe, however it is rarely found in its elemental form. Hydrogen is often extracted through the process of electrolysis, where energy is inputted to split water into hydrogen and oxygen gas molecules. The advantage of using hydrogen as opposed to hydrocarbons is that when reacted with oxygen to produce energy, the only by-product is water and thus the energy storage process can theoretically be entirely carbon free. Hydrogen has a higher energy density than batteries (142 MJ/kg vs 0.95 MJ/kg) [24].

Despite all these promises for hydrogen as a long term storage method, the need for additional components for the production, storage and consumption of hydrogen makes it inaccessible as an energy storage method in many cases eg. individual households. However, when implemented on a large scale, such as in a neighbourhood or town, it may be more feasible both in terms of cost and of sizing. One disadvantage of hydrogen is the low, final round trip efficiency of around 30% [103]. In addition, hydrogen's the wide range of flammability in air (4-74% concentration) and the self discharge causing potentially dangerous situations are other disadvantages to the storage method [86]. Therefore, great care must be taken when implementing hydrogen storage.

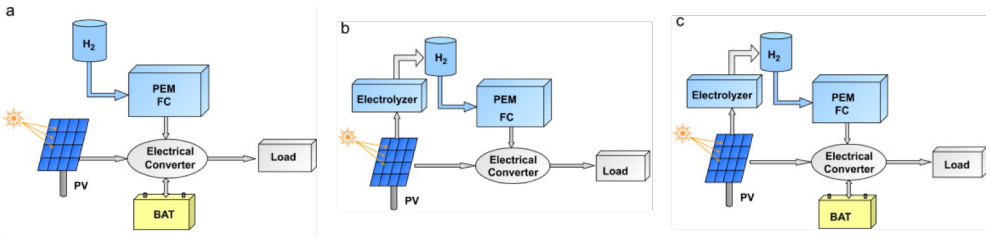

Figure 1.2: Configurations of the system studied by Lagorse. (a) A PV, Battery and FC with an external hydrogen tank. (b) A PV, Electrolyzer, FC and storage tank. (c) A PV, Battery, Electrolyzer, FC and storage tank. [85]

1.2 HYBRID SOLAR SYSTEMS

Hybrid Solar Systems are energy systems combining PV energy generation and energy storage in the form of a battery bank or, more recently, a hydrogen fuel cell. Despite the abundance of hydrogen in many chemical processes and industrial process, high costs and lack of technological development mean that it is still rarely used as an option in residential based energy systems.

Typically such systems are designed for stand-alone situations. Extensive research has been performed optimising, analysing comparing stand alone renewable system combining PV/Battery/Electrolyzer/FC in various configurations. One such study by Jérémy Lagorse et al. [85] modelled and sized based on intuition the configurations of (a) PV/Battery/FC, (b) PV/Electrolyzer/FC and (c) PV/Battery/-Electrolyzer/FC, shown in Figure 1.2, to match the demand. The costs of each system respectively came to 0.519 € /kWh, 4.943 € /kWh and 0.645 € /kWh. Both configurations (a) and (c) showed that such systems could be built at acceptable costs.

With studies of stand-alone hybrid PV-Electrolyzer-Battery-FC (PEBF) energy systems yielding such promising results, the academic world has been bolstered to pour more research into the topic and aid the energy transition towards a hydrogen economy. This promotes an ideology for a future with a clean, energy economy. A hydrogen economy focuses on producing, storing and transporting hydrogen for energy purposes and the conversion of hydrogen to electricity as a low-carbon energy source (when combined with renewable generation) to match global energy needs. The design of this hydrogen economy, however, requires in depth economic and feasibility studies for its use in residential applications.

In reality, most residential loads around the world are connected to the electricity grid. Comparatively few studies have been performed comparing the costs of stand-alone hybrid systems to grid connected ones, especially in OECD countries. One 2011 study by Turkay and Telli [138] made this comparison for the Electrics and Electronics Faculty of Istanbul Technical University, using the HOMER (Hybrid Optimization Model for Electric Renewables) optimization software. The optimisation process aimed to find the best sizing of the system with the given components whilst minimising the LCOE and the total cost of the system. It found that the high cost of a stand alone system meant that it was only suitable for 'regions that are far from the grid where it is uneconomical to install any utility line'. The corresponding grid-connected PV-Electrolyser-FC system, however, yielded economic costs as low as 0.307 $/kWh. This low cost was in part due to large reliance on the grid for the electricity supply. However, a sensitivity analysis found that increasing electricity prices to 2 $/kWh decreased this grid reliance from 75% to 12% but significantly increased costs. Bettayeb and Ghenai [50] modelled a grid-tied PV-Electrolyser-FC hydrid system for the University of Sharjah administration building in United Arab Emirates. For a 500kW PV and 100kW fuel cell, the levelised cost

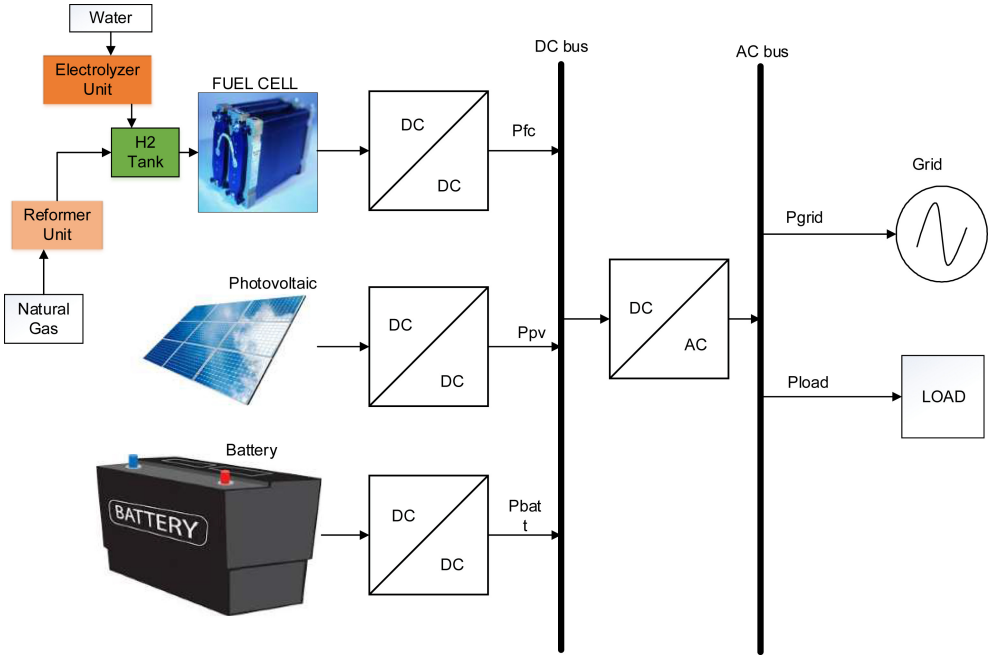

Figure 1.3: Proposed Hybrid Renewable Energy System for a hospital in Malaysia [70].

of electricity (LCOE) was found to be as low as 0.071 $/kWh with 40.1% of power supplied by the PV generation. Only 5% of the power generated was sold back to the grid. A simple optimization analysis to find the optimal sizing from discrete steps to minimise the LCOE was used for this study.

The idea of integrating grid-connected hybrid systems into commercial buildings with a significant load is not uncommon. In another study, Isa et al. [70] performed a techno-economic analysis on the feasibility of a PV-Electrolyser-Battery-FC system in a hospital in Malaysia, the configuration of which is shown in Figure 1.3. The HOMER software was used to optimise for the lowest LCOE and total net present cost. They found the LCOE for the grid connected PV/Battery system, PV/FC system and PV/Battery/FC system to be 0.133 $/kWh, 0.085 $/kWh and 0.091 $/kWh. Comparing this to a LCOE of 0.128 $/kWh for grid-connected PV system alone, this demonstrates the feasibility of installing an optimally sized PV-Battery-FC hybrid system in such commercial buildings. Feed-in tariffs are discussed as an incentive to reduce electricity costs but are not included in the final LCOE of the system. Zhang et. al [156] modelled and optimised the sizing of a PV-Battery-Electrolyser-FC Hybrid system for a rental multi-apartment building in Gothenburg under different operation strategies. The authors used the Genetic Algorithm (GA) to optimise the size of the system whilst aiming to minimise the net present value (NPV) and maximise self consumption. This paper is the only one found that aimed to minimise exchange with the grid, using an indicator known as the Self Sufficiency Ratio (SSR) that represents the percentage of the load that is met by the system. Variable hourly electricity prices for selling and buying electricity are used. When looking at both pessimistic and optimistic cost scenarios, battery and hydrogen storage are recommended when the goal is to reduce the negative impact on the grid. A sensitivity analysis was performed on the lifetime of the various components and the different operation strategies used.

Real, operational cases of such systems are few in number. One extensive study of a stand alone hybrid solar-hydrogen energy system was published by Oystein Ulleberg [139] in 1998. In this PhD dissertation, the system is simulated using the TRNSYS (Transient System Simulation Tool). Combining this with results from the demonstration PV-Electrolyzer-Battery-FC system in Jülich, Germany named

PHOEBUS, it was concluded that the developed models were accurate enough to carry out long-term simulations. The PHOEBUS system is currently in operation to provide the load demand of Central Library in Forschungszentrum [94]. In 2014, a grid connected PV-hydrid-battery system for an experimental case in Germany was developed. The study showed that the system was feasible for the handling of daily and seasonal fluctuations in PV generation and demand [26]. Another system was constructed in 2007 for the Clean Energy Center in Denzili, Turkey [155]. However, an economic analysis was not performed for either of these cases.

This literature study shows several stand-alone and grid connected hybrid solar-hydrogen systems which are either optimized using an intuitive methods [85], [141], [26], [155] or a numerical approach [138], [70], [50]. Some optimizations are performed to optimise technical aspects [85], [155] and one based on self sufficiency from the grid [156]. However, most studies focused economic factors [138], [50], [156], [70], incorporating investment, maintenance and replacement costs as well as the cost of the grid connection as the sale and purchasing of electricity from the grid. Although most studies consider seasonal fluctuations in the load demand (i.e. hot summers and cold winters), all of these except Zhang et al. were performed for locations that have high temperatures all year round (and thus have fluctuations that depend heavily on air conditioning and not on heating) and high annual radiation. This raises the question of whether the cost effectiveness and reliability of the hybrid solar-hydrogen systems in these studies will also be viable for locations with less solar radiation like the Netherlands. Finally, none of these papers discuss extensively the prospect of utilising such systems in the future under the premise that electrolyzers, batteries and fuel cells undergo a similar learning curve to that of PV modules in the last 20 years.

1.3 PROBLEM STATEMENT

This thesis project attempts to extend the previously discussed literature on grid connected hybrid solar-hydrogen systems and the performed study for a stand alone hybrid system. The optimally-sized, grid-connected, hybrid energy system is found based on solar generation as a primary electricity source combined with battery and hydrogen storage, including an electrolyser and a fuel cell for the conversation of electricity to/from hydrogen. This system can help tackle the daily and seasonal fluctuations in energy demand and resolve the problems of using solely battery or hydrogen as as storage method.

Multiple systems are proposed to solve this problem, all including PV generation, a battery system, a fuel cell, an electrolyser, a hydrogen storage system and a controller. This can be abbreviated as a PV-Electrolyzer-Battery-FC system. Different scenarios will look at differing levels of de-centralisation of the system used to meet different load demand profiles. The system is optimally sized to meet these differing load profiles for the lowest Levelized Cost of Energy over the 25 year lifetime and a Self-Sufficiency ratio of 1%. Different cases of load demands and of components prices are also analysed.

The literature study detailed in the previous section combined with the motivation for deepening the level of this research has allowed for the formulation of the following research objective:

Assess the feasibility of current and future grid-connected hybrid PV-Electrolyzer-Battery-FC energy systems from a techno-economical point of view, based on the optimal system sizing for the neighbourhood of Ackerswoude.

This research objective can be divided into sub-objectives:

- Develop a computer simulation model of a grid-connected hybrid PV-Electrolyzer-Battery-FC energy system for the neighbourhood of Ackerswoude.
- Develop scenarios for the assessment of the hybrid energy system to fulfill electrical, heat and mobility demand, as well as incorporating smart load management.
- Use the PSO - Hooke Jeeves optimisation algorithm to obtain the optimal sizing of the hybrid system in each scenario to minimise the LCOE of the system.
- Assess the techno-economical feasibility of the hydrid system for current and future cases based on the optimisation results.

1.4 THESIS APPROACH

The structure of this thesis project follows the sub-objectives mentioned in the previous section to gain an understanding of hybrid PV energy systems. This chapter detailed the motivation for this thesis topic and a small literature review of research into grid-connected hybrid energy systems. Chapter 2 provides the physical, chemical and mathematical details of each component in the simulation and the motivation to justify the chosen technologies used for the TRNSYS (Transient System Simulation Tool) simulation environment. In addition, an overview of the hybrid system for each scenario, the master controller and the economic modelling are also described. Chapter 3 explains the chosen optimization algorithms - particle swarm optimization (PSO) and Hooke-Jeeves - as implemented in the TRNSYS Optimization (TRNOPT) and Generic Optimization Program (GenOpt) optimization environment. The optimisation approach used in this study to minimise the LCOE and set the SSR to 1% are subsequently detailed, along with the different scenarios and different load profiles cases that are studied in this project. The final results of this are discussed in Chapter 4. Chapter 5 proceeds to detail the literature review performed into the learning curves for different technologies in the PV-Electrolyser-Battery-FC energy system, using them to calculate the a final price for the technologies in 2030, and presents some preliminary results found for these cases. Lastly, Chapter 6 gives the conclusions and future recommendations of the work.

2 SIMULATION

The designed grid-connected PV-Battery-Electrolyser-FC energy system in this thesis is powered through solar energy, provided by PV. Excess energy from the PV can be stored in the battery bank (short term) or in the form of hydrogen (long term) that can be converted to electricity using an electrolyser and fuel cell. To study the behaviour of this system, a simulation model has been built in the simulation environment TRNSYS. Section 2.1 initially describes TRNSYS and how it was used. This is followed by a summary of the chosen technologies for the hybrid system and detailed mathematical description of how each of the main components are modelled in Section 2.2. A schematic overview and differing layouts of the simulation model for each scenario is given in Section 2.3. Section 2.4 then continues by explaining the master controller of the system. Finally, the economic modelling methodology, including the levelised cost of electricity (LCOE) and system performance metrics, are outlined in Section 2.5.

2.1 TRNSYS SOFTWARE

The software used in this study is the TRNSYS software, which stands for Transient System Simulation Tool. This software was developed at the University of Wisconsin using the coding languages Fortran and C++. It comes with a standard library containing 150 components [143]. The standard models for these components use a 'black box' approach. Each component is linked to others and the output of one component will be sent to the input of another, known as the successive substitution method of solving. This method allows for the design and optimisation of a system without having detailed knowledge of each component. In this way, the user can study the behavior of system as a whole. Furthermore, more experienced users can modify the component models to eliminate the 'black box' approach if desired. This study uses the version TRNSYS17. Some of the standard components have been previously modified by the Photovoltaic Materials and Devices (PVMD) group. Others are developed especially for this thesis and have been modified by the author.

2.2 TECHNICAL MODELLING

The following section justifies the chosen technology for each component in the PV-Battery-Electrolyzer-FC system and details how they are technically modelled. The rated power for each component (except the PV modules) is left undefined intentionally to prevent unwanted constraints during the optimisation process.

2.2.1 Location

Chapter 1 details some of the studies conducted to asses the feasibility of grid connected PV-Battery-Electrolyser-FC system. Yet most of these studies, have been performed in locations with high radiation levels. Few studies have been performed on places with lower radiation levels, such as the Netherlands, despite the fact that

hydrogen and battery storage are considered a vital part of the energy transition in such places.

For this reason, the chosen location for this study is a neighbourhood called Ackerswoude in Pijnacker-Nootdorp, The Netherlands [27]. This is one of many neighbourhoods in the Netherlands that has a similar layout and construction planning and, as of 2020, it is still in the planning and construction phase. Designing a PV-Battery-Electrolyser-FC system that is technoeconomically feasible for such a neighbourhood could result in implementation of the system into future designs of many neighbourhoods across the Netherlands.

Ackerswoude is a neighbourhood comprising of 630 households. The layout of Ackerswoude can be found in Figure 2.1.

Figure 2.1: Plan of Ackerwoude, the chosen neighbourhood for this study [27]. The areas highlighted in red have not been included in this study.

2.2.2 Meteorological Data

The PV power output of a PV-Battery-Electrolyser-FC system depends greatly on the weather in that given location. There are currently many weather stations and systems that already collect meteorological data throughout the world. Such data files contain many parameters that are influenced by the weather conditions, but the noteworthy parameters in the solar energy sector are solar radiation, wind speed, ambient temperature and ambient humidity [58].

To calculate the power output of a PV module, the incident irradiance on the plane of array (POA irradiance) is used. This takes into account: the position of the Sun, the orientation of the array and ground reflectivity. Calculating the POA irradiance (G_{POA}) requires three radiation components, the beam radiation (G_{beam}), diffuse radiation (G_{beam}) and ground reflected radiation (G_{ground}), as is shown in Equation 2.1. Beam radiation is determined from the direct normal irradiance on the surface whilst accounting for the angle between the tilted surface and the Sun's position in the sky (aka. angle of incidence). The diffuse radiation is the indirect light

in the sky. Many approaches have been developed to calculate this but the most comprehensive, and thus the method used here, is the Perez Sky Diffuse model [124]. Finally, the ground reflected radiation is the reflected irradiance received from the ground, found from the irradiance incident on the ground, the reflectivity coefficient and the tilted angle of the surface.

$$G_{POA} = G_{beam} + G_{diffuse} + G_{ground} \tag{2.1}$$

The data for the global solar radiation was collected from Meteonorm for the year 2017 [147]. Table 2.1 summarises the parameters used for this location.

Parameter	Value	Description
Latitude	52.03°	(North being 0°)
Longitude	4.45°	(East being 0°)
Altitude	40°	(Horizontal is 0°)
Albedo (snow)	0.7	-
Albedo (no snow)	0.2	-

Table 2.1: Weather parameters regarding the location of Ackerswoude in The Netherlands

2.2.3 Solar Panel

Chosen technology: Mono-crystalline PV module

The primary source of energy in the hybrid system will be from the PV modules, which convert electromagnetic radiation from the Sun into electricity. PV modules are most commonly manufactured from crystalline silicon, either mono-crystalline silicon and poly-crystalline silicon. Both are made from the same material but their manufacturing methods are different and thus result in different efficiencies. Commercially available mono-crystalline modules have an efficiency of 24% and poly-crystalline modules have an efficiency of 17-21% [44]. Even though mono-crystalline modules are more expensive, their higher efficiency means they are the preferred choice for use in residential installations.

Most houses built in the Netherlands use black, high power solar panels as these are considered more aesthetically pleasing. For this reason, the chosen module used in this study is the Panasonic HIT N340 PV module [11]. The parameters for the PV module are taken from the data-sheet of the manufacturer and are listed in Table 2.2.

Electrical Model

Irradiating a PV module will generate a voltage and a current that can be plotted in a characteristic current-voltage (IV) curve dependant on environmental conditions, such as the irradiation and the solar cell's temperature. This curve is determined by plotting the product of the voltage and the current for all possible values between the the open-circuit voltage (V_{OC}) and the short circuit current I_{SC}. V_{OC} occurs when there is no load connected to an illuminated solar cell. I_{SC} flows through the solar cells when the positive and negative connectors are connected together. The maximum power point (P_{MPP}) occurs at the maximum of the power-voltage curve, with voltage V_{MPP} and current I_{MPP}.

The final power output of a PV module is shown in Equation 2.2, where FF is the fill factor.

$$P_{MPP}(T, G_M) = FF \cdot I_{SC}(T, G_M) \cdot V_{OC}(T, G_M) \tag{2.2}$$

Here, $P_{MPP}(T, G_M)$ differs from the reference P_{MPP} due to the effects temperature and incident irradiance, thus resulting in a different efficiency. It is possible to model these effects without knowing the exact electrical characteristics of the solar panel, only using meteorological data and values from the data sheet of the chosen solar panel. This method is simpler as it does not involve solving time consuming iterative equations.

The temperature effects on the PV power output are modelled using the fluid-dynamic model based on a detailed thermal energy balance model between the module and its surroundings. This calculates the module temperature based on external parameters such as the ambient air temperature, the incident irradiance on the module and the wind speed. From this, the change in the I_{SC}, V_{OC}, P_{MPP} and the efficiency can be calculated using the temperature dependant coefficients listed on the data sheet. The detailed equations can be found in Solar Energy Book Appendix G [124].

The effects of irradiance on the efficiency of the module can be found as a function of the incident irradiance over the irradiance at standard test conditions. The I_{SC} of the module scales linearly with this ratio and the V_{OC} logarithmicly. The equations used to determine this dependence can be found in Appendix A.1.

Parameter	Value	Description
Pmpp	340 W	Power at maximum power point
Voc	71.3 V	Open circuit voltage
Isc	6.04 A	Short circuit current
Vmpp	59.7 V	Voltage at maximum power point
Impp	5.7 A	Current at maximum power point
NOMT	44°C	Normal Operating Module Temperature
μ_{Voc}	-0.235 % °C	Temperature coefficient open circuit voltage
μ_{Isc}	0.055 % °C	Temperature coefficient short circuit current
μ_{Pmpp}	-0.258 % °C	Temperature coefficient maximum power point
η_m	20.3 %	Module efficiency
A_m	1.67427 m^{-2}	Area of module
γ	1.5	Ideality factor crystalline silicon

Table 2.2: External and internal parameters Panasonic HIT N340 PV module at STC [11]

In this study, it is assumed that the power output of each PV module is always at the maximum power point for that given moment, temperature and incidence irradiance. Furthermore, there is a warranty on the solar panel efficiency. By the end of the 25 year lifetime of the modules the efficiency will have degraded to a lower level. To take this into account, the panel is assumed to have a constant efficiency of 93% over the entire lifetime [11].

2.2.4 Electrolyser

Chosen technology: Alkaline Electrolyser

To convert electricity into electrochemical energy in the form of hydrogen, electrolysis is used. In electrolysis, two metal electrodes are connected through an 'electrolyte' that transmits an applied current through ionic transfer. When a direct current is applied, this will cause the molecules in the electrolyte to break down and form new products. To generate hydrogen, electrolysis splits an electrolyte of water solution into hydrogen and oxygen gas. This allows for the chemical storage of energy of the electricity in the form of hydrogen.

Background information

The most common technologies used for water electrolysis are alkaline electrolysis and Proton Exchange Membrane (PEM) electrolysis, each containing different materials in the electrolyte and electrodes. Currently, the PEM electrolyser is not readily available for use in a large-scale energy systems and thus is still relatively costly. As a result, the alkaline electrolyser is the chosen technology for this study.

Alkaline electrolysers use a basic solution as an electrolyte, containing potassium hydroxide (KOH) or sodium hydroxide (NaOH) and water to enable ions to flow between the two electrodes. The alkaline electroyser has an efficiency of 65-75% and an operating temperature ranging from 80°C to 90°C. In addition, their long lifetime (60000-90000 hours) means that, if treated correctly, there should be no need for replacement within the lifetime of the system. As a mature technology, alkaline electrolysers have lower investment costs than other technologies and are already readily available on the market. This is especially true for the large scale electrolysers (above 500kW) given their use in industry for many decades. The main disadvantages include the low current density of operation and the fact that they cannot be easily turned on and off [92]. More details of this technology can be found in Appendix B.

Electrical and thermal model

In this study, the optimisation process is used to determined the rated power of the electrolyser. This rated power is a product of the input current to the electrolyser (I_{ely}) and the cell voltage ($V_{cell_{ely}}$). Electrochemical power losses in the electrolyser are caused irreversible losses to the voltage potential, namely the concentration overpotential (V_{con}), the ohmic overpotential (V_{ohm}) and the activation overpotential (V_{act}). Thus, the required voltage to the electrolyser must be higher than the thermoneutral voltage (V_{tn}) of 1.48V needed for a 100% efficient electrolyser. When the electrolyser is operational, these overpotentials generate thermal losses that must be also accounted for.

$$V_{cell_{ely}} = V_{tn} + V_{con} + V_{ohm} + V_{act} \tag{2.3}$$

The electrochemical and thermal electrolyser model selected for this study is the empirically verified model for an alkaline electrolyser used in the PHOEBUS system by Meurer and Ulleberg [94], [141]. This model takes the I_{ely} and the ambient air temperature as inputs. This original model was designed for a small scale electrolyser. For the large scale electrolysers simulated in this study, the HyProvide Large-Scale Alkaline Electrolyser Project by GreenHydrogen is modelled with some parameters provided for by Meurer and Ulleberg [55]. The empirical equations used for the electrochemical and thermal models, along with a full list of the parameters used, is detailed in Appendix A.2.

The reversible voltage and the effect of the overpotential terms on the voltage are demonstrated in Figure 2.2 as a function of current density. More details about the origins of these terms and the effect the have on the voltage curve can be found in Appendix A.2.

2.2.5 PEM Fuel Cell

Chosen Technology: Proton Exchange Membrane Fuel Cell (PEMFC)

To convert electrochemical energy stored as hydrogen back into electricity, a combustion device in the form of a fuel cell is required. The structure of a fuel cell is similar to the electrolyser, containing two electrode and an connecting electrolyte.

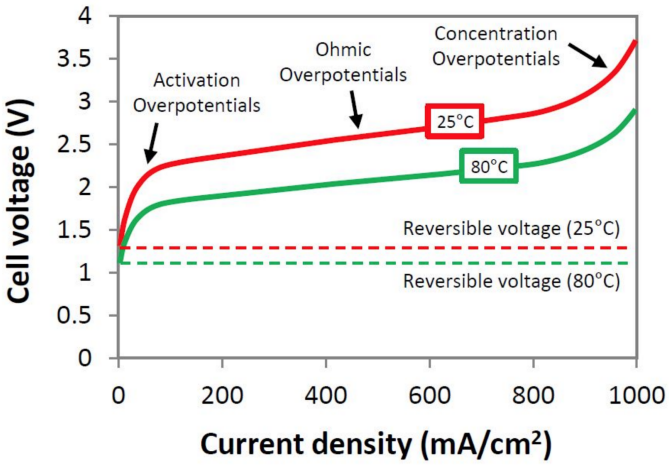

Figure 2.2: The polarisation curve of the concentration, activation and ohmic overpotentials that defines the practical cell voltage of an electrolyser at 25°C and 80°C. [16]

However, the reactions contained in a fuel cell are spontaneous and thus will generate energy (in the form of electricity) when the fuel is inserted. In this case, hydrogen and oxygen (from the air) are inserted into the fuel cell. H^+ ions are transported through the electrolyte where they react with oxygen to produce direct current electricity with a by-product of water [25].

Background information

Although the low costs and maturity of the technology make the alkaline electrolyser the most suitable choice for the electrolyser, this technology is not as mature for use in fuel cells. Moreover, alkaline electrolysers also have a low current density and can cause carbon dioxide poisoning if air is used instead of pure oxygen, meaning this technology is not suitable for use here. Other possible technologies, such as solid oxide fuel cell, either have very high operating temperatures and costs or can be damaging to the environment [97]. Consequently, the chosen technology for this study is the PEMFC.

The PEMFC has a solid electrolyte of a thin, permeable sheet and electrodes on both sides of the membrane made of porous carbon with a platinum catalyst. The efficiency is about 40-50% and the operating temperature ranges from 60°C to 80°C [116]. Their high power makes them very suitable for use this study and the recent increase in usage of PEMFCs in electric cars mean that they are available on the market today, even for larger scales [116]. They also have a long stack lifetime (20000-40000 hours) and so do not have to be replaced often. The main disadvantage of the PEMFC is the high component and installation costs. More details of this technology can be found in Appendix B.

Electrochemical and thermal model

The optimisation process in this study is used to determine the rated power of the fuel cell. This rated power is a product of the fuel cell input current (I_{fc}) and the operational voltage ($V_{cell_{fc}}$). Electrochemical power losses in the fuel cell are caused by irreversible losses in the potential. A 100% efficient fuel cell can retrieve the maximum amount of electrical energy when operating at the reversible voltage (V_{rev}) of 1.23V at standard conditions (25°C and 1 bar pressure). In reality the practical $V_{cell_{fc}}$ is lower than this due to the concentration overpotential (V_{con}), the ohmic overpotential (V_{ohm}) and the activation overpotential (V_{act}), thus altering the

fuel cell efficiency. These electrochemical losses also generate heat, contributing to the thermal power losses in the fuel cell.

$$V_{cell_{fc}} = V_{rev} - V_{con} - V_{ohm} - V_{act} \tag{2.4}$$

For these simulations, both the electrochemical and thermal loss mechanisms are accounted for using a model developed by Amphlett et al. [17]. The model uses empirical equations to determine voltage losses and thermal power losses in the fuel cell, using I_{fc} and the ambient air temperature as inputs. The Amphlett model was originally designed for a small scale fuel cell and thus has been adapted to fit the industrial size (above 500kW) fuel cells used in this work. The empirical equations and a a full table of the list of parameters used are reported in Appendix A.4.

2.2.6 Battery

A battery is an electrochemical storage device used to store excess energy or to supply energy on a short term basis. Although, the fundamental chemistry is similar to an electrolyser or a fuel cell, the energy in a battery is instead stored as electrochemical energy inside the electrodes and electrolyte of the battery.

Electrical Model

Much like the electrolyser and fuel cell, electrochemical losses in a battery can occur from the concentration overpotential, ohmic overpotential and activation overpotential. However, the relationships between current, voltage and internal resistance in batteries are complex to model for a large scale system. Additionally, connecting the load to the grid through an inverter reduces the importance of the relationship between the battery voltage and the power delivered to the load.

As a result, a simple, quasi-static energy model is used in this study, recommended by Raszmann et al. for simulating large scale battery storage systems [109]. The optimisation process determines the rated capacity of the battery system ($E_{batt_{rated}}$), related to the state of charge of the battery SOC_{batt} by Equation 2.5.

$$SOC_{batt}(t) = SOC_{batt}(t-1) \pm \frac{P_{batt}.\Delta t.\eta_{batt}}{E_{batt_{rated}}} \tag{2.5}$$

where:

- $SOC_{batt}(t)$ is the battery SOC at time t
- $SOC_{batt}(t-1)$ is the battery SOC at time t-1
- $P_{batt}(t)$ is the instantaneous power to/from the battery at time t
- Δ t is the timestep
- η_{batt} is the battery round-trip efficiency
- $E_{batt_{rated}}$ is the rated capacity of the battery

The lifetime of batteries can be extended by limiting the maximum and minimum of available energy capacity ($E_{batt_{max}}$ and $E_{batt_{min}}$ respectively), determined by the maximum and minimum SOC:

$$\begin{aligned} E_{batt_{max}} &= SOC_{batt_{max}} \cdot E_{batt_{rated}} \\ E_{batt_{min}} &= SOC_{batt_{min}} \cdot E_{batt_{rated}} \end{aligned} \tag{2.6}$$

Although there are many battery technologies available, the most well-established are ones lithium-ion batteries and lead-acid batteries. The choice of technology for this project is dependant on whether the battery system is centralised or decentralised. This model will be applied for both batteries technologies, assuming they have similar charging and discharging characteristics.

Table 2.3 summarises the assumed characteristics of the both the lithium ion and lead-acid battery models, with details discussed below. In addition to the external efficiency quoted here, it is assumed that the degradation rate to 80% of capacity at the end of the battery lifetime causes a constant efficiency of 90% [32].

Coefficient	Description	Li-ion Value	Lead-acid Value
η_{batt}	Battery efficiency	-	78%
$SOC_{batt_{max}}$	Maximum state of charge	85%	100%
$SOC_{batt_{min}}$	Minimum state of charge	20%	50%
C-rate	Charging rate	0.5	0.2

Table 2.3: The battery characteristics for the lithium ion and lead acid battery models [109], [127], [21].

Centralised system chosen technology: Lithium-ion battery

The use of a large scale centralised battery system in a neighbourhood sized PV-Battery-Electrolyser-FC system will reduce the overall costs of the system and make management of the system simpler. However, such a system requires a technology that is cost effective and energy efficient and thus lithium-ion battery is chosen. Recent findings demonstrate this technology offers the best option in terms of performance, cycle life, and technological maturity [96] and is justified by the increasing share of lithium-ion as the technology of choice in newly built battery storage projects over the past few years [68]. Lead-acid batteries offer a better option in terms of cost (a priority for a residential household system), however their limited cycle life means they must be replaced every 3 years and thus are not suitable for a centralised system.

Lithium-ion has a high depth of discharge (DoD) of 90-100% [24]. In addition, lithium-ion batteries are maintenance free. This is why they are often used in portable systems such as cars or mobile phones. However, they can only run above zero degrees (0°C to 45°C) [77] and as a result it is assumed that during cold months the temperature of the battery system is kept above 0°C using waste heat from other components.

In this model, the self-discharge rate 5% a month is assumed to be negligible in the daily cycle of the batteries and a charge/discharge rate (C-rate) of 0.5C (2 hours at 1A) is used. Other parameters have been listed in Table 2.3.

The efficiency of the lithium battery is greatly dependant on the operating temperature. Kuo has developed a comprehensive model to represent the effects of temperature on the coulombic efficiency in a lithium ion battery [83], given by Equation 2.7.

$$\eta_C = a_1.e^{b_1 T_{batt}} + a_2.e^{b_2 T_{batt}} \tag{2.7}$$

where T_{batt} is the operating temperature and a_1, a_2, b_1 and b_2 are empirical parameters established during the study. For a C-rate of 0.5C, these values are respectively $7.2 \cdot 10^3$, $-3.130 \cdot 10^2$, $2.799 \cdot 10^{-3}$ and $-9.669 \cdot 10^{-2}$. For simplicity, the voltaic efficiency is taken as 100% for this study.

Decentralised system chosen technology: Lead acid battery

A decentralised battery system places a battery pack in every household, as is common practise today. This would allow PV generated power to be stored directly in the battery without added transportation and losses. A residential-sized battery has different requirements to that of micro-grid sized battery storage. The smaller size of the unit and the need for additional installation work would mean higher costs. The low cost of lead-acid batteries is therefore attractive to those living in residential households [77].

A lead-acid battery operates in an acidic environment, with electrodes made of lead and lead dioxide. As a low cost, well-known and mature technology, it is appealing for adoption in the energy industry. Although the batteries are most commonly found in cars, they are also used in stationary, residential systems where cost is a driving factor [75]. When the batteries are located in the homes of residents, it is far easier to perform the required maintenance (every 3-6 months) and system replacement. However, having a DoD limited to 50% has the potential to drive up the costs long term. Additionally, the environmental impact of the acidic electrolyte disposal should also be considered [24].

In this model, the efficiency of the lead acid battery is taken as 78%, as was experimentally determined by Tarmarzians [134], and a C-rate of 0.2C is used [21]. Placing the batteries inside allows the temperature dependence of the efficiency and the overall cycle life to be neglected for this study as homes are kept at a relatively constant temperature.

2.2.7 Hydrogen Storage

Chosen Technology: Compressed Storage

The low volumetric density of hydrogen makes storing it in a cost-effective and safe manner a significant challenge. There are currently three methods of storing hydrogen in development: as a compressed gas, as a liquid at temperatures of -253°C or stored in metal hydrides like Lanthanum Nickel ($LaNi_5$) [151], [159].

The chosen technology for this study is compressed gas storage. Other methods of hydrogen storage are inefficient and/or are still in the research phase [82]. Compressing hydrogen gas allows it to be stored at pressures up to 800 bar, corresponding to a relatively high volumetric density [43]. This storage method is the most mature, cost effective and widely used technology. The main disadvantage is the large amount of energy required to compress the gas, up 17% of the higher heating value of combustion [159].

Once the hydrogen gas has been compressed, it is stored in a cylindrical storage tank. The volume of this tank (V_{tank}) is determined during this study by the optimisation process. This storage method is modelled in this study using a the modified TRNSYS library model as developed by Goetzberger [53]. This uses the ideal gas law, dependant on the gas' pressure (p_{gas}), volume (V_{gas}) and temperature (T_{gas}), to calculate final p_{gas}, V_{gas} and the state of charge of the hydrogen tank (SOC_{tank}). The amount of gas sent from the compressor (n) is the only input.

$$p_{gas}.V_{gas} = n.R.T_{gas} \tag{2.8}$$

Is it possible to store hydrogen at pressures up to 800 bar to overcome the low volumetric energy density of hydrogen. However, due to potential safety issues and the high costs of storage tanks for such high pressures, the maximum pressure (p_{max}) is set to 500 bar. At this pressure, the low volumetric density of hydrogen can be tackled while also reducing costs.

2.2.8 Compressor

The alkaline electrolyser produces hydrogen at the conditions of 40 bar and 25°C [65]. Given hydrogen's low volumetric energy density at 40 bar, it must be compressed with a compressor before it can be stored. The model used is from the TRNSYS library and calculates the power the compressor uses when compressing the gas. This power is dependant on the type of gas (in this case hydrogen) and the input and output temperature and pressure of the gas. More details of the model used for the compressor can be found in Appendix A.6.

The compressor chosen for this model is the RIX Model 4VX3BG-65. This is able to compress hydrogen to pressures of 500 bar, with a maximum flow of 170 m^3/h [7]. The output pressure is defined by the pressure level of the hydrogen gas currently in the storage tank. The compressor is only activated when the electrolyser is producing hydrogen that needs to be stored. It is assumed that no external cooling is required as all heat produced will be lost of the environment.

2.2.9 DC-AC Inverter

The electricity used in households is AC however the power generated by PV modules is DC. Thus, to deliver this power to households a DC-AC inverter is required. The inverter has an efficiency that reduces the final AC output power (P_{AC}) depending on the input power (P_{DC}) and the input voltage (V_{DC}). The Sandia Inverter Model has been chosen to predict the final AC power output of the inverter [79]. This can represented using the following equations:

$$\begin{aligned} P_{AC} = (\frac{P_{AC0}}{A-B} - C(A-B))(P_{DC}-B) + C((P_{DC}-B)^2) \\ A = P_{DC0}(1 + C1(V_{DC} - V_{DC0})) \\ B = P_{S0}(1 + C2(V_{DC} - V_{DC0})) \\ C = C_0(1 + C3(V_{DC} - V_{DC0})) \end{aligned} \tag{2.9}$$

where:

- P_{AC0} is the maximum AC power rating for inverter at reference conditions.
- P_{DC0} is the maximum DC-power input to inverter.
- V_{DC0} is the DC-voltage level at which the AC-power rating is achieved.
- P_{S0} is the DC-power required to start the inversion process
- C_0, C_1, C_2 and C_3 are empirical coefficients that are dependant on the inverter type.

All of these parameters are dependant on the chosen inverter. The inverter used for a centralised system will differ from the one used for decentralised PV generation. Table 2.4 lists the parameters used for the chosen inverters for each situation.

Metric	PV (centralised)	PV (de-centralised)
Inverter	Power Electronics: FS3000CU15	Fronius Primo: 3.8-1 240
P_{AC0} [W]	3201170	3800
P_{DC0} [W]	3.26e+06	3911.35
V_{DC0} [V]	1030	650
P_{S0} [V]	11384	53.25
C_0 [W^{-1}]	-3.12e-09	-3.14e-06
C_1 [V^{-1}]	8.34e-06	-3e-05
C_2 [V^{-1}]	7.11e-04	-4.8e-05
C_3 [V^{-1}]	2.21e-03	2.76e-04

Table 2.4: The chosen DC-AC inverter and the parameter values for the Sandia Inverter Model for the centralised and de-centralised PV generation [79].

A DC-AC inverter will also be needed to operate the fuel cell. Research has shown that most DC-AC inverters are designed for use with PV modules. High power inverters, such as the one used for the fuel cell, in general will have a more constant efficiency than those used in conjunction with PV modules. Thus, for simplicity, a constant efficiency of 97% is assumed for this inverter.

2.2.10 Pump

Two water pumps are required in this system to pump de-mineralised water to the electrolyser and cooling water to the electrolyser and fuel cell. The water pumps are only activated when they are needed. The power required for pumping de-mineralised and/or cooling water is defined as:

$$P_{pump} = \frac{\phi_{pump} \cdot \rho_{H_2O} \cdot h \cdot g}{\eta_{pump}} \tag{2.10}$$

where ϕ_{pump} is the volumetric flow of the water and the only dependant variable. The density of water (ρ_{H_2O}) and the gravitational acceleration (g) are constant. In this study, the pump is assumed to have an overall efficiency (η_{pump}) of 67.5% [45]. Furthermore, the maximum height difference (h) is assumed to be 2 metres for simplicity. Any heat produced due to the pump's inefficiencies is dispersed into the environment, thus increasing the water temperature.

2.2.11 Grid

Despite the fact that the system in this study is grid-connected, it is still necessary to have an internal grid within the centralised location. All components listed above operate at different voltage levels and the high power flows through this system require a higher voltage level than the traditional 240V for households to minimise losses. Therefore, an AC microgrid will be used for this study. An AC microgrid was chosen over a DC microgrid or hybrid micro grid as it is simpler to construct, is more commonly used in higher power situations such as this and will reduce power losses by minimising the use of DC cabling. A schematic of this micro-grid is shown in Figure 2.3.

The medium-voltage level for the distribution grid in the Ackerswoude neighbourhood is 6kV [133]. To ensure the grid can attach to a local substation in the vicinity, 6kV will be the chosen voltage level for the AC microgrid. All high power DC components, such as the fuel cell, electrolyser and centralised battery, will be connected to the 6kV grid through AC-DC converter or DC-AC inverter. The high power pump and the compressor will also be connected to this grid.

When the PV modules are located on rooftops and the battery inside households, they will be connected directly to 240V distribution grid for the households through DC-AC inverter. Therefore, all power flows between the PV modules and the battery system or electrolyser or between battery or fuel cell and the households must pass through an AC-AC transformer.

2.2.12 Additional Components

AC-DC Converter

In order to utilise the alkaline electrolyser, it must be connected to the AC micro grid through an AC-DC converter. For simplicity it has been assumed that this converter has no power or current limitations and thus is able to provide the required current and power at any given time. However, in practical situations normally multiple converters aligned in series and/or parallel are needed to overcome any large voltage decrease/increase and the resulting current. The efficiency AC-DC converters, as with the inverter, depends on the power input. It can range from 70% for low power to 95% for the nominal power in large devices. In this study, a constant efficiency of 93% has been assumed [81].

Bidirectional Converter

A centralised battery storage system will need to be connected to the grid using a bi-directional DC-AC inverter. A typical bi-directional DC-AC inverter has efficiencies around 96 % [23]. For simplicity, a constant efficiency of 96 % is used.

AC-AC Transformer

The AC micro-grid operates at medium voltage level of 6kV. To convert the voltage level from this to that which is used in households (240V), a step-down transformer is required at a local substation. Any power that is transported to/from the battery, fuel cell or electrolyser must be sent through this transformer.

In general, AC-AC transformers operate at very high efficiencies, ranging between 95% to 99% depending on the power rating [30]. For simplicity, a constant efficiency of 97% will be assumed for the transformer used in this model.

DC-DC Converter

Every component used in this PV-Battery-Electrolyser-FC system operates at a different DC voltage. In some scenarios, a DC-DC converter will be needed to connect different DC components (such as the PV modules and the battery) when they are in decentralised locations. For simplicity it has been assumed that the converters have no power or current limitations and thus they are able to provide the required current and power at any given time. In practise, however, several converters in series are usually required and/or in parallel to deal with the large changes in voltage and current. DC-DC converters usually have an efficiency between 91-97%, but here a constant efficiency of 95% has been assumed for simplicity [93].

Cable losses

Due to safety reasons and operating logistics, all centralised components of the PV-Battery-Electrolyser-FC system must be located in a separate location from the residents of Ackerswoude. Power must be transferred by overhead distribution lines to households. This transmission of power will result in power losses in the form of heat dissipation through the cables. Nominally, depend on the length and the voltage level of the cables. However, given that these losses will be minimal compared to the overall losses and to maintain simplicity, they have been taken as an average of 2% for the entire system.

2.3 OVERVIEW HYBRID SYSTEM

Previously in this chapter, the individual components of the PV-Battery-Electrolyser-FC system and how they have been modeled have been described. However, how the components are structured in the system depends on the scenario being simulated. This section will detail the scenarios that will be simulated, their system structure and how the master controller will function in each of these systems.

This study will look at three different system scenarios: a fully centralised system (Scenario 1), a system with de-centralised PV generation (Scenario 2) and a scenario with de-centralised PV and battery storage. As detailed before, the centralised components in this system will be connected to an AC micro-grid. Each scenario will consist of the same components: PV generation and MPPT, load, a battery system, an electrolyser, hydrogen storage tanks, a fuel cell and other auxilliary components.

In all scenarios, Radiation from the Sun is received by the PV system and converted into electricity, with the MPPT charge controller extracting the maximum available power. Subsequently, depending on the load demand, the converted solar power will either be used to meet the demand, to store on a short term basis in a battery system or on a long term basis in the form of hydrogen gas in compressed cylindrical gas tanks. When it is delivered to the long term storage, this excess solar power along with demineralised water is fed to the electrolyser to produce the hydrogen gas. When the PV power output is not sufficient to meet demand, the battery system and/or the fuel cell are used to meet this demand. All components in the system will be connected to the grid at a distribution level due to the high power flows. This AC micro grid will operate at a medium voltage level of 6kV. Therefore, all power flows to and from the battery, fuel cell and the electrolyser must pass through a transformer within a local power substation. The energy management the storage methods and the load demand is regulated by the master controller. This will be described in the Section 2.4.

2.3.1 Scenario 1: Centralised System

This scenario will be the base case scenario for this study. Within this scenario, all components of the system, both generation and storage, will be in a centralised location. The advantage of this system is that all components can be easily controlled from the master controller. The aim of studying this centralised system will be to find the lowest possible LCOE for the given load demand and constraints. This scenario uses a limited number of largest scale components rather than a large number of smaller components, thus reducing the costs.

Given that the PV generation is centralised, excess generation that is sent to grid will be 'sold' on the wholesale market for wholesale electricity prices. Electricity taken from the grid will be purchased for the household electricity price. More details are given in Section 2.5.1. For the battery system, the lithium ion battery technology will be used, connected to the 6kV AC micr-grid.

2.3.2 Scenario 2: Decentralised PV Generation

All components of this scenario are found in a centralised location except the PV generation. The PV generation will distributed onto the roofs of the Ackerswoude households. The advantage of this scenario is the lack of need for additional space for the centralised PV array. Disadvantages include the need for an inverter and MPPT charge controller in every household, increasing overall costs, and the difficulty in energy management. The final layout for Scenario 2 is depicted in Figure 2.5.

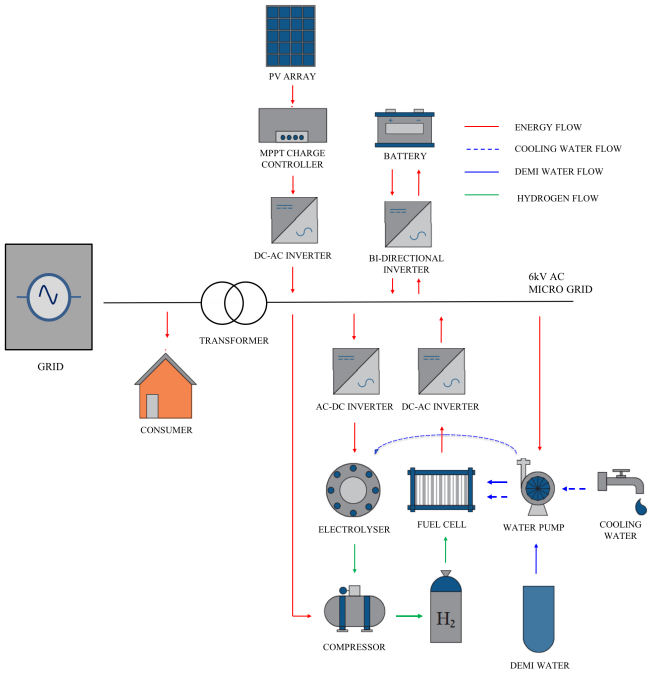

Figure 2.3: Schematic overview of the proposed stand-alone hybrid PV-Battery-Electrolyser-FC system for Scenario 1.

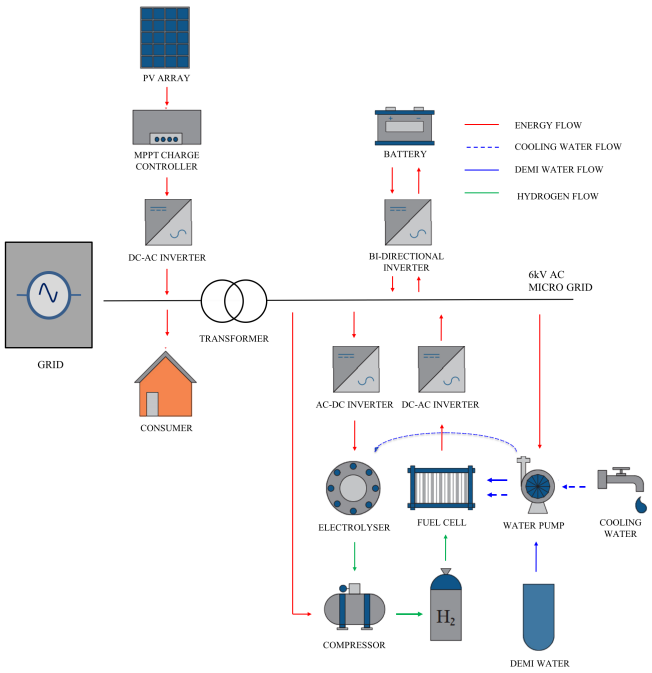

Figure 2.4: Schematic overview of the proposed stand-alone hybrid PV-Battery-Electrolyser-FC system for Scenario 2.

The orientation of the PV modules are dependant on the orientation of the houses. Of the 630 houses in Ackerswoude, 40% face SSE, 58% face SWW and 2% face S. More detail about how the modules are arranged are explained in Section 3.2.3.

The aim of studying this scenario is to demonstrate the feasibility of the more realistic scenario where PV modules are located on the roofs of households. Although

the LCOE of this scenario is likely to be higher due to increased costs, it is important to simulate a system where PV is incorporated into the urban environment.

2.3.3 Scenario 3: Decentralised Battery Storage

This system layout out will be the same as in Scenario 2 except that the battery system will be at a de-centralised location inside households. As explained in Section 2.2.6, lead-acid battery are the chosen technology for the de-centralised battery system. As a result, a 48V DC mini grid will be located in each household, attaching the battery system to the PV generation with a charge controller to help charge and discharge the battery. The household load demand can then easily be met with either the PV generation or battery storage. Only when there is excess generation or an energy deficit will power be transported to the centralised electrolyser and hydrogen storage or from the fuel cell.

The aim of studying this scenario is to compare another realistic scenario with respect to Scenario 2 where the generation/load mismatch is solved as locally as possible. Advantages of this scenario include lower power losses due to transmission, no need for converters to the battery storage system. Disadvantages include the need for maintenance every year and the difficulty with the management of the energy flows. The layout for Scenario 3 is depicted in Figure 2.5.

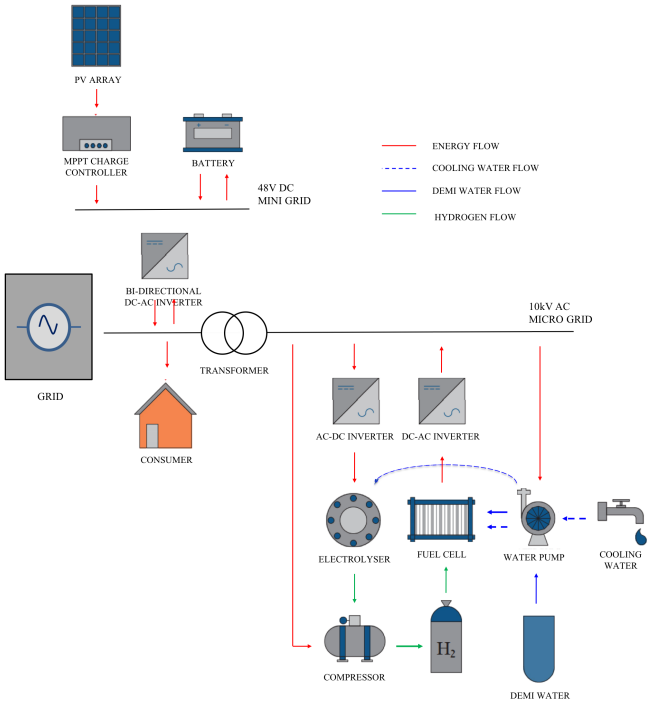

Figure 2.5: Schematic overview of the proposed stand-alone hybrid PV-Battery-Electrolyser-FC system for Scenario 3.

2.4 MASTER CONTROLLER

In a large and complex energy system such as this one, a power management controller is needed. The master controller determines the power flows to each of the 630 houses in the neighbourhood, the power to or from the battery, the power to the electrolyser (to produce hydrogen), the power extracted from the fuel cell and

the power necessary for the auxiliary components. It does this in 0.125 hour (7.5 minutes) increments. The power to and from these energy sources are sent to the converters and/or the inverter where necessary. Power flows from the PV array or from the grid enter the system and thus are considered positive. Power to the load or to the grid must leave the system and thus are negative. All other power flows occur within the system boundary.

The flow chart for the logic for the master controller is shown in Figure 2.6. This control strategy can operate in one of three operation modes. The mathematical equations for each operation mode can be found in Appendix C.1. In this Figure, P_{to_tank} represents the power used by the electrolyser and auxiliary components for producing and storing the hydrogen. P_{from_tank} represents the net power produced by the fuel cell, accounting the power consumed by the auxiliary components before being delivered to the system. The orange circle labelled 'Battery Management' in the flow chart adds additional conditions for the battery discharge. When the power generated by the solar array is not sufficient to meet the load demand, power is extracted from the battery if the following conditions are met. First, that the current state of charge of the battery (SOC_{batt}) is larger than the minimum state of charge (SOC_{min}). Second, if the SOC_{batt} is to drop below SOC_{min} the controller will ensure that the battery charges to the maximum state of charge (SOC_{max}) before it can be discharged again. This extra constraint is in place to prevent accelerated degradation within the battery due to a repeated full discharging, thus limiting the battery capacity and its lifetime.

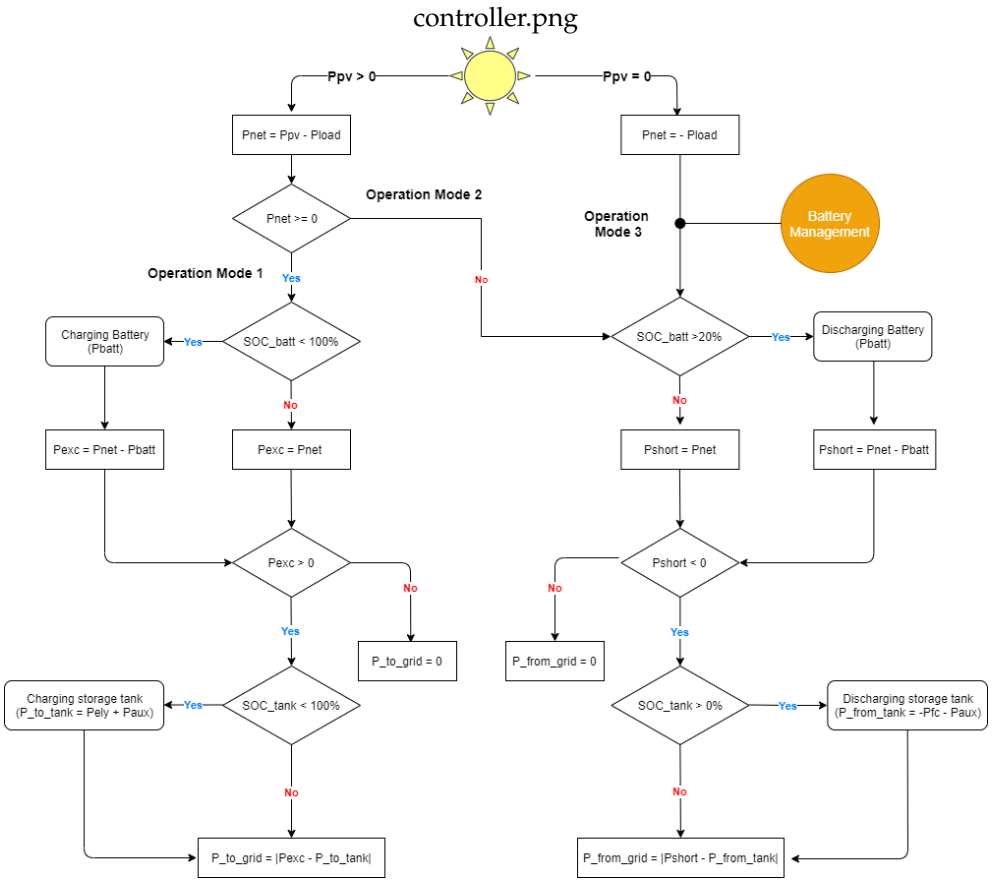

Figure 2.6: Flowchart of the energy strategy for the energy management of the hybrid PV-Battery-Electrolyser-FC energy system for the master controller.

Operation Mode 1

This operation mode represents the case when the PV generation (P_{pv}) is greater than the load demand (P_{load}) once the inverter efficiency has been accounted for. It is

represented by the left hand branch in Figure 2.6. This results in a net positive power flow ($P_{net} > 0$). If the SOC_{batt} is below SOC_{max}, this power is delivered to the battery (P_{batt}) until the battery is charged to SOC_{max}. If there is still excess power ($P_{exc} > 0$) this power will be directed to the electrolyser and the auxiliary components (e.g. compressor, water pump) until the level of hydrogen in the storage tanks reaches 100% (SOC_{tank}). Any excess power is directed to the grid (P_{togrid}). If SOC_{tank} is already at 100% then the P_{exc} is sent directly to the grid.

Operation Mode 2

This operation mode encompasses the case when the PV generation PV array (P_{pv}) is not sufficient to meet the load demand (P_{load}). This results in a negative net power ($P_{net} < 0$). If the SOC_{batt} is above SOC_{min} and is not required to reach SOC_{max} before dischargin again, the required net power is taken from the battery system ($-P_{batt}$). If the remaining shortage of power is less than zero ($P_{short} < 0$), power will be extracted from the stored hydrogen through the fuel cell and auxiliary components. Hydrogen is consumed until the load demand is met or the hydrogen tank is emptied. In the latter case, power must be taken from the grid (P_{from_grid}) to provide for the remaining demand. This value is taken as positive in these calculations.

Operation Mode 3

This operation mode is represented by the right hand branch of the flow chart in Figure 2.6. The control logic is comparable to Operation Mode 2. However, in this case there is no PV power generation ($P_{pv} = 0$).

2.5 ECONOMIC MODELLING

The most commonly used metric to measure the economic feasibility of an energy system is to look at the overall cost of the system throughout its lifetime. This is found through the levelised cost of electricity (LCOE) of a system, defined as:

$$LCOE = \frac{\sum_{d=1}^{d=y} \frac{I_{C_d} + M_{C_d} + R_{C_d} + F_{C_d}}{(1+r)^y}}{\sum_{d=1}^{d=y} \frac{E_{gen-load}}{(1+r)^y}} \tag{2.11}$$

where:

- I_{C_d}, investment costs in year d
- M_{C_d}, maintenance costs in year d
- R_{C_d}, replacement costs in year d
- F_{C_d}, fuel costs in year d
- $E_{gen-load}$, generated energy delivered to the load
- y, project lifetime
- r, discount rate

The total generated energy delivered to the load ($E_{gen-load}$) over the time period is defined as:

$$E_{gen-load} = \sum_{j=1}^{j} P_{gen-load_j} . \Delta t_j \tag{2.12}$$

Parameter	Value
Project lifetime (y)	25 years
Discount rate (r)	5%
Installation costs	10%
Conversion GBP to EUR	1.1
Conversion USD to EUR	0.9

Table 2.5: Economic parameters. Exchanges rates dates from 01-04-2020

where $P_{gen-load_j}$ is the instantaneous power delivered to load by the system, comprising to the power send to the load and the auxiliary components from the PV generation, from battery storage and from the fuel cell. This does not include power sent to or taken from the grid.

In Table 2.5 the economic parameters used within the analysis are given. Table 2.6 displays the current and future costs and the lifetime of PV modules, electrolyser, different battery technologies and the fuel cell. In addition to the main components, the LCOE also takes into account the cost of: the storage tank (€/kg); the compressor (€/unit); the water pumps (€/unit); the inverter, rectifier and converter (€/W); the gas dryer (including the driete material needed for drying the hydrogen); the gas boiler or heat pump, depending on the load profile case; the costs for the cooling water and de-mineralised water; costs of purchasing any deficit in energy from the grid and selling excess electricity to the grid. The costs of the infrastructure needed for transporting the electricity to/from households are not included here as well as the costs of the AC-AC transformer found in Figure 2.3. This transformer is needed to connect the medium voltage level AC-grid to the low voltage level of the households. It is assumed that it will already be present in an existing substation.

Finally, the LCOE also incorporates any energy deficit in the hydrogen storage tank at the end of the year. An equality constraint is implemented to ensure the state of charge at the beginning of the year is the same as at the end of the year (see Section 3.2.2). However, it is possible to put a monetary value on this deficit by multiplying it with the Dutch electricity price. This equates the energy deficit to electricity that would be purchased from the grid at a later time.

In the tables, the investment cost is the initial cost of purchasing the component. The maintenance cost is the percentage of the investment cost spent on maintenance every year. The replacement cost depends on the component's lifetime, measured in calendar years (e.g. batteries, MPPT, storage tank, inverter), operational hours (e.g. electrolyser, compressor) or when the material is chemically worn out in the case of drierite material. Finally, a 10% installation cost is added to the total cost of the system [57].

The discount rate is assumed at 5% based on the average value from other papers that also evaluate the LCOE of renewable energy systems [37], [69], [119], [146], [145].

Component	Ic 2020	Ic 2030	Mc	Rc	Lifetime
PV Module System - Commercial	0.88 €/Wp [88]	0.16 €/Wp [31]	3% [74]	-	25 years [72]
PV Module System - Residential	1.30 €/Wp [71]	0.16 €/Wp [31]	3% [74]	-	25 years [72]
Lead Acid Battery	0.11 €/Wh [107]	0.06 €/Wh [107]	2% [18]	100%	5 years [18], [33]
Lithium-ion Battery	0.47 €/Wh [96]	0.21 €/Wh [107]	-	100%	15 years [84], [61]
Alkaline Electrolyser	1.1 € /W [119]	0.7 € /W [119]	2.5 % [22]	15 % [22]	30,000h [119]
PEM Fuel Cell	2.57 €/W [67]	1.55 €/W [67]	6% [15], [73]	50% [152]	10,000h [125]

Table 2.6: Individual investment cost (I_C), maintenance cost (M_C), replacement cost (R_C) and lifetime of PV modules, lead-acid battery, lithium-ion battery, Alkaline electrolyser and PEM fuel cell in the year of 2020 and 2030. Maintenance and replacement cost are given as a percentage of the investment cost. (X) Assumed by author.

Component	Ic	Mc	Rc	Fc	Lifetime
Storage Tank	950 € /kg [101]	1% [149]	-	-	25 years
AC Compressor	€130,000 [2]	6% [148]	100%	-	60000h [10]
Demi water pump	250 €/pc [9]	5% [95]	100%	-	15 years [12]
Cooling water pumps	0.09 €*h/m^3 [9]	5% [95]	100%	-	8 years [12]
DC-AC Inverter (uni/bi-directional)	0.16 €/W [114]	3 % [36]	100%	-	10 years [117]
AC-DC Rectifier	0.22 € /W [49]	1% [X]	100 %	-	25 years [78]
DC-DC Converter	0.75 € /W [3]	-	100%	-	10 years [126]
Gas Dryer (incl. drierite)	820 €/pc [5]	-	8% [5]	-	95 m^3 (100% RH) [6]
AC Heat Pump Boiler	€9,000 [110]	4 % [99]	100 %	-	20 years [56]
HR Gas Boiler	€2,000 [110]	4 % [99]	100%	-	x
Hydrogen Boiler	€10,000 [1]	4 % [99]	100%	-	x
DEMI-Water	-	-	-	30 € /m^3 [*] [4]	-
Cooling Water	-	-	-	0.93 € / m^3 [40]	-

Table 2.7: Individual investment cost (I_C), maintenance cost (M_C) replacement cost (R_C) fuel cost (F_C) and lifetime of the auxiliary system components. Maintenance and replacement cost are given as a percentage of the investment cost, although in some cases were converted from fixed values. (X) Assumed by author.

Several things can be noted about the values in Table 2.6. First, the costs for each element are based on the estimated size of the element that will be used. For example, the lithium ion battery and the centralised fuel cell are based on a 500kW+ sized system. However, the values for the lead acid battery are based on a household system. The fuel cell lifetime is assumed to be shorter than is generally the case. This more conservative lifetime was chosen to take into account the effect of accelerated startup-shutdown of the fuel cell (occurring repeatedly) throughout its lifetime. An assumed shorter lifetime is also used for the alkaline electrolyser when it undergoes similar conditions. In addition, the estimated costs for each technology for 2030 are also listed in this table. These costs are used to assess the cost of a PV-Battery-Electrolyser-FC system as if it were to be built in 2030, explained in more detailed in Section 2.3.

Furthermore, many things can also be noted It about Table 2.7. The drier and drierite material for the hydrogen was not discussed in the previous section. For modelling purposes, it is assumed that the hydrogen is compressed and stored without the need for drying. This is to maintain simplicity in the model by not including another component. However in practice, a drying unit would be required and so this has been taken into account in the economic modelling. The lifetime of the hydrogen drier unit and drierite depends on the absorption capacity of the drierite and therefore has been defined using the total volume of hydrogen given to the drier. Moreover, for simplicity and due to lack of proper information, all electric auxiliary components are replaced in their entirety and thus the replacement costs amount to 100%. The AC water pump has been determined to meet the maximum water flow needed to supply the electrolyser. In practise, one water pump will be needed for supplying de-mineralised water to the electrolyser, one for replacement in case of failure and another to pump cooling water to the electrolyser and fuel cell. Thus, a total of three pumps must be purchased. Finally, the cost of the DEMI-water is based on an order of 100 tonnes of water.

2.5.1 Electricity Prices

When excess electricity is generated by the centralised PV system, the electricity is sold to the grid at the wholesale electricity price. When there is a deficit of electricity, electricity must be purchased from the grid at the retail electricity price. The retail electricity price is assumed to constant throughout the year. During 2019, the average electricity rate for households in the Netherlands was 0.206 €/kWh [29]. The wholesale electricity price, however, is dependant on whether the PV generation is centralised or de-centralised.

For the centralised system, the hourly electricity spot price from the day ahead electricity market on EPEX is used. For the de-centralised system, the government net metering scheme is in place for households with PV modules on their roofs. According to the Rijksoverheid, this scheme has three phases over the next 10 years [111]. The first phase, running from present day until 2023, allows households to subtract PV generation from the grid consumption, running the meter backwards and reducing the money spent on purchasing electricity. The final phase, to be implemented fully in 2031, allows households to receive a fixed amount (between 0.04-0.11 €/kWh) for energy delivered to the grid after self-consumption. The amount paid for electricity will remain the same and depends on the electricity provider. The second phase transitions between these two phases at a rate of 11% a year. During phase two, an average 'price' has been calculated for energy delivered to the grid after self-consumption for each year. This is used to calculate the money that was received by each household for the energy send to the grid over the course of a year. All prices are assumed to be constant throughout the lifetime of the project.

2.5.2 System Performance

In order to gather a better understanding of the performance of this system, a few metrics can be used, including the the self-sufficiency ratio (SSR) and the energy payback time (EPBT).

SSR

The hybrid PV-Battery-Electrolyser-FC system designed to meet the load demand of Ackerswoude must be mostly self sufficient in order to be fully utilised before it relies on the grid. By optimising the sizing of the system with a self sufficiency that is suitably low, an assessment of the full capability of the performance of the system can be conducted.

To measure the system's self sufficiency fully, the self-sufficiency ratio (SSR) can be used. Used in many studies, it represents the percentage of the load demand that is *not* supplied by the PV generation, battery and fuel cell [156], [60], [157], [102]. The parameter uses instantaneous power values and thus is only valid at the end of each simulation run.

$$SSR = \frac{\sum_{j=1}^{j} P_{fromgrid_j}}{\sum_{j=1}^{j} (P_{load_j} + P_{aux_j})} \cdot 100\% \tag{2.13}$$

Where:

- j is the time step
- $P_{fromgrid_j}$ is the power taken from the grid at time step j
- P_{load_j} is the power sent to the load at time step j
- P_{aux_j} is the power sent to the auxiliary components at time step j

Energy Payback Time

The energy payback time (EPBT) is the amount of time an energy system requires to generate the amount of energy it uses in its entire life cycle. This starts from raw materials extraction and follows through to the decommissioning phase. Calculating the EPBT allows for comparison of energy generated compared to the energy invested.

For this study, only the EPBT of the PV system is used. The typical energy payback time for a mono-silicon PV system in northern Europe is 3-6 years [87]. It is also possible to find the EPBT for the enitre PV-Battery-Electrolyser-FC hybrid system. However, there are few studies conducted into the energy used in the life cycle of every component studied here and thus compiling such data would not yield an accurate enough result.

The EPBT is defined as:

$$EPBT = \frac{E_{invested}}{E_{agen} - E_{OM}} \tag{2.14}$$

Where:

- $E_{invested}$ is the primary energy invested in PV system
- E_{agen} is the annual electricity generation

- E_{OM} is the annual primary energy used for operation and maintenance

$E_{invested}$ encompasses the energy needed to produce the materials of the PV system, transport the materials, to manufacture and install it and for the end of life management. In most cases, this energy invested can be summarised by the cumalative energy demand (CED), measured in MJ/m^2. Many estimates have been made over for this value over the past 20 years and thus a short literature study was performed to find a final value. Only papers published after 2000 were used in this study. Given that the CED is dependant on so many variables, the values found in this literature study ranges from 1123-8174 MJ/m^2. Ludin et al provided a comprehensive review of all the lifetime cycle analyses for various PV technologies, including mono-crystalline silicon, between 1990-2016 [87]. Fthenakis et al provides a comprehensive analysis of the CED of three types of solar panel, with the closest fitting one used in this study [48]. Finally, Tariq performed life cycle analysis on utility scale solar parks in Germany, providing a CED for mono-crystalline silicon [135]. For this study, an average value was from this literature review as 4562 MJ/m^2. For this study, E_{OM} has been neglected as it is minimal compared to E_{agen}.

Energy flow metrics

Finally, it is also possible to analyse a given system based on the energy flows within the system. The following energy quantities have been used for analysis of the results:

- **Solar energy** - the total solar energy produced by the PV system in one year
- **Energy sent to the grid** - the total electrical energy sent to the grid in one year
- **Energy from the grid** - the total electrical energy taken from the grid in one year
- **Generated energy delivered to the load** ($E_{gen-load}$) - the total energy delivered to the load demand, including the energy delivered directly from the solar generation, from the battery system and from the fuel cell. Energy taken from the grid or sent to the grid is not included in this metric. However, this metric does take into account the system losses, including cable losses, transformer losses and converter/inverter losses.

3 SYSTEM OPTIMISATION

Previous studies have shown that grid connected hybrid PV-Battery-Electrolyser-FC systems can be cost-effective when they are optimally sized. By optimising the hybrid systems designed in this study based on techno-economical parameters, it should be possible to find their optimal size and improve their technical and economic performance. Section 3.1 describes the classic form of the optimisation problem and explains in detail the chosen optimisation methods of Particle Swarm Optimisation and Hooke-Jeeves. The optimisation approach for the hybrid energy systems, including the chosen constraints, will be described in Section 3.2. The different scenarios that are used and the optimisation objective function and constraints for each case are explained in Section 3.3. Finally, Section 3.4 details how different the load profiles used in this study are established.

3.1 OPTIMISATION METHOD

TRNSYS contains an optimisation component called TRNOPT. This is the implementation of the Generic Optimisation Program (GenOpt) using the TRNSYS environment. Created by the Lawrence Berkeley National Laboratory, GenOpt consists of multiple optimisation algorithms for both single-dimensional and multi-dimensional optimisation with multiple starting points [154]. For this study, the Particle Swarm Optimisation (PSO) and Hooke-Jeeves method was chosen. This method uses multiple starting points for the variables and thus reduces the chances of getting stuck at a local minimum. The resulting minimum found by the PSO algorithm is then used as the base point for the Hooke-Jeeves method. Subsequently, the Hooke-Jeeves method carries out a pattern search to allow for a solution closer to the global minimum to be found.

3.1.1 Particle Swarm Optimisation

The Particle Swarm Optimisation method was developed by Kennedy, Eberhart and Shi to optimise continuous, non-linear functions [34], [76]. The behaviour of a swarm of birds was used as a basis. When they are a part of swarms, birds share information regarding their velocity and location. By processing this gathered information, the birds are able to reach their final goal as a collective. Within the PSO algorithm, a set of particles is used instead of a swarm of birds, with each particle containing its own velocity and location.

In their papers, Erdinc and Uzonoglu describe the PSO algorithm visualised in the flowchart in Figure 3.1 [39]. Initially, a random set of particles is generated with each particle representing a combination of the control variables. Each control variable can be increased or decreased by its given step size within the given domain. This initial set is then scattered randomly in the domain as defined by the bounds of the control variables. After this first 'generation' of particles has collected its results, the particles can share information in the swarm about the results, velocity and location.

Next, the location and velocity is updated for each particle, resulting in a new 'generation'. Additionally, if a global best location or personal best location is found,

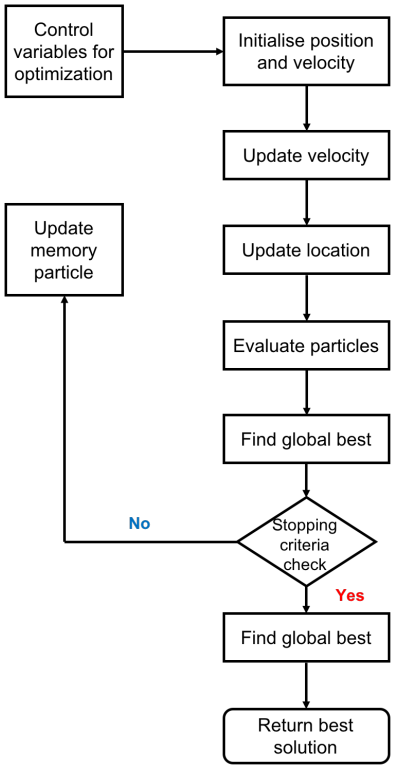

Figure 3.1: Flowchart depicting the PSO algorithm [39].

this is stored in each particle. This process is repeated iteratively until the specified number generations has been searched. Following this, the lowest optimal solution is found within the particles and presented as the global optimum.

3.1.2 Hooke-Jeeves

Robert Hooke and T.A. Jeeves describe their "direct search" optimisation method as the "sequential examination of trial solutions involving comparison of each trial solution with the 'best' obtained up to that time together with a strategy for determining (as a function of earlier results) what the next trial solution will be" [63].

The Hooke-Jeeves direct search optimisation method combines two different actions: an exploratory move and a pattern move. To initialise, a base point is chosen, in this case by the PSO algorithm, and is evaluated according to the objective function. This is followed an exploratory move, adjusting the coordinates of the base point by the defined step sizes in either an increasing or decreasing direction. If one of these directions yield a better solution, the variable will continue moving in this direction. If neither direction shows an improvement, the pattern move is launched using the best point of the exploratory move. It should be noted that only one variable can be adjusted with exploratory move at one time.

The pattern move will search in the most favourable direction according the exploratory move. A new base point is created after the pattern move has been performed and is evaluated with an exploratory move before being evaluated itself. If this new point offers a better solution, the pattern move is performed again. This is continued until the pattern move offers no improvement, after which the exploratory move is utilised again until the best solution for the objective function is found. The final step is to decrease the given step size after which the entire process of the exploratory and pattern moves is performed again until no improvement is shown. This yields the global optimum.

3.2 OPTIMISATION APPROACH

The aim of this study is to find the optimal size of different proposed PV-Battery-Electrolyser-FC energy systems for the Dutch neighbourhood of Ackerswoude. The proposed systems are extensively explained and the layout for the each scenario displayed in Chapter 2. For this study, the optimal sizing has been defined as: "a system size that yields the lowest possible levelised cost of energy (LCOE) over a lifetime of 25 years for a self sufficiency ratio (SSR) of 1%". The SSR and LCOE have been explained in Chapter 2.5.2, given by Equations 2.11 and 2.13. For the optimisation, the hybrid method of Particle Swarm Optimization (PSO) and Hooke-Jeeves is used. A time step size (Δt) of 0.125 hours (7.5 minutes) has been chosen for the optimisation process. This time step is small enough to allow the simulation to run correctly as well as being a multiple of time step of the input data (0.25 hours).

The standard optimisation problem is expressed by an objective function, bound constraints and equality or inequality constraints. The objective function defines the optimisation problem. The minimum of the objective function is found by varying the control variables within the domain given by the bound constraints. Additionally, the equality and inequality constraints have to be met by the solution of the optimisation problem. The optimal solution to the problem can be found in the space defined by these constraints.

The objective function, to be minimised during the optimisation process, for each scenario of the hybrid energy system is defined as:

$$f(x) = LCOE(x) \tag{3.1}$$

3.2.1 Constraints

As already mentioned, this study utilises TRNOPT to find the optimal solution to the objective function. In TRNOPT, the settings of the chosen optimisation method (here PSO+Hookes-Jeeves) can be tuned, for example the number generations and particles on the PSO algorithm. However, the TRNOPT program lacks the prospect of including equality or inequality constraints.

To solve this problem, a penalty function is incorporated to add constraints. For this optimisation problem, the penalty function is added to the objective function to generate an 'augmented' objective function that suffers an additional penalty when the given constraints are not met. The penalty function can either be an interior penalty function, which adds a penalty as the constraint is approached, or an exterior penalty function, which adds a penalty only if the constraint has been breached.

The penalty function used in this study is an interior penalty function. This adds a penalty to the objective function that grows larger as the constraint is breached further. This then pushes the point or particles back towards a more feasible optimum. In this way, using an interior penalty function allows the constraint to be reached more quickly than if an exterior penalty function had been used, thus speeding up simulation time.

This penalty function can be applied for any constraint type: equality, inequality or bound constraint.

3.2.2 Equality Constraints

Although equality constraints can be in any form, a quadratic loss functions is used in this study. Using a quadratic loss function will ensure a greater penalty is applied as the optimisation process moves further from the given constraint. A quadratic function also eliminates any problems negative differences can contribute. Finally, a quadratic function only has one global minimum (as opposed to a quartic that has multiple minima), thus reducing the chance of finding a local optimum [89].

This optimisation problem has two equality constraints. The first ensures that the $SSR = 1\%$. This SSR equality constraint is taken into account with the given interior penalty function:

$$b_{SSR}(x) = c_1.(SSR - 1\%)^2 \tag{3.2}$$

where b_{SSR} is the interior penalty function and c_1 is the multiplier for this penalty function. b_{SSR} will add a value or 'penalty' to the final objective function. The value of 1% has been chosen to ensure the system has adequate self sufficiency and to fully asses the established hybrid system's ability to meet the load demand. An SSR that is too high means the grid will be used to meet the demand when little power is available, making the role of hydrogen storage less clear. It is also likely that when the grid is used it will be a non-sustainable electricity source generating the energy.

The second equality constraint encompasses the state of charge (SOC) of the hydrogen tank. The optimisation procedure is run for the lifetime of the project of 25 years. However, given that the system in this study is deterministic and to keep computational time to a minimum, the simulation is performed only for a one year period. It is possible to find a system size that minimises the LCOE and fulfills SSR requirement using this time period. However, in this case the initial SOC of the hydrogen tank (SOC_{tank_i}) and the final SOC of the tank (SOC_{tank_f}) can differ. This difference in size would result in a shortage of energy if the final SOC was lower or energy that would have to be dumped if the final SOC was larger. This would mean the sizing of the system would not be optimal in reality.

As a result, it is necessary to set the initial SOC and final SOC of the hydrogen tank to be equal using an equality constraint. These are integrated into the optimisation problem using an interior penalty function in the form:

$$b_{tank}(x) = c_2.(SOC_{tank_i} - SOC_{tank_f})^2 \tag{3.3}$$

This interior penalty function will add a value or a 'penalty' to the objective function as this optimization problem will minimise the LCOE.

The values for c_1 and c_2 depend on the weighting given to each constraint. For this study, a sensitivity analysis was performed on the values for c_1 compared to c_2. An optimal value for c_2 was established, however, it was found that varying c_1 does not have a direct effect on the final result. Instead, it yields a margin of error on the results as a local optimum is often reached instead of the global optimum. As a result, each scenario and case was run multiple times with different values for c_1. The best of these runs, with the c_1 value resulting in the lowest LCOE, is presented in this work. Performing multiple runs provides insight into the deviation from the global optimum solution and thus the reliability of the optimisation process. This deviation is represented as an error margin on the final results, indicating the range of values found as result of different c_1 values.

3.2.3 Bound Constraints

All the control variables altered in the different scenarios and used by the optimisation process are bound to constraints. Table 3.1 displays the domain of the bound constraints of each variable.

Control Variable	Domain	Stepsize	Description
Centralised			
N_{SSE}	0 - ∞	20	Number of modules facing SSE
N_{SWW}	0 - ∞	20	Number of modules facing SWW
N_S	0 - ∞	20	Number of modules facing S
De-centralised			
N_{SSE}	0 - 20	0.5	Number of modules on SSE houses
N_{SWW}	0 - 20	0.5	Number of modules on SWW houses
N_S	0 - 20	0.5	Number of modules on S houses
$E_{rated_{batt}}$ (centralised)	0-∞	50kWh [128]	Rated energy capacity of centralised battery
$E_{rated_{batt}}$ (de-centralised)	0-∞	1kWh	Rated energy capacity of de-centralised battery
V_{tank}	0 - ∞	50^3	Rated volume hydrogen storage tank
$P_{max_{Ely}}$	0 - 10,000kW	120 kW [65]	Maximum power electrolyser
$P_{max_{FC}}$	0 - 10,000kW	120kW [64]	Maximum power fuel cell

Table 3.1: Control variables for optimisation with domain and stepsize.

All other components in the hybrid energy system not designated as control variables are considered unconstrained. For example, it is set that the water pump, gas dryer, compressor, DC-AC inverters (uni and bi-directional) and the AC-DC rectifier are all able to deliver or receive any level of power without restriction on the maximum rated power. If the rated power of the chosen component is exceeded, an additional component (eg. pump) is purchased. Note, the power flows, number of each of the components in the system and the number of panels is taken into account when calculating the LCOE of the system.

PV array

De-centralised

In Ackerswoude, there are a total of 630 households available for use for PV generation with 45103m^2 of roof space. Table 3.2 displays the area of roof and the number of panels facing in each direction (S, SSE and SWW).

Direction	Area	Number panels
S	268m^2	360
SSE (NNW)	14603m^2	5060
SWW (NEE)	21139m^2	7340

Table 3.2: The roof area coverage and number of panels for each direction in Ackerswoude [27].

When the PV modules are located on the roofs of households, the maximum number of panels is physically constrained by the available roof surface on each house. Most of these households will consist of slanted roofs, resulting in a roof with two

possible orientations for PV modules. As a result, there will be four separate variables to represent the number of PV modules on every roof facing in each direction: SSE, SWW, NNW and NEE. To reduce computing time, the number modules on the south facing roofs will be kept constant at the maximum.

In Ackerswoude, the average area of each roof is $70m^2$. Thus, only half of the roof surface ($35m^2$) will orientated in any given direction. This results in a maximum of 20 PV modules when using the chosen Panasonic HIT N340 PV module with an area of $1.67m^2$. The required spacing between the modules is neglected in this calculation. Therefore, the domain of these variables runs from 0 - 20.

It should be noted, the step size of 0.5 does not equate to adding half a panel on each roof. If every roof facing SSE gains one PV module, this will increase the total number of modules by 253. Similarly, this total number will increase by 367 if N_{SWW} increases by 1. Therefore it is possible to increase these steps by 0.5, in a sense increasing the number of panels by 1 on every *other* roof.

Centralised

For the centralised scenario, the PV system is located in a central location. In order to draw a comparison between the centralised and de-centralised PV array, the panels will be optimisable in the same orientations as the roofs of Ackerswoude. It is assumed panels are connected together in strings of 20 panels, resulting in a step size of 20. No upper bound is placed on the number of PV modules in this scenario.

Battery

To account for the daily fluctuations in solar power generation, battery storage is utilised. The battery system must be sized appropriately based on the physical constraints seen in the system. Often when purchasing large-scale battery storage systems, such as will be used for the centralised system, these systems cannot be purchased for any size. Most commercial batteries on the market store energy in discrete steps. For the centralised system, these steps are 50kWh. For the decentralised system energy, these steps were 1kWh (80Ah at 12V) [105]. No upper bound was chosen for the battery system as the limit on the number of solar panels will ensure the battery system sizing does not reach unfeasible levels.

Hydrogen Storage Tank

To resolve the seasonal fluctuation of solar power generation, hydrogen storage is favoured as a storage method. A certain tank volume is required that can meet the load demand in the winter when the solar irradiance is at a minimum.

Given that the hydrogen gas will be stored in many hydrogen tanks, the step size for the hydrogen will incrementally increase with the size of one of these tanks. Each tank can hold the equivalent of around $50m^3$ of hydrogen gas at room temperature and pressure [101]. Once again, no upper bound was chosen for the hydrogen storage as the limit on the number of solar panels will ensure the tank volume does not reach unfeasible levels.

Electrolyser and Fuel Cell Power

The electrolyser and the fuel cell are needed to convert the generated electricity to hydrogen and then back to electricity. As they are in a centralised location, large amounts of power will be sent to these components and thus their sizing will be considerable. When purchasing electrolysers and fuel cells at such sizes, they can only be acquired in incremental steps depending on the provider. For this study, steps of 120kW have been chosen, based on research of currently available fuel cell and electrolyser systems [65], [64].

3.3 SCENARIOS

This section will detail the control variables to be optimised to find the system size of the hybrid PV-Battery-Electrolyser-FC energy system for each scenario. These control variables will include: (1) number of PV modules, (2) battery bank capacity, (3) hydrogen storage tank volume, (4) rated power fuel cell and (5) rate power of the electrolyser. An overview of the layout and the master controller for each system is detailed in Section 2.3.

3.3.1 Scenario 1: Centralised System

This scenario will be the base case scenario for this study. The aim is to find the techno-economical optimal size of the hybrid PV-Battery-Electrolyser-FC energy system with centralised PV generation, battery storage and hydrogen storage for the neighbourhood of Ackerswoude. This scenario will allow for the assessment of the lowest possible LCOE for the neighbourhood demand. The control variables for this scenarios are listed in Table 3.3. The objective function is defined as:

$$\begin{aligned} \min_x f'(x) &= \min_x [f(x) + b_{SRR} + b_{tank}] \\ f(x) &= LCOE(x) \end{aligned} \tag{3.4}$$

For this Scenario, 630 different load profiles summed together were used to simulate the entire load demand of Ackerswoude. One simulation takes about one minute to run and thus the entire optimisation process takes up to 24 hours. For each different load profile, five simulations were run to find the global optimum and to calculate the error margins on the final results.

Control Variable	Domain	Stepsize	Description
N_{SSE}	0 - ∞	20	Number of modules facing SSE
N_{SWW}	0 - ∞	20	Number of modules facing SWW
N_S	0 - ∞	20	Number of modules facing S
E_{batt}	0 - ∞	50kWh	Energy capacity of battery
V_{tank}	0 - ∞	50 m^3	Volume hydrogen storage tank
$P_{rated_{FC}}$	0 - 15,000kW	120kW	Rated power of fuel cell
$P_{rated_{Ely}}$	0 - 15,000kW	120kW	Rated power of electrolyser

Table 3.3: Characteristics used to optimise the system size for the minimum LCOE and for varying levels of SSR for the PV-Battery-Electrolyser-FC system for Scenario 1.

3.3.2 Scenario 2: De-centralised PV Generation

This scenario differs from Scenario 1 in that the PV generation is now located on the roofs of the houses in Ackerswoude. As a result, the objective function remains the same but different control variables are needed, as listed in Table 3.4.

For this Scenario, 90 different load profiles are used to represent the load demand of Ackerwoude. Each roof orientation is matched with these 90 different profiles to allow for a detailed representation of how PV generation matches with differing load profiles. The PV generation in each household is first used to meet the load. Then, the final difference between PV generation and the load demand is scaled to match the percentage of roofs orientated in that direction and then multiplied by 7 to replicate the 630 households in the neighbourhood. One simulation takes about one to three minutes to run and thus the entire optimisation process takes 24-36

hours. For each different load profile, three simulations were run to find the global optimum and to calculate the error margins on the final results.

Control Variable	Domain	Stepsize	Description
N_{SSE}	0 - 20	0.5	Number of modules on SSE facing roofs
N_{SWW}	0 - 20	0.5	Number of modules on SWW facing roofs
N_{NNW}	0 - 20	0.5	Number of modules on NNW facing roofs
N_{NEE}	0 - 20	0.5	Number of modules on NEE facing roofs
E_{batt}	0 - ∞	50kWh	Energy capacity of battery
V_{tank}	0 - ∞	$50m^3$	Volume hydrogen storage tank
$P_{rated_{FC}}$	0 - 15,000kW	120kW	Rated power of fuel cell
$P_{rated_{Ely}}$	0 - 15,000kW	120kW	Rated power of electrolyser

Table 3.4: Characteristics used to optimise the system size for the minimum LCOE and for varying levels of SSR for the PV-Battery-Electrolyzer-FC system for Scenario 2.

3.3.3 Scenario 3: De-centralised Battery Storage

In this scenario, the battery storage system will be de-centralised in the houses of Ackerswoude. The aim of this scenario is still to find the techno-economical optimal system size and thus the objective function will be the same as Scenario 1. However, the boundary constraints are different and are listed in Table 3.5.

For this scenario, 30 different load profiles were used to represent the load demand of Ackerwoude in order to reduce simulation time. As with Scenario 2, each roof orientation was matched with these 30 different profiles. The PV generation in each household is first used to meet the load. The final load difference was then scaled to match the percentage of roofs orientated in that direction and multiplied by 21 to match the number of houses in the neighbourhood. One simulation takes about 45-50 minutes to run and thus the entire optimisation process takes 3-5 days. For each different load profile, three simulations were run to find the global optimum and to calculate the error margins on the final results.

Control Variable	Domain	Stepsize	Description
N_{SSE}	0 - 20	1	Number of modules on SSE facing roofs
N_{SWW}	0 - 20	1	Number of modules on SWW facing roofs
N_{NNW}	0 - 20	1	Number of modules on NNW facing roofs
N_{NEE}	0 - 20	1	Number of modules on NEE facing roofs
E_{batt}	0 - ∞	1kWh	Energy capacity of battery
V_{tank}	0 - ∞	$50m^3$	Volume hydrogen storage tank
$P_{rated_{FC}}$	0 - 15,000kW	120kW	Rated power of fuel cell
$P_{rated_{Ely}}$	0 - 15,000kW	120kW	Rated power of electrolyser

Table 3.5: Characteristics used to optimise the system size for the minimum LCOE and varying levels of SSR for the PV-Battery-Electrolyzer-FC system for Scenario 3.

3.3.4 Case Studies

For each scenario, it is possible to simulate multiple 'cases' concerning different load profiles. How the these different load profiles are established is detailed in the following section whilst a summary is listed below:

- **Electricity demand** - The load profile incorporates only the electricity demand of the neighbourhood
- **Smart Load Management** - The load profile incorporates the electricity demand adjusted for smart load management

- **Electricity and heat demand** - The load profile incorporates the electricity and heat demand (as supplied by heat pumps) of the neighbourhood
- **Electric Vehicles** - The case incorporates the electricity demand and load generated by electric vehicles in every house instead of gasoline vehicles

3.4 LOAD DEMAND

In this section, the approach used for modelling the electrical and heat demands of the neighbourhood of Ackerswoude will be discussed. This includes the electricity demand (with and without smart load management), the heat demand and the use of electric vehicles. Each of these different load demands will be tested for each scenario.

3.4.1 Electricity demand

The neighbourhood of Ackerswoude contains 630 households. Each of these households will have a different load profile for both electricity and heat depending on the types of people living in the given household. A collection of individual household load profiles were assembled using the software Load Profile Generator [100]. Having different profiles not only is more reflective of reality but also prevents unnatural peaks in the load demands that can occur when simply multiplying the load for a limited number of households.

To establish the demographic of a neighbourhood such as Ackerswoude, the national demographic of Dutch households was analysed, taking into account: the percentage of the population in each age bracket, the number of people living in a household, the number of children in households and the number of retired people in the Netherlands [8], [121]. Given that Ackerswoude is a neighbourhood containing relatively large houses (usually two bedrooms or more) and assuming that it requires a household with an income equal to or above national income to purchase such houses, it was assumed that the number multi-person houses with and without children would be higher than the national demographic. In addition, the number of households where all working members are unemployed would be lower than the national demographic. This is reflected in the final demographic of each household type. Finally, for simplicity it was assumed that anyone over the age of 65 is retired.

The Load Profile Generator allows for different electricity load profiles to be chosen for the same household type. This is utilised to ensure the final load profile is closer to reality. The final load profile for one day in winter (blue) and one day in summer (orange) can be seen in Figure 3.2.

3.4.2 Heat demand

In a zero-carbon world, future households may not only have their electricity powered by PV-Battery-Electrolyser-FC systems but also their heating. In 2017, residential gas heating contributed to 10% of Dutch CO_2 emissions. Already, Dutch households are starting to be disconnected from gas heating and using electric sources (such as heat pumps) to heat their homes [47]. Therefore, it is important to model scenarios where the heating demand is met in these manners.

To model the electric demand for heat pumps, it is first necessary to model the space heating demand pattern for Ackerswoude. This calculates the necessary power required to heat a dwelling to the temperature set by a thermostat at each time step.

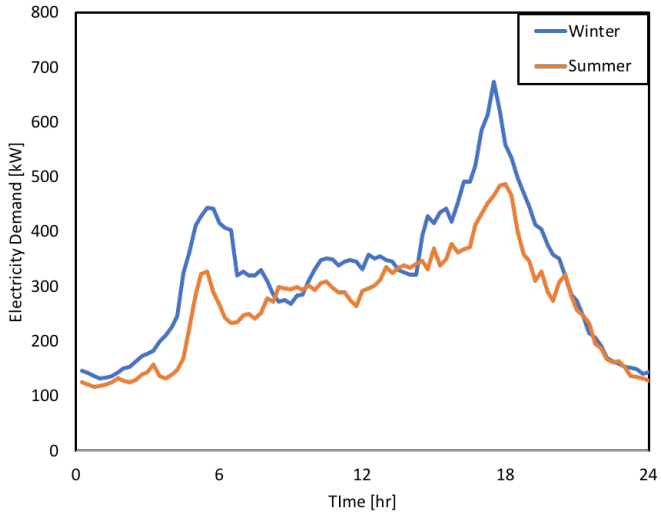

Figure 3.2: The profile of the electricity demand for the neighbourhood of Ackerswoude [100].

The thermostat settings for each household are taken from the report by Elshof (2016). Each day is divided into five time blocks, each with constant thermostat settings. On the weekends, the day is divided into two time blocks. Although Elshof uses different values for the weekend, daytime thermostat settings, for simplicity here every household is assumed have the thermostat set at 19.8 °C. Table 3.6 displays the final thermostat settings for each time period in the day.

Week	Temperature (°C)	Weekend	Temperature (°C)
23:00 - 06:00	15.8	23:00 - 08:00	15.8
06:00 - 08:00	17.5	08:00 - 23:00	19.8
08:00 - 16:00	18.8		
16:00 - 19:00	19.3		
19:00 - 23:00	20.0		

Table 3.6: Thermostat profile per week used in the model [35]

The heating demand for each 15 minute interval can be found by calculating the heat losses and the heat gains within each household. The heat flows taken in account into this model are shown in equation 3.5, namely: conduction, ventilation and infiltration, and internal heat flows [90], [35]. The equations for these terms are presented Appendix D. The final heat demand for all 630 houses is shown in Figure 3.3.

$$Q_{heatdemand} = Q_{conduction} + Q_{ventilation} - Q_{internal} \tag{3.5}$$

where,

- $Q_{heatdemand}$ is the total heat lost in each household
- $Q_{conduction}$ is the heat lost through conduction
- $Q_{ventilation}$ is the heat lost through ventilation
- $Q_{internal}$ is the internal gains from objects that emit heat within the house

Heat pumps are one of the most common ways to meet this heat demand using electricity. The addition of heat pumps will increase the electricity demand. For

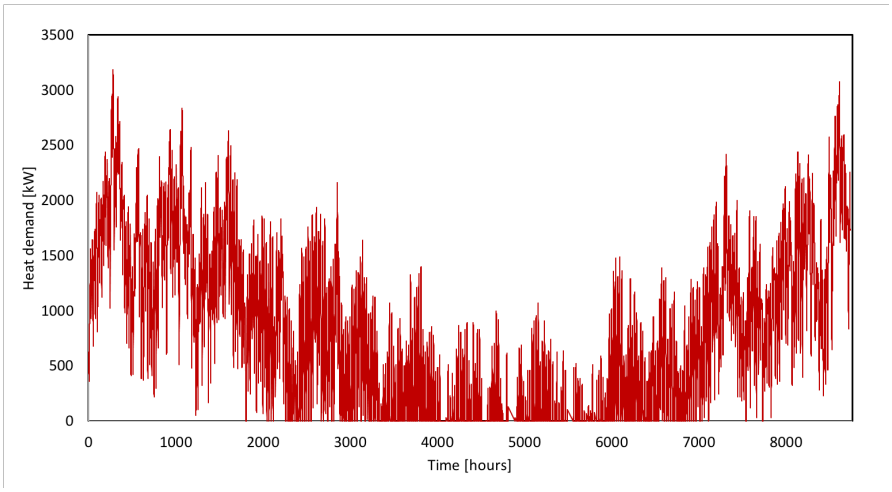

Figure 3.3: The profile of the heat demand for the neighbourhood of Ackerswoude for an entire year (1st January to 31st December).

this study, it has been assumed that all households use air heat pumps. These have an average seasonal performance factor of 4.0 [35]. The seasonal performance factor is the ratio of heat energy output throughout the season compared to the input electrical energy. The heat demand is divided by the specific performance factor to yield the required electricity input at each time step.

3.4.3 Smart load management

A crucial part of the grid after the energy transition involves smart load management by consumers. This will help to sychronise electricity production and consumption, reduce the energy mismatch and reduce the need for storage. On the consumer side, smart load management involves changing the time of use of so called 'flexible' household appliance loads, such as washing machines and electric car charging. In the future, this can be done using an automated system that will turn such loads on during the daily peak in PV generation.

Although the implementation of smart load management would require shifting the times of loads of individual household appliances, in reality this is too complex too model for 630 households. Therefore, for simplicity, the load has been altered such that 20% of the load is higher than average between 9:00 and 15:30 and lower than average otherwise, as detailed in equation 3.6. The load still uses the same amount of energy over the entire time period.

$$Load_{SLM} = 0.2 \cdot Adjustment factor + 0.8 \cdot Originalloadprofile \tag{3.6}$$

The load profile with and without the demand response is plotted alongside the adjustment factor is plotted in Figure 3.4. For the decentralised scenario, this process was performed for each load profile individually, with the adjustment factor being scaled based on the average of the that load profile.

3.4.4 Electric Vehicles

The Dutch government is aiming "for all new cars to be emission-free by 2030" [113]. As a result, many major car companies have committed to producing electric vehicles (EVs) and the Dutch government are providing incentives for the purchase of EVs. There is a high possibility that soon many residents living in neighbourhoods like Ackerswoude will own EVs instead of gasoline fueled cars.

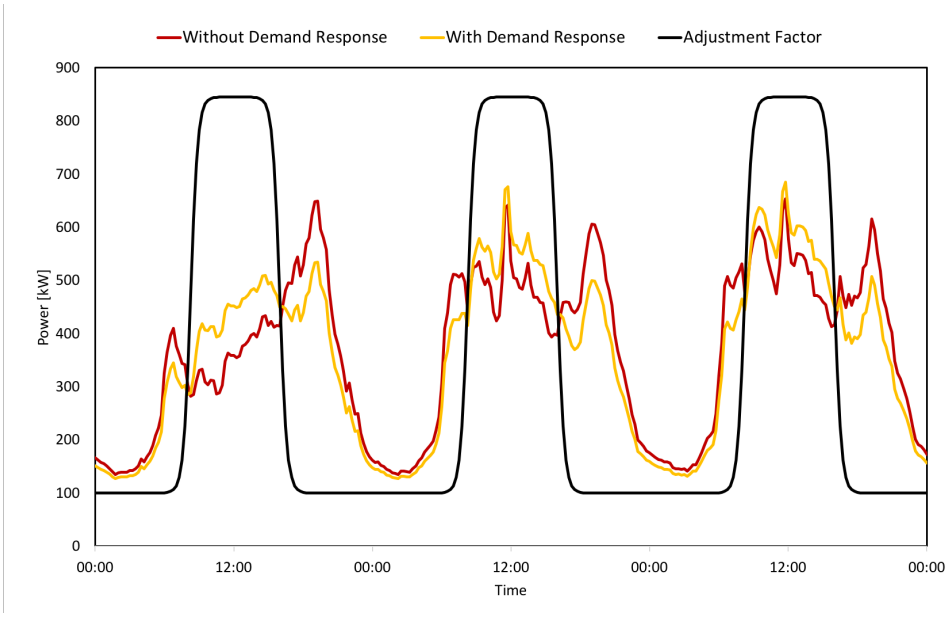

Figure 3.4: The effects of demand response on the final load profile, plotted against the correction factor.

This transition from gasoline cars to EVs could significantly increase the electric load of the neighbourhood. It is possible to simulate this by adding an additional contribution to the electric load for each scenario. The EV load profile is generated by the Load Profile Generator for each household.

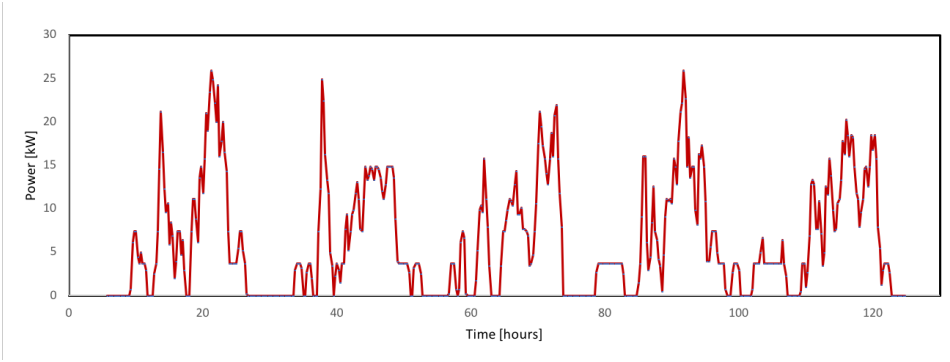

Figure 3.5: The profile of the EV electricity demand for 30 households in Ackerswoude with 3.7kW charging capacity.

The load profile for EV charging for one week for 30 households is shown in Figure 3.5. This profile is generation by the Load Profile Generator [100]. It has been assumed that all EV owners prefer to charge their vehicle at home and that each EV charging point charges the car at 3.7kW.

3.4.5 Electricity demand 2030

By 2030, it is likely that electricity demand in Dutch households will have changed. This must be taken into account when simulating the neighbourhood of Ackerswoude in the future. The ECN, working with CBS, RVO and PBL, devised a forecast for the future development of electricity use in the residential sector [59], [122]. This forecast takes into account the increased number of houses, the increased number of appliances in one household and improvements in appliance efficiency. The forecast concluded that baseline electricity will reduce by 1.9% each year. For this

study the same electricity demand pattern is assumed with an overall decrease of 1.9% each year until 2030.

3.4.6 Heat demand 2030

The heat demand is likely to change as well in the future, with changes in external temperatures being the largest contributing factor. Increasing outdoor temperatures due to global heating will result in a lower energy usage for space heating in the Netherlands. The Royal Netherlands Meteorological institute (KNMI) has presented predicted temperature data for different climate scenarios in 2030 [19]. The central estimate for 2030 temperatures predicts an average increase of $1°C$ compared the reference period of 1981 - 2010. Assuming a linear increase between 2015 (the year of publication) and 2030, this would mean an increase of $0.6°C$ between 2020 and 2030. For this system, any additional cooling power in residential homes due to hotter temperatures has not been accounted for.

It is assumed that the thermostat temperature settings in households are the same in 2020 as in 2030. In addition, as this neighbourhood is composed of newly built households designed to be fully insulated, it is assumed that there is no significant change to the insulation between 2020 and 2030.

4 RESULTS AND DISCUSSION

This chapter discusses the results for each scenario and load profile. The objective function for these systems aims to fulfil the load demand at the lowest possible LCOE whilst constraining the SSR to 1%. The electrical load demand of the 630 households in Ackerswoude is provided for by the PV system, battery storage and hydrogen storage. 1% of the instantaneous demand may be met by the grid. For each scenario, the simulation was run at least three times (five times for Scenario 1) to minimise the chances of the simulation getting stuck in a local optimum. This provides insight into the deviation from the global optimum solution if a limited number of simulations is performed and thus into the reliability of the optimisation process. This deviation is represented as an error margin on the final value for the LCOE and total costs, represented here in Figures 4.1 and 4.2.

The first scenario in this study looks at optimising the size of the centralised hybrid PV-Battery-Electrolyser-FC system, with the aim of finding the lowest possible LCOE for the given load demand and constraints. Scenario 2 simulates the hybrid system with PV generation located on the roofs of households. The aim of studying this scenario is to demonstrate the feasibility of the more realistic scenario where PV is incorporated into the urban environment. Scenario 3 simulates the system with PV generation on rooftops and battery storage inside households. Studying this scenario allows for the comparison of another realistic scenario where the generation/load mismatch is solved as locally as possible

The metrics used for analysis and comparison in this section are the LCOE, the total costs, the SSR, the generated energy delivered to the load ($E_{gen-load}$) and the energy payback time (EPBT). $E_{gen-load}$ is defined here as the total energy delivered to the load demand, including energy directly from the PV generation, from the battery system and from the fuel cell. Energy taken from the grid or sent to the grid is not included. The EPBT is the amount of time the PV system requires to generate the amount of energy it uses in its entire life cycle. Note, the EPBT does not include the energy used to generate the entire PV-Battery-Electrolyser-FC hybrid system, just the PV system.

To test the ultimate economic feasibility of each scenario and case, the LCOE can be compared to Dutch electricity prices. During 2019, the average electricity rate for households in the Netherlands was 0.21 €/kWh [29]. It should be noted that using this metric does not allow for a perfect comparison. However, a comparison cannot be made with the LCOE of a fossil fuel based power plant as this would neglect a large proportion of important costs, including for the transmission infrastructure. Although these additional costs are not taken into account in this study, they are likely to be significantly less for this hybrid system due to proximity of the microgrid to the load and the lower voltage levels used. Finding a comparable LCOE is outside the scope of this study given that the aim is to assess the expense and technical feasibility of building a hybrid PV-Battery-Electrolyser-FC system in the Netherlands.

Section 4.1 displays the overall final results and comments on trends that are common across all scenarios and load profiles. Section 4.2 discusses the results of each scenario for the electricity base case load profile. Section 4.3 does this for the smart load management load profile, Section 4.4 for the heat and electricity demand load profile and Section 4.5 for the electric vehicle load profile. Finally,

4.6 draws a comparison between the results of each load profile and explains their differences.

4.1 GENERAL RESULTS

This section displays the overall results of the simulations and the optimisation process. A complete overview of the results of the optimal system size for each scenario and load profile case are given in Table 4.1. Almost all of the system sizes displayed here are technically feasible within the constraints of the optimisation problem. The exceptions to this are the heat and electricity load profiles for scenarios 2 and 3. In these cases, the limit on the number of panels means that the PV generation is not enough to meet the load of the system throughout its lifetime whilst keeping costs low and and keeping the SSR at 1%. This is explained in more detail in Section 4.4.2. The final optimisation results are displayed in Table 4.2.

4.1.1 LCOE

Figure 4.1 compares the LCOE of each scenario for the different load profile cases. The general trend evident from this figure indicates the more de-centralised the system becomes, the greater the LCOE of the system. Intuitively this is logical. A more de-centralised system requires additional costs for purchasing and installing individual components, such as the battery system, compared to a centralised system. In reality, however, the de-centralised components in the neighbourhood will also be bought in bulk and will benefit from the reduced losses of a localised storage system.

To further analyse these differences in the LCOE, the metric can be broken down into two components: the total costs and the generated energy delivered to the load ($E_{gen-load}$). In all load profile cases, $E_{gen-load}$ is relatively consistent across all three scenarios. Thus, any change in the LCOE originates from the change in total costs. Figure 4.3 shows that the increase in costs between Scenario 1 and Scenario 2 mostly occurs from the increase in the costs of the PV system and the battery. For the PV system, this is to be expected given the costs per kWp for a residential PV system are larger. The limit on the number of solar panels in the de-centralised system also limits the amount of solar energy that can be produced. To compensate for this and for the transport losses incurred by separating the PV and battery system requires a larger (and more costly) battery system.

On top of this, the change in technology for the de-centralised battery system also play a part in increasing the LCOE between scenarios 2 and 3. The lower costs of the lead acid battery system were seen as the driving factor for choosing it as the de-centralised battery technology. However, it also has a lower depth of discharge (DoD), only 50% compared to the 75% of the lithium ion battery. This lower DoD means a larger battery is needed to store the same amount of energy. Furthermore, the drop in efficiency from around 90% to 78% also requires larger battery size. This drop in efficiency is compensated in part by the fact there are no transport losses to and from the centralised location. However, when combined with the lower DoD, this results in a slight increase in costs for the battery system compared to Scenario 2, despite the lower costs per kWh for lead acid batteries. On top of this, charge controllers are required in the de-centralised battery system, further adding to the costs in the 'other' section in Figure 4.3.

Finally, it should be noted that the LCOE of every load profile and scenario is significantly higher than the Dutch electricity prices of 0.21 €/kWh, thus indicating that this hybrid system would not currently be competitive with grid electricity.

However, as stated above, this conclusion should be taken with the knowledge that this metric does not allow for a perfect comparison.

To make a fair comparison with the heating demand, the average prices for gas in the Netherlands must be included. This price in 2020 is 0.08 € /kWh [52]. Thus, the total price of 0.29 €/kWh is still must lower than the LCOE for the heating demand and so indicates the system is still not competitive.

4.1.2 SSR

When comparing the SSR of each scenario and load profile, it is possible to see that only in a few cases is it close to the 1% that the constraint specifies. It is expected that an SSR closer to 1% will result in a higher LCOE as more energy can be supplied by the grid and thus a smaller storage system is needed. However, in reality the LCOE is not dependant on such small changes in the SRR.

Instead, a more dominant factor is the step size used in the optimisation process for variables such as the rated power of the fuel cell and the electrolyser. The step size of 120kW is larger than most other variables, chosen to reflect the reality of what is available for large scale fuel cells and electrolysers currently on the market. However, these step sizes make it more difficult for the optimisation process to find an optimum that fits exactly within the constraints. For example, in the base case and SLM scenarios, altering the final rated power of the fuel cell of 0.48MW by one step will change this value by 25% and thus will significantly alter the final SSR and LCOE. Consequently, these large steps can result in an SSR that is up to 80% smaller than the 1% constraint but still yields the optimal LCOE, depending the load profile.

4.1.3 Energy flows

The energy flows used to meet the electricity load demand are plotted in Figure 4.4. The full plot can be found in Appendix E. As shown in the figure, $E_{gen-load}$ is always consistent across all three scenarios within the same load profile. At the same time, the proportion of $E_{gen-load}$ met by each of the components is very similar for all scenarios and every load profile sees a slight increase in the reliance on the battery system between scenarios 2 and 3. $E_{gen-load}$ does, however, differ depending on the nature of the load profile, as explained below.

Conversely, the energy sent to the grid shows stark contrasts between each scenario. For all load profiles, the energy sent to the grid is much larger in Scenario 1 than in scenarios 2 and 3. This is caused by the sizing of the centralised PV system in Scenario 1. Given that the centralised PV system is cheaper per kWp (and there are no sizing constraints), it is possible to build a PV system that is oversized to reduce the reliance on the storage components. It should be noted that the *denominator* of the LCOE is not affected by this over production; $E_{gen-load}$ does not take into account excess energy sent to the grid. Instead, this excess energy sent to the grid is incorporated into the total costs in Scenario 1 by being sold on the wholesale market, although this only contributes to a 2-3% difference in the total costs. Finally, in most load profiles the energy taken from the grid is minimal compared to that sent to the grid due to the 1% constraint for the SSR.

4.1.4 EPBT

The EPBT of Scenario 1 ranges from 3.33 years to 3.71 across different load profiles. However, for Scenario 2 this range is 4.44 to 4.96 and for Scenario 3 it is 4.65 to 4.69, demonstrating that the de-centralised scenarios yield a higher EPBT for all load profiles. As this EPBT is only applicable for the PV system, there are two main

reasons for this trend. First, less solar energy is generated in the de-centralised scenarios due to the upper bound on the number of solar panels. The solar generated energy forms the numerator of Equation 2.14 for the EPBT. Secondly, many of the PV modules are facing either NNE or NWW. As these solar panels are not facing in a southerly direction, they will generate less energy overall and thus it will take a longer time to payback the energy these panels use in their lifetime.

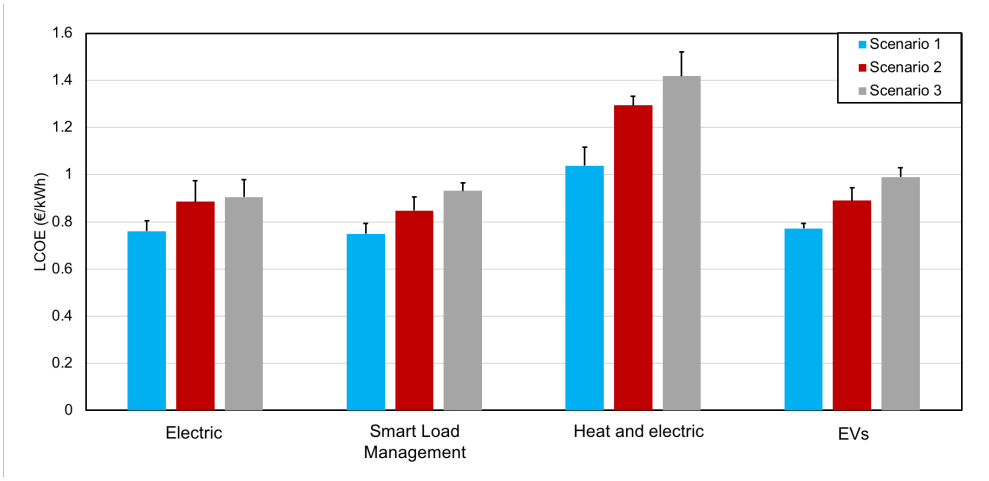

Figure 4.1: The LCOE for each load profile and scenario. The black lines represent the error from the 5 different runs of the scenarios.

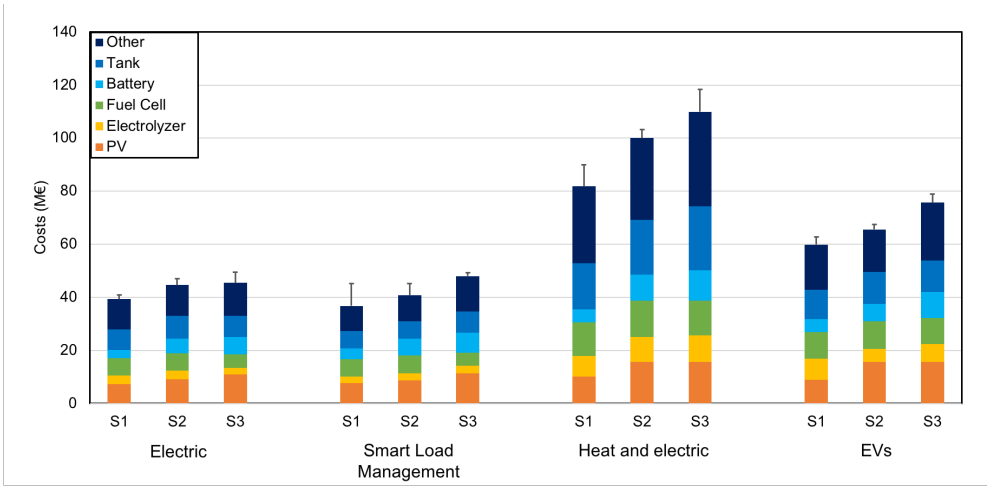

Figure 4.2: The total costs for each load profile and scenario. The different colours in each bar represent the percentage of the total costs made up by each component. The black error bars represent the range of the multiple simulation runs performed to test the reliability of the optimisation process. The final value used is the minimum of these error bars.

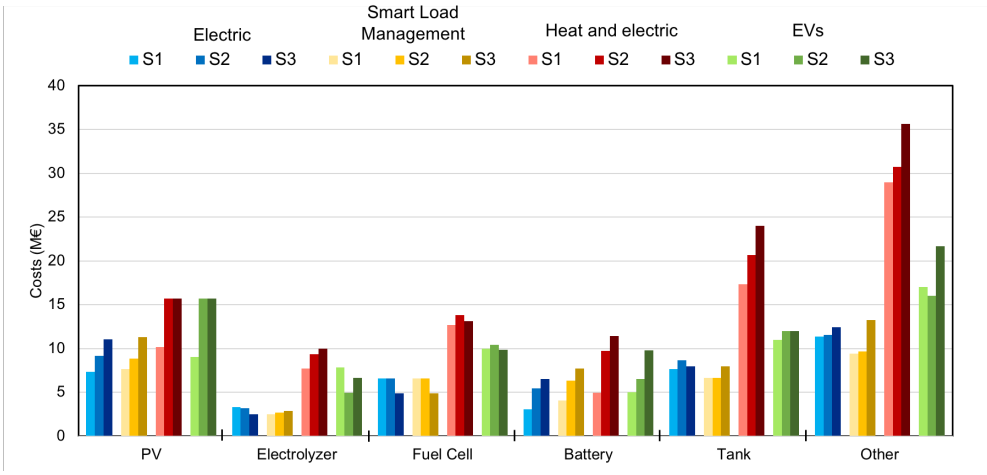

Figure 4.3: The costs for each component for each load profile and scenario, allowing for direct comparison between scenarios. The black error bars represent the range of the multiple simulation runs performed to test the reliability of the optimisation process. The final value used is the minimum of these error bars.

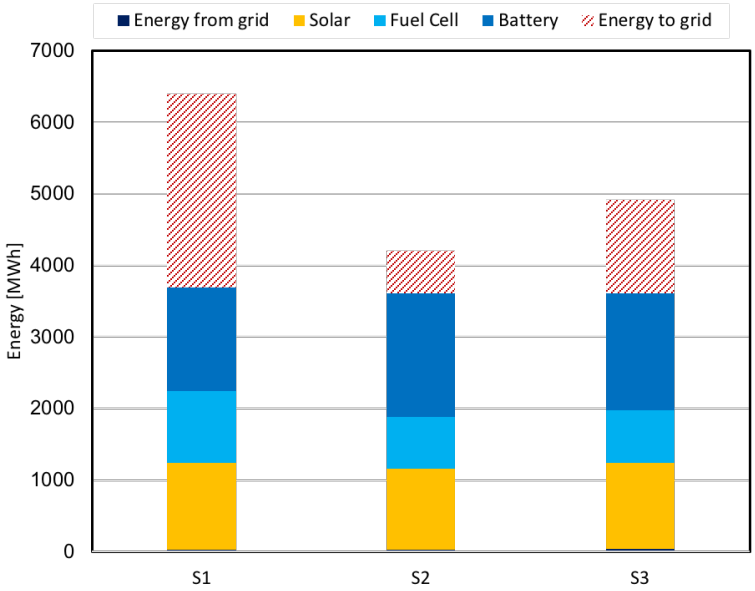

Figure 4.4: Generated energy delivered to the load for each scenario when providing for the electricity demand. The different colours represent what percentage of the energy was met by the PV generation, battery storage, the fuel cell or the grid. The dashed section represents the excess generated energy that was sent to the grid.

Load Profile	Scenario	N_S	N_{SSE}	N_{SWW}	N_{NNW}	N_{NEE}	Battery (kWh)	Tank volume (m^3)	Rated power electrolyser (MW)	Rated power FC (MW)
Electric load	1	15160	1400	600	-	-	4400	600	1.92	0.48
	2	-	16.5	17	2.5	9	7850	650	2.16	0.48
	3	-	19	14	20	6.5	27 (per house)	600	1.68	0.36
Smart load management	1	15940	1440	560	-	-	5800	500	1.44	0.48
	2	-	19.5	15.5	7	4	9100	500	1.8	0.48
	3	-	20	12	20	9	31 (per house)	600	1.96	0.36
Heat and electric	1	23580	320	60	-	-	10475	1300	4.48	0.92
	2	-	20	20	20	20	14000	1550	6.28	1
	3	-	20	20	20	20	46 (per house)	1800	6.72	0.96
EVs	1	19660	960	620	-	-	7550	800	3.6	0.72
	2	-	20	20	20	20	12850	750	1.92	0.72
	3	-	20	20	20	20	40 (per house)	900	4.48	0.72

Table 4.1: Final system sizing for each load profile and scenario.

Load Profile	Scenario	LCOE (€/kWh)	SSR (%)	EPBT (years)	Energy to the system (MWh)	Energy from the grid (MWh)	Energy to the grid (MWh)	Total costs (M€)
Electric load	1	0.761	0.79	3.71	2705	30.4	3663	39.27
	2	0.885	0.75	4.44	3580	28.1	592	44.6
	3	0.905	1.19	4.66	3561	45.6	1316	45.43
Smart load management	1	0.749	0.18	3.69	3484	6.89	4009	36.8
	2	0.848	0.92	4.42	3411	33.2	1079	40.74
	3	0.932	1.05	4.67	3660	41.70	1105	48.06
Heat and electric	1	1.038	1.034	3.33	5592	1972	60.53	81.8
	2	1.295	1.11	4.96	5504	64	2.62	100
	3	1.418	1.08	4.69	5499	62.22	2.76	109.93
EVs	1	0.772	0.99	3.54	5237	54	1861	56.99
	2	0.841	0.75	4.96	4912	38.44	2408	58.19
	3	0.989	0.92	4.694	5426	2.76	62.22	75.68

Table 4.2: Final optimisation results for each load profile and scenario.

4.2 ELECTRICITY LOAD PROFILE

While simulating this 'base case' load profile, only the electricity demand of the neighbourhood of Ackerswoude is analysed for each scenario. A comparison between the results of these simulations will be made in this section. The details of how this load profile is established is found in Section 3.4.1.

4.2.1 LCOE

Figure 4.1 demonstrates clearly how the LCOE increases as the scenarios become more de-centralised. Between Scenario 1 and Scenario 2, the LCOE increases 16% from 0.761 € /kWh to 0.885 € /kWh. In Scenario 3, it increases another 2% to 0.905 € /kWh. This small increase places the LCOE for Scenario 3 within the uncertainty range for Scenario 2, indicating that for some simulation runs the LCOE of Scenario 3 was smaller than that of Scenario 2. Given that $E_{gen-load}$ is very similar for all three scenarios, these changes are caused by the increase in total costs.

As shown in Figure 4.3, the increase in costs between Scenario 1 and Scenario 2 mostly occurs from the increase in the costs of the PV system and the battery. This is to be expected given the costs per kWp for a residential PV system are larger. More details are explained below. Between Scenario 2 and Scenario 3, the increase in costs occurs from the battery and the 'other' components. There is also slight decrease in the size and costs of the electrolyser and the fuel cell, hence why the LCOE increase is minimal.

4.2.2 System Sizing

The PV system is the largest in Scenario 1. In fact, the large amount of energy sent to the grid (2705MWh in Scenario 1 compared to 270MWh in Scenario 2) indicates that the PV system here is oversized. Scenario 3 has the next largest PV system, followed finally by Scenario 2. The de-centralised PV systems are smaller due to the increased costs for a residential system. The larger PV system in Scenario 3 is related to change in battery technology from lithium ion battery system to a lead acid battery system. The efficiency of lead acid batteries is 78% compared to around 90% for the lithium ion battery and thus requires additional PV generation to store the same amount of energy.

The sizing of the battery system also changes significantly between the three scenarios. The battery system increases from 4400kWh in Scenario 1 to 7850kWh in Scenario 2, a relative increase of 78%. Between scenarios 2 and 3, this increased another 140% to 18900kWh. The larger battery storage between scenarios 1 and 2 is most likely to compensate for the lower amount of solar energy generated. The difference between scenarios 2 and 3 is caused by the change in the battery technology. When the battery system is inside houses, it is more efficient to store the energy directly in the battery rather than sending it to the hydrogen system, thus increasing the reliance on the battery system. In addition, DoD of the lead acid battery is 50% compared to 75% of the lithium ion battery. This lower DoD means a larger battery is needed to store the same amount of energy, thus resulting in a slight increase in costs for the battery system compared to Scenario 2, despite the lower costs per kWh for lead acid batteries.

Finally, the rated power of the electrolyser is always significantly higher than that of the fuel cell. This higher rated power is necessary given that electrolyser is only used for a few hours each day to charge the hydrogen tank and thus a higher power is needed to store more solar power. In contrast, the power of the electricity load demand does not exceed 0.8MW and thus the fuel cell power does not need to

exceed this value. Given the higher costs of the fuel cell, a lower fuel cell rated power will help reduce the final LCOE.

4.3 SMART LOAD MANAGEMENT

This load profile incorporates smart load management of the residents of Ackerswoude, imagining that some of the electric load has been shifted to when PV generation is highest. The details of how this load profile is established can be found in Section 3.4.3.

4.3.1 LCOE

As with the electricity load profile, Figure 4.1 shows that the LCOE increases between the different scenarios. The LCOE rises from 0.749 € /kWh to 0.848 € /kWh between scenarios 1 and 2, a change of 13%, with the error bars indicating this increase is consistent for all runs. Between scenarios 2 and 3 it increased another 10% to 0.932€ /kWh. Given that $E_{gen-load}$ is very similar for all three scenarios, these changes are caused by an increase in the total costs

In Figure 4.3, it is possible to see how the costs of each component changed between the scenarios. Between scenarios 1 and 2 only the PV system and the battery costs increased, as was to be expected given the greater expense of the residential PV system. This is explained in more detail below.

Between scenarios 2 and 3 the costs of the batter system, the hydrogen storage tank and the 'other' components also increased. The increased costs of the battery system is caused by the larger system sizing, explained in detail in the next section. The increase in the costs of the 'other' components originates from the need for additional charge controllers in the de-centralised battery system as well as the need for a larger dryer to match with the hydrogen storage tank. The PV system, the battery system and the 'other' components contribute the most to the overall costs according to Figure 4.2.

As expected, the LCOE of this load profile is lower than the base case scenario. This is to be expected given that more of the PV generation can be met directly by the load. However, it should be noted that the LCOE in Scenario 1 is the lowest of all the scenarios and cases, yet at 0.18% the SSR is also the furthest away from 1%. It is expected that a higher SSR will yield a lower LCOE as it allows for more of the load to met by the grid. As explained previously, this discrepancy is likely to be caused by the 120kW step size used for optimisation of the rated power of the fuel cell and the electrolyser, chosen to reflect what is currently available on the market. However, these step sizes make it more difficult for the optimisation process to find an optimum that fits exactly within the constraints. If final rated power of the fuel cell in Scenario 1 were to increase by one step, this changes the value by 25% from 0.48MW to 0.60MW. As a result, these large steps can result in the low SSR seen here but still yield the lowest LCOE.

4.3.2 System sizing

Between scenarios 1 and 2, the sizing of the PV system decreased overall due to the increase in costs per kWp. A smaller PV system results in a lower amount of PV generation at peak hours and thus a larger battery storage system to compensate. The battery system increases by 56% from 5800kWh in Scenario 1 to 9100kWh in Scenario 2. This resulted in an increase of costs of the battery system. At the same time, the hydrogen storage system remains the same size and thus the reliance on

the battery storage system has increased. The percentage of energy provided by the battery has increased from 47% to 52%.

Between scenarios 2 and 3, the battery system increases by 117% from 9100kWh to 19800kWh, as does the size of the hydrogen storage tank and the PV system. As explained previously, this change in sizing is caused by the change in technology to the lead acid battery. The lead acid battery is less efficient than the lithium ion battery and thus a larger PV system is needed to store the same amount of power. Furthermore, the lower DoD results in a larger battery system size overall that eventually increases the costs of the battery system despite the lower costs per kWh.

4.4 ELECTRICITY AND HEAT DEMAND

In addition to the electricity load, it is also possible to incorporate the heating demand of Ackerswoude with the use of heat pumps. The details of how the heating demand was established can be found in Section 3.4.2.

4.4.1 LCOE

The same trends seen for other load profiles is also reflected in this case. The LCOE increases 25% from 1.038 € /kWh to 1.295 € /kWh between Scenario 1 and Scenario 2. Another 10% increase to 1.418 € /kWh is seen between Scenario 2 and Scenario 3. Both of these increases are outside the range of the error bars, indicating they are valid for all simulations runs. For this load profile, $E_{gen-load}$ is larger than others due to the additional heat demand, however it is still consistent across all three scenarios within this load profile. Thus, it is changing the total costs that causes the differences between the LCOE's.

According to Figure 4.3, the costs of *every* component increases between scenarios 1 and 2. The de-centralised PV system is more expensive and thus has a smaller size. This generates less energy throughout the year and thus a larger storage system is needed to meet the larger load demand, thus increasing the total costs. On top of this, de-centralising the battery system in Scenario 3 also requires a larger hydrogen storage system. The lead acid battery technology used for the de-centralised battery system has lower costs but is also less efficient and has a lower depth of discharge. Combining these two with a lower PV generation requires an increase in the size (and so the costs) of the battery system and also a further increase in the costs from the electrolyser, the tank and the 'other' components. This means that despite the lower costs per kWh for lead acid batteries, changing technologies has increased the total costs overall. However, the increase in costs between scenarios 2 and 3 is smaller than between scenarios 1 and 2 as the PV system and the fuel cell do not increase in costs. This is explained further in the next section.

Moreover, Figure 4.2 demonstrates that the 'other' components contribute the largest proportion to the total costs. This is caused by the additional costs of the heat pumps in this scenario. The increase in the costs of the 'other' components between scenarios is caused by the larger dryer needed for the larger hydrogen storage tank and the need for charge controllers for the de-centralised battery system in Scenario 3.

4.4.2 System sizing

As mentioned previously, the size of every system component increases between Scenario 1 and Scenario 2. This is caused by the limit on the PV generation in Scenario 2. The large load demand causes the PV system to reach its maximum size

(20 panels on every roof orientation) and yet it is still smaller than the PV system in Scenario 1. To compensate this, a larger storage system is required.

The increase in the battery system size from 10475kWh to 14000kWh reflects the trends of other load profiles, however there is also an increase in the size of the the electrolyser and tank. As mentioned previously, between scenarios 2 and 3 this increase is in part caused by the change in battery technology from lead acid battery to lithium ion battery. However, the seasonal variation in the heat load profile will also affect the increase across all scenarios. The total load demand is higher in the winter than in the summer and thus requiring a larger seasonal (hydrogen) storage system.

Despite reaching the maximum PV system sizing in Scenario 2 and Scenario 3, this PV generation is still not enough to meet the load of the system throughout its lifetime at low cost. This is indicated by the deficit in the state of charge (SOC) of the hydrogen tank at the end of the year. The difference between the initial SOC and final SOC for Scenario 1 is 0.41%. However, for Scenario 2 it is 10.6% and for Scenario 3 it is 18.98%. This implies that the system with de-centralised PV generation would not supply enough energy to meet the load over the 25 year lifetime with an SSR of 1%.

The deficit is larger in Scenario 3 because of the change in the battery technology. As mentioned previously, the smaller DoD of the lead acid battery system requires a larger battery capacity. This contributes to more to the total costs and a requires a larger tank and electrolyser to compliment, thus making it more difficult to meet the load at low cost.

Finally, throughout all the scenarios, the fuel cell is the only component that does not significantly increase in size. This is logical given the load demand does not exceed 1.4MW thus a larger fuel cell is not needed to meet the load demand.

4.4.3 Energy flows

As seen with previous load profiles, $E_{gen-load}$ and the proportion of energy provided by the battery, fuel cell and and PV generation are similar across all scenarios. More interestingly, however, is how the energy sent to the grid differs. As expected, in Scenario 1 much more energy is sent to the grid due to the larger and cheaper PV system. However, as mentioned previously, the maximum size of the de-centralised PV system is insufficient to meet the load demand over the 25 year lifetime. As a result, the energy sent to the grid in scenarios 2 and 3 is minimal, only 2.6 and 2.7 MWh compared to the 1972MWh of Scenario 1. This is a reflection of this energy deficit as all the energy must be stored and used to meet the load demand.

4.5 ELECTRIC VEHICLES

In addition to electric or heat demand, it is possible to model the neighbourhood of Ackerswoude as if each resident had an electric vehicle (EV). The details of how the load profiles for EVs was established can be found in Section 3.4.4.

4.5.1 LCOE

As with the other load profiles, the more de-centralised the hybrid system becomes, the more the LCOE increases. Between scenarios 1 and 2, the LCOE increases 15% from 0.772 € /kWh to 0.848€ /kWh. This increases again by 11% to 0.990 € /kWh between scenarios 2 and 3. These increases are within the error bars in Figure 4.1, indicating this is the case for all simulation runs. Similar to the heat load

profile, $E_{gen-load}$ here is larger than the base case scenario (5237MWh compared to 3663MWh in Scenario 1) but it is relatively constant between the three scenarios. Given this, it is the changes in total costs that cause the increase in the LCOE.

According to Figure 4.3, the increase in total costs mostly occurs from an increase in the PV system costs, battery costs and slight increase in the size of the tank. The costs of the PV system increase 73% from €9.0 million to €15.7 million. This is to be expected given the use of the more expensive residential system. This more expensive system results in a smaller system sizing that, along with added transport losses to the centralised battery system, also causes an increase in the battery costs. Between scenarios 2 and 3, the increase in costs originates from the battery system and the 'other' components. As with other load profiles, the de-centralised battery system is the cause of these increases. The technology changes from lithium ion technology to lead acid battery technology reduces the DoD 50% compared to 75% for lithium ion battery. This means a larger battery system is required to meet the load demand. Combining this with the lower efficiency (78% compared to 90%), this means that the battery system has increased in costs despite the lower costs per kWh of the lead acid batteries. A larger battery system also requires more electronics in the form of charge controllers, and thus significantly increases the contribution of the 'other' components.

It should also be noted that the LCOE of the EVs load profile is similar, and at times lower, than that of the base case scenario. For example in Scenario 1 there is only a 1.4% difference from 0.761€/kWh in the base case to 0.772€/kWh in the EV load profile. This is in contrast to the heat load profile where the increase in costs leads to a significant increase in the LCOE. More details about this is explained in Section 4.6.

4.5.2 System sizing

As with other load profiles, the de-centralised PV system is smaller than the centralised one due the limit in the size of the system. The de-centralised PV system reached the maximum size of 20 panels in each roof orientation in order to meet the higher load demand.

As explained previously, the battery system size also increased for both Scenario 2 and Scenario 3. Between scenarios 1 and 2, the battery system increased by 18.5% from 7550kWh to 8950kWh. For scenario 3, this increased another 228% to 29400kWh. The increase between scenarios 2 and 3 is mostly caused by the change in battery technology for the de-centralised system. The slightly lower efficiency and the lower DoD results in a far larger system size. However, the extent of this increase also demonstrates the reliance on the battery to meet the demand in this load profile case.

4.6 LOAD PROFILES

This section aims to compare the results of the different load profiles and reflect on the reasons for these differences.

Firstly, it should be noted that for most scenarios the LCOE of the SLM profile was lower than the electricity load profile. This is to be expected, reflecting the increased amount of the load demand that is met directly by the PV generation. In theory, this should reduce the need for storage and thus reduce the size of the battery system. However, in contrast to expectations, the size of the battery system is higher in the SLM case (7550kWh compared to 4400kWh for the case case in Scenario 1) and the size of the hydrogen storage system lower. In Scenario 1, the

resulting energy provided to the load by the fuel cell has in turn decreased from 27.4% in the base case to 21.3% in the SLM case, demonstrating a decreased reliance on the hydrogen storage. This is most likely caused by the higher overall costs per kW of the hydrogen storage system. Reducing the size of the hydrogen storage system will result in a larger reduction of the total costs compared to the battery system.

Scenario 3 is the exception to this trend, where the LCOE of the SLM profile is greater than the base case at 0.932 € /kWh and 0.905 € /kWh respectively. $E_{gen-load}$ in this case is similar for both the base case and the SLM case, thus it is the increase in costs of the PV system and the battery system that has caused the LCOE to increase. The change in the battery system technology may have contributed to this. The lower efficiency and the lower DoD of the lead acid battery means that a larger battery size is needed to meet the load demand and thus results in an increase in the costs.

In reality, however, it is most likely that something in the optimisation process that caused this anomaly. Less simulations were run for Scenario 3, thus making it less likely for the global optimum to be found. In addition, less load profiles were used to reduce the simulation time (only 30 in Scenario 3 compared to 90 in Scenario 2) and thus any discrepancies would become emphasized when the system is multiplied to represented the 630 houses in the neighbourhood.

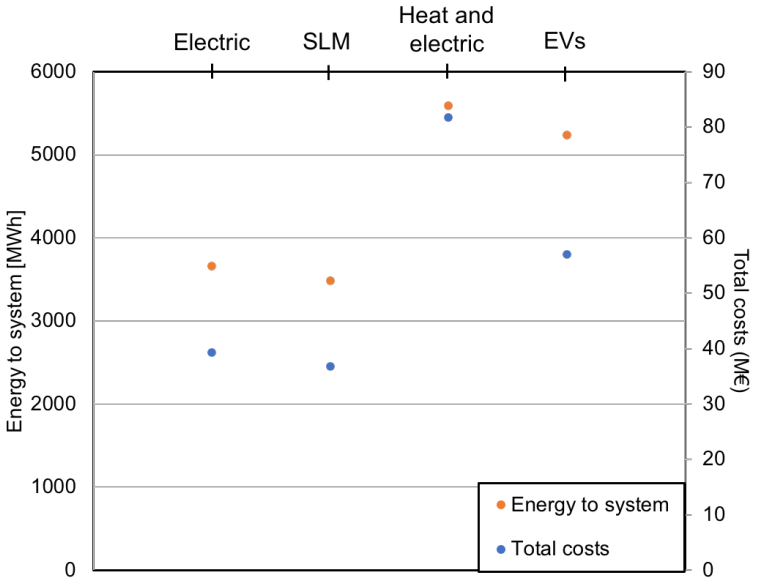

Figure 4.5: Generated energy delivered to the load ($E_{gen-load}$) and total costs plotted side by side of each load profile for Scenario 1.

Furthermore, it is also important to note the relatively low LCOE of the EV load profile, demonstrated in Figure 4.1. For all scenarios, it is only slightly higher than that of the base case electricity load profile, with a maximum difference in Scenario 3 of 8.5% between the 0.905 €/kWh of the base case and the 0.990€ /kWh of the EV load profile. This is surprising when you compare this to the heat demand load profile. Both the heat load profile and the EV load profile have a higher load demand and so see a significant increase in $E_{gen-load}$ compared to the base case.

This can be explained by breaking the LCOE down into its two contributing factors: the total costs and $E_{gen-load}$. Figure 4.5 plots these side by side for each load profile for Scenario 1. For the heat profile, the higher load demand requires a system with larger storage components, resulting in total costs that are twice that of the base case, €81.8 million compared to €39.3 million respectively. For the EV load profile, however, the increase in the system size is smaller and thus the increase in total

costs is proportionally smaller, reaching only € 57.0 million. This results in the ratio between the total costs and $E_{gen-load}$ remaining similar to the base case and thus yielding a similar LCOE.

This difference can be explained by comparing the nature of the additional load for the EV and the heat load profile. The EV additional load is added during the day, when residents of the neighbourhood come home from work and charge their cars. This means that often this load can be met directly with the PV generation and thus comparably less storage is needed and fewer losses occur. The heat load profile contributes the additional load in the evening/night and during the winter, when the hydrogen storage system is often used to meet the demand. This means a larger storage system is required with additional contribution from the expensive and inefficient hydrogen storage. In addition, the costs of the heat pumps are also taken into account in the heat load profile, contributing further to the increase in total costs.

5 FUTURE SCENARIOS

Previous chapters have discussed the technical and economic feasibility of a PV-Battery-Electrolyser-FC system as if it were built in 2020. However, many technologies used in this study are still in the early stages of commercialisation and thus their costs are considerably higher than they will be in ten years time. This results in an LCOE that is not low enough to be economically competitive with Dutch electricity prices.

However, as these technologies commercialise, economies of scale will ensure prices will drop as production expands, thus lowering the costs of building such a system in years to come. As a result, it is important to look at the feasibility of building such a system in the future when costs are lower.

Section 5.1 of this chapter will present the literature review conducted to find the learning curves of each components, establishing an average, upper and lower bound of the prices in 2030. Some preliminary results of the optimisation using these values are presented in Section 5.2

5.1 LEARNING CURVES

The relationship between the expansion of production and the decrease in costs is known as the learning curve. It is possible to model such a curve based on the observations of past trends of the commercialisation of each technology (or a similar technology). By analysing the data of past technologies, and predicting their growth patterns, it is possible to predict the cost reduction as a function of time and thus the costs in any given year and thus the costs of such systems in 2030. A literature review has been performed, predicting the 2030 prices of PV systems, lithium ion batteries, alkaline electrolyser, PEM fuel cell, heatpumps and the hydrogen boiler.

In literature, the learning curve is usually represented by a metric known as the learning rate. The learning rate represents the percentage that the costs of a given technology fall when the production rate doubles. The learning rate is then coupled with a predicted growth rate for the technology to yield final cost of the technology as a function of time.

For each technology, the final predicted learning curves (plotted in red) are found by averaging the results and fitting the data to a trend line. The upper-bound (plotted in blue) and the lower-bound (plotted in yellow) for the learning curves are established by taking the maximum and minimum values from this data and fitting them with trend lines. For the PV systems, the lithium ion battery, the fuel cell and the heat pump, the starting price for each paper is different depending on the location of the study and the year of publication. For some papers, the starting price was not given and so the learning rate and growth rate has been combined with starting price from this study. The starting price and learning rate for each paper can be found in Appendix F. The final trend line equations used are also located in Appendix F.

5.1.1 PV system

The costs for PV systems have been falling steadily for over a decade. As a result, substantial research has been conducted into the learning curves of PV systems, both on a residential level and for utility scale. PV systems are inclusive of both PV modules and the balance of system (BOS) components, such as inverters and the racking. An example of the learning curve for PV modules can be found in Figure 5.1. For simplicity, the costs and learning rates of BOS and PV modules have be combined into one value for this study. In reality, this method is not entirely accurate. The sizing of the BOS and the number of PV modules do not necessarily increase in parallel. In addition, both BOS and PV modules have different learning rates. Thus the proceeding literature studies are inclusive of both of learning curves. All the research conducted here is focused on systems with crystalline silicon PV modules.

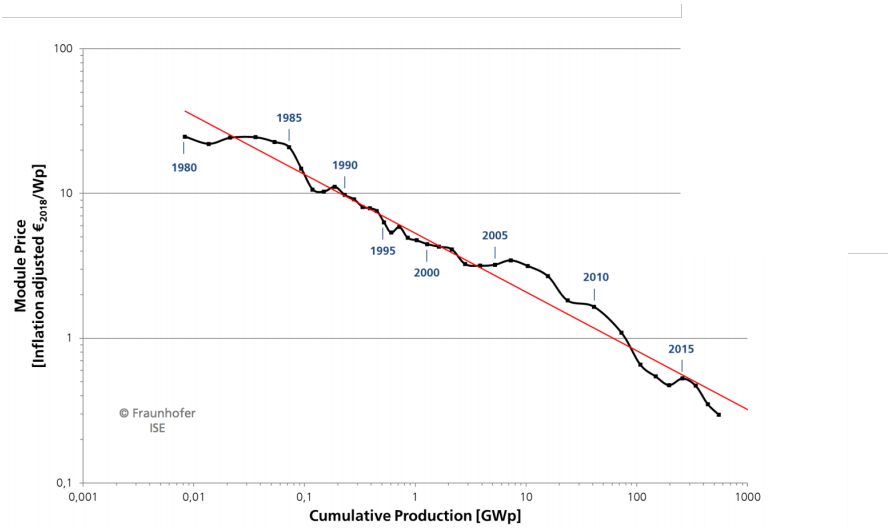

Figure 5.1: The historical price learning curve of PV modules from 1980-2014 [106]

Utility-scale PV

Six different papers were used to establish a learning curve for utility-scale PV, [[146], [37], [158], [54], [137], [108]] with three of them yielding results from multiple scenarios. The data and the resulting learning curves are plotted in Figure 5.2. The final price for a PV system in the year 2030 is 0.59 € /Wp, a decrease of 32.9%. The upper bound is 0.80 € /W and the lower bound is 0.32 € /W.

In terms of the growth rate for the utility scale PV systems, Vartiainen et al. used a compound annual growth rate (CAGR). For the slow scenario, a 5% CAGR is used. For the moderate scenario there is a 10% growth until 2035 before decreasing linearly to 2.5% by 2050. For the fast scenario, a 20% CAGR is used until 2030 before decreasing linearly to 5% in 2040 and to 0% in 2050. Fraunhofer ISE has four different growth rate scenarios using S curve growth with differing saturation points and a CAGR of 5%, 7.5%, 10% and growth until PV represents 40% of electricity generation in 2050. Zhou and Gu represented a growth of PV systems in US, with a growth rate for utility-scale solar of 6GW a year in the slow scenairo and 11.1GW a year in the fast scenario. Tsiropoulos et. al present three scenarios. The "Baseline" scenario represents the 'business as usual' where renewable energy supplies 30% of global electricity consumption. The 'Diversified' scenario represents the moderate case where renewable energy supplies 74% of electricity. The 'ProRES' scenario represents the the most ambitious scenario where 93% of electricity is generated by renewables. The growth rates from each scenario are taken from other papers.

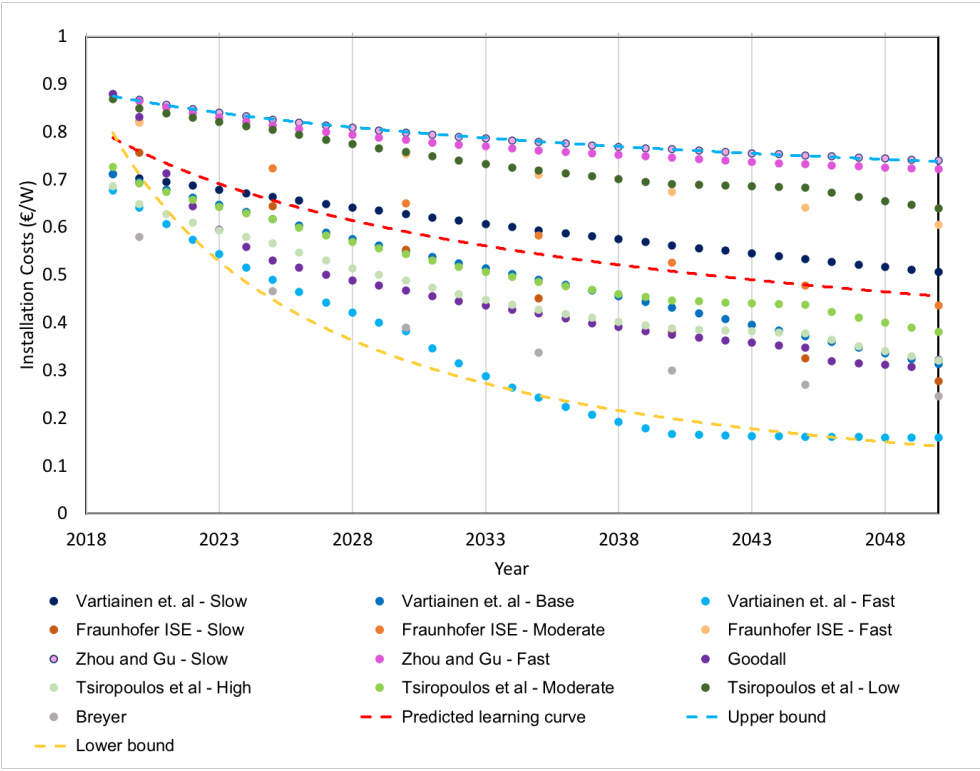

Figure 5.2: The learning curves for the utility scale PV system based on historical data and future growth prediction. The red is the average predicted learning curve, blue the upper bound and yellow the lower bound.

Breyer models the growth rate with a CAGR of 10%. Goodall does not present their PV growth strategy in detail.

Residential PV

Five different papers were used to establish a learning curve for residential PV, [[106], [158], [54], [137], [108]] with two yielding results from multiple scenarios. The data and the resulting learning curves are plotted in Figure 5.3. The final price for a residential PV system in the year 2030 is 0.80 € /W, a decrease of 36.2%. The upper bound is 1.08 € /W and the lower bound is 0.49 € /W.

Each paper has chosen a different growth rate for different scenarios. Zhou and Gu represented growth of residential PV systems in US, with a growth of 1.7GW a year in the slow scenario and 3.1GW a year in the fast scenario. The growth strategy for Tsiropoulos et. al and Breyer is the same as for utility-scale PV. Fraunhofer ISE and Goodall did not provide details of a growth rate, having sourced that data from external studies.

5.1.2 Lithium ion battery

The costs for lithium ion batteries have been falling for the last few years as the industry for residential and utility scale lithium ion battery storage has expanded. However, lithium ion batteries today are used for many different purposes, from battery packs in electronics to storage systems, and thus can have a range of different prices. Some studies have been conducted on the learning rates of lithium ion batteries over the past five years.

The final learning curve is found by using the learning rate and the growth rate of each paper to predict the prices of lithium ion batteries to 2050. Data has been

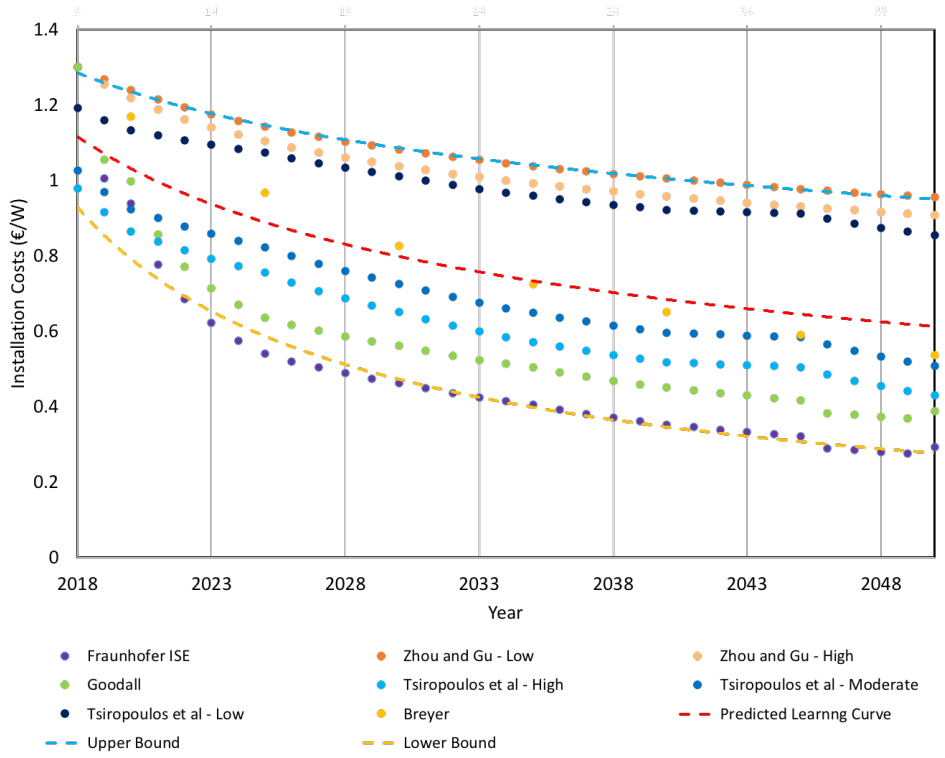

Figure 5.3: The learning curves for residential PV systems based on historical data and future growth prediction. The red is the average predicted learning curve, blue the upper bound and yellow the lower bound.

taken from six papers [[136], [120], [42], [104], [Fell], [108]] ranging from 2010 - 2017. Three papers have presented results from three different scenarios. The final data and predicted learning curves are plotted in Figure 5.4. The final price for a lithium ion battery in the year 2030 is 266 € /kWh, a decrease of 43.3%. The upper bound is 547 € /kWh and the lower bound is 37.7 € /kWh.

Smchidt et al. specifically looked at the growth of utility-scale lithium ion storage between 2010 and 2015. The predicted growth had an S-curve shape with a growth rate of 0.326 and a saturation annual capacity of 96 GWh by 2050. BNEF researches data for lithium-ion battery packs for 2010-2017 but does not detail its growth rate assumptions. Breyer and Tsiropoulos et al. conducted research for stationary lithium ion storage system. The growth rates for the for the different scenarios, have been collected from other papers. IRENA only provided data points for 2016 and 2030, having not used historical data to find learning curves but instead the expertise of those in industry and academic research of lithium ion battery development.

It should be noted, finally, that many of these prices are likely to be an overestimate when based on the study of past data. The lithium ion battery industry is still not mature at collecting and presenting data on cumulative capacity and prices. Thus, the historical data presented here may not be entirely reflective of reality and thus may skew the final results.

5.1.3 Alkaline Electrolyser

Alkaline electrolysis is a comparatively mature technology, having been in use in industry since the early 20th century. Despite this, the volume of alkaline electrolysers being produced on the market is still relatively small. As a result, the costs of al-

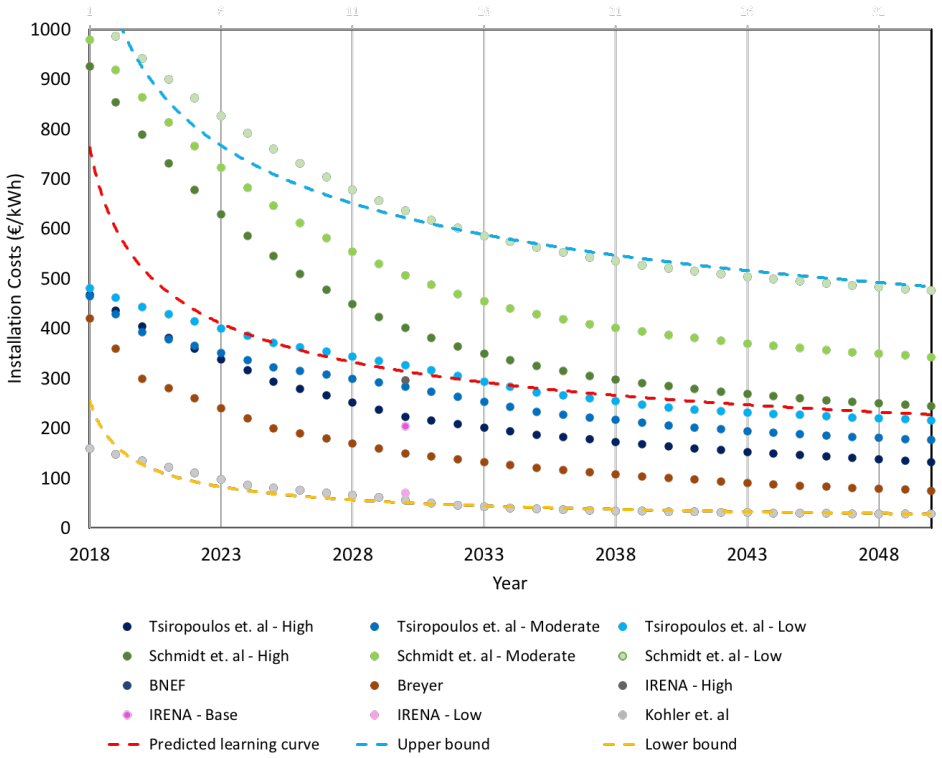

Figure 5.4: The learning curves for lithium ion batteries based on historical data and future growth prediction. The red is the average predicted learning curve, blue the upper bound and yellow the lower bound.

kaline electrolysers are unlikely to decrease because of technological developments but could still benefit from large scale production.

Data from five papers [[115], [51], [119], [108], [91], [150]] ranging from 2000-2017 was used to determine the alkaline electrolyser learning curve. Unlike for the PV systems and lithium ion battery, the data collected for the alkaline electrolyser is either historical data or estimates of future prices sourced from expert opinions in industry or in academia.

The final data and predicted learning curves are plotted in Figure 5.5. The final price for the alkaline electrolyser in the year 2030 is 0.66 € /W, a decrease of 48.2%. The upper bound is 0.88 € /W and the lower bound is 0.42 € /W.

Saba et al. conducted a literature review to evaluate published data (from academic and manufacturing sources) on investment costs of electrolysers (alkaline and PEM) from the 1990s through 2017, resulting in a final learning rate of 18%. Glenk et. al used 'hand-collected data from manufacturers, operators of PtG plants, articles in peer-reviewed journals and technical reports' to predict the price of alkaline electrolysers in the future, resulting in an exponentially fitting curve for the costs as a function of time. This data ranged from 2003-2016. Schmidt et. al obtained estimates for the costs of electrolysers in 2020 and 2030 from structured discussions with experts in industry and academia. This resulted in a final learning rate of 18%. Element energy sourced their data from previous studies and industry publications. Breyer took research from other papers that predicted the cost of alkaline electrolysis as the industry expands.

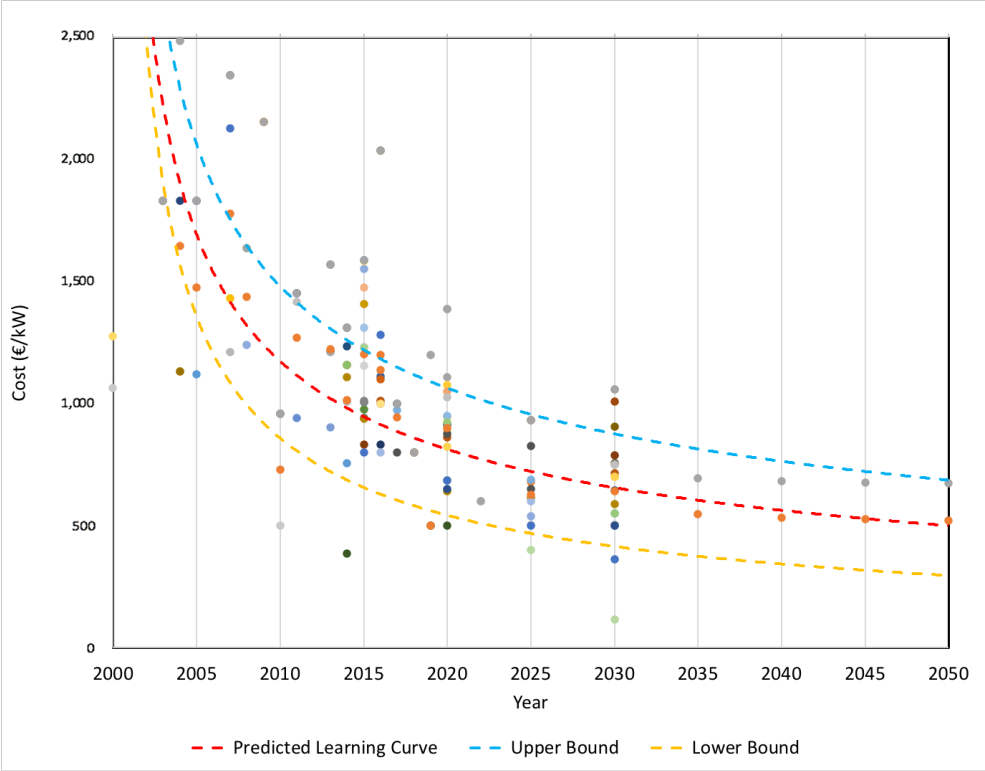

Figure 5.5: The learning curves for alkaline based on future growth prediction. The red is the average predicted learning curve, blue the upper bound and yellow the lower bound.

5.1.4 PEM Fuel Cell

Little research has been conducted in the learning curves of PEMFCs. Residential PEMFCs have only been commercially available for a few years, mostly in Japan and Korea. Utility scale PEMFCs are even more uncommon and are still in the development phase in most countries. As a result, the research presented here has been conducted on residential PEMFCs. As this is technologically very similar to utility scale PEMFCs, it is possible to utilise the learning rates and growth rates from these papers and combine it with current known prices for utility-scale PEMFCs to find future prices.

Data from three papers [[120], [129], [130]] were used to determine the PEMFC learning curve, using data from 2004-2017 and presenting different learning curve scenarios.

The final predicted learning curve and the data used are plotted in Figure 5.6. The final price for the PEMFCs in the year 2030 is 1.09€ /W, a decrease of 59.7%. The upper bound is 1.75 € /W and the lower bound 0.54 € /W. Given that these learning rates have been established for residential fuel cells, the starting price for 2020 has been used in this study for most scenarios. The learning rates from each paper can be found in Appendix F.5.

When predicting the growth of PEM fuel cells, Green and Staffell used an S shape growth curve. The slow curve has a growth rate of 20% and a saturation capacity of 1GW per year. The moderate growth scenario uses a growth rate of 40% and a saturation capacity of 10GW per year. The fast growth scenario has a growth rate of 80% and saturation capacity of 100GW per year. Schmidt et al. uses an S shape growth curve with a growth rate of 0.5 and a saturation capacity of 97GW. Staffell et al. used data from Japan and Korea for fuel cell capacity from 2000 - 2015 to establish an annual growth rate of 25%.

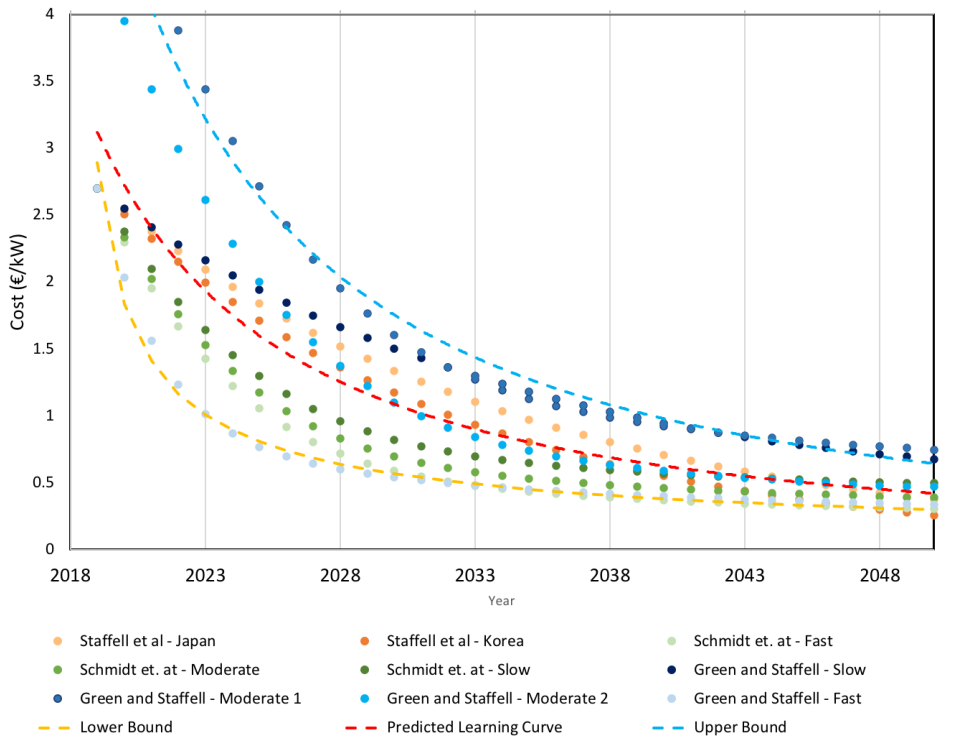

Figure 5.6: The learning curves for fuel cells based on historical data and future growth prediction. The red is the average predicted learning curve, blue the upper bound and yellow the lower bound.

5.1.5 Heat pump

Although heat pump technology is relatively mature, there are few places where heat pumps have been distributed on a large scale into households for use in heating. As a result, few studies have been conducted into the learning curves of heat pumps.

Data from five papers [[104], [46], [13], [80], [153]] are used to determine the heat pump learning curves, with one paper presenting multiple scenarios. These and the data used are plotted in Figure 5.7. The final price for the heat pump in the year 2030 is 1054.5 € /kW or 7381.5 for a 7kW unit, a 18% decrease. The upper bound and lower bounds are 1361 € /kW (no change in price) and 837.68 € /kW respectively.

In terms of growth rate and data collection, Kohler et al used external sources to predict the growth of heat pumps and literature to establish the learning rate. Kiss et al conducted a study into the production and distribution of heat pumps in Switzerland and Sweden to determine the learning rate. No details about a future growth rate of heat pumps were given. This same data was used by EnergiNet, combined with more recent prices, for their predictions. Element Energy established their costs reductions through a literature review and stakeholder consultation. Finally, Weiss et al used data published from Switzerland on heat pumps prices to establish a learning rate. However, no details of a growth rate was given.

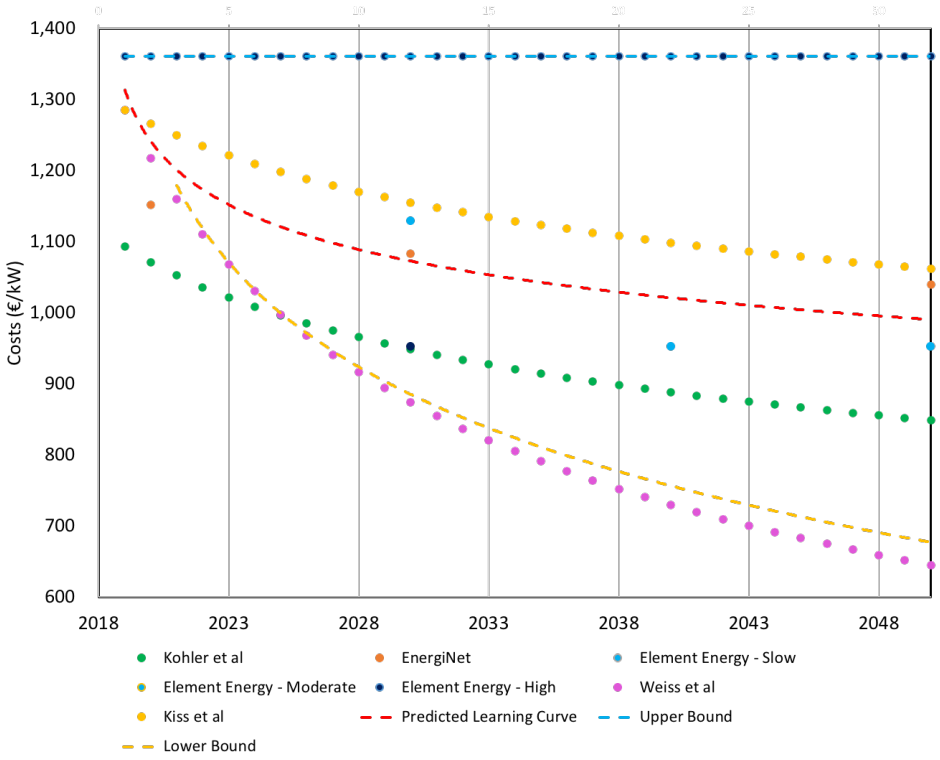

Figure 5.7: The learning curves for heat pumps based on historical data and future growth predictions. The red is the average predicted learning curve, blue the upper bound and yellow the lower bound.

5.2 RESULTS AND DISCUSSION

This section details the preliminary results found for 'future scenario' simulations, using the predicted costs for 2030 for each component, as found by the average trend line presented in Section 5.1. Due to time constraints, only one run for each case was performed, resulting in no error bars on the results. Furthermore, only results for Scenario 1 were obtained.

The metrics used for analysis and comparison in this section are the LCOE, the total costs, the SSR and the generated energy delivered to the load ($E_{gen-load}$). $E_{gen-load}$ is defined here as the total energy delivered to the load from the PV system, battery system and from the fuel cell.

The costs of auxiliary components, such as the pump, compressor, the converter and the bi-directional inverter are assumed to be the same in 2030 as in 2020. The electricity prices and the wholesale market prices are also assumed to be the same as in 2020. However, in reality it is likely that these costs will have also changed.

Load Profile	N_S	N_{SSE}	N_{NEE}	Battery (kWh)	Tank volume (m^3)	Rated power electrolyser (MW)	Rated power FC (MW)
Electric load	15280	2040	1000	2700	600	3.24	0.48
Smart load management	19660	1980	860	2050	400	2.04	0.36
Heat and electric	19280	3080	1240	10000	1000	3.4	1.04
EVs	20100	920	760	7500	800	3.36	0.72

Table 5.1: Final system sizing for each load profile of Scenario 1 with 2030 prices.

Load Profile	LCOE (€/kWh)	SSR (%)	EPBT (years)	Energy to the system (MWh)	Energy from the grid (MWh)	Energy to the grid (MWh)	Total costs (M€)
Electric load	0.596	0.79	3.93	4006	33.02	1513	33.67
Smart load management	0.542	0.89	3.75	3392	32.09	5381	25.93
Heat and electric	0.815	1.02.	4.01	4798	51.23	3671	55.14
EVs	0.566	0.998	3.55	5220	54.40	2270	41.70

Table 5.2: Final optimisation results for each load profile of Scenario 1 with 2030 prices.

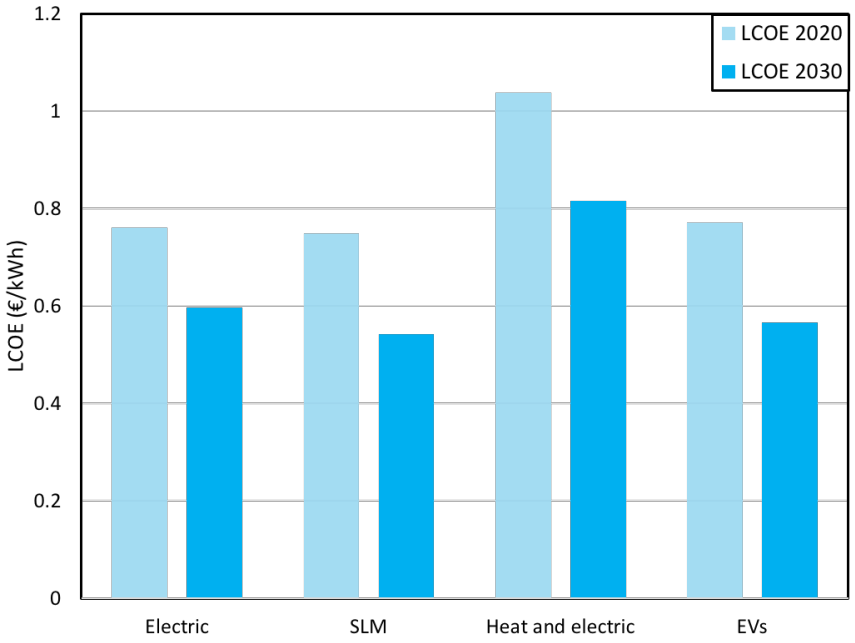

Figure 5.8: The LCOE for Scenario 1 for each load profile, comparing the results of the simulations with the 2020 and the 2030 costs of components.

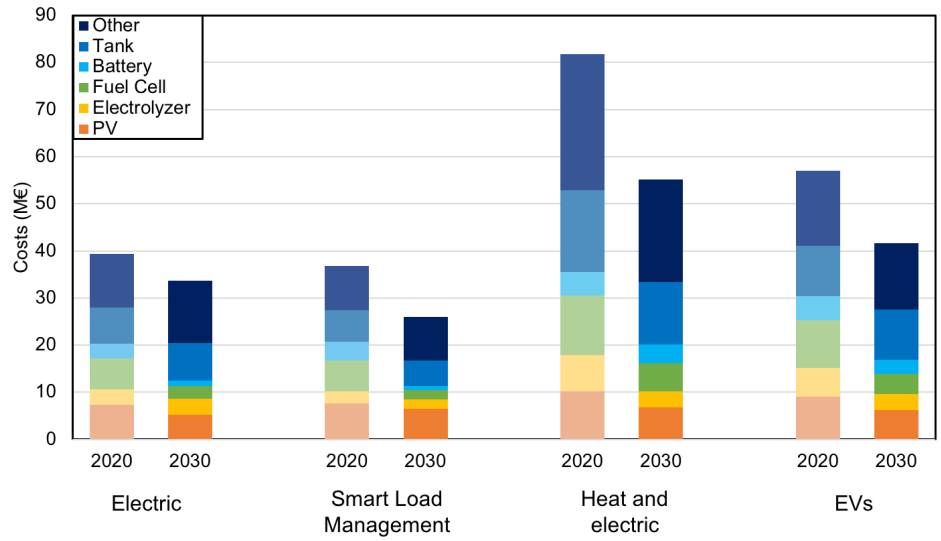

Figure 5.9: The total costs for each load profile for Scenario 1, comparing the results of the simulations with the 2020 and the 2030 costs of components. The different colours in each bar represent the percentage of the total costs made up by each component.

5.2.1 General comments

A complete overview of the results is given in Table 5.1. Figure 5.8 compares the LCOE of each of the different load profile cases, demonstrating that, in these preliminary results, the LCOE of every load profile has decreased in the future scenarios. This reduction is a combination of the reduction in costs as well as an increase in $E_{gen-load}$ in some cases. The electricity demand is modelled to increase slightly in 2030 compared to 2020.

Despite this however, none of the LCOE's in these results are lower than the Dutch electricity prices of 0.21 € /kWh. However, the drawbacks of using the Dutch electricity prices as a metric are described in Chapter 4 and are especially apparent here given that electricity prices are expected to increase by 2030 [123].

Moreover, Figure 5.9 compares the total costs of each case in the 2030 simulations to the original 2020 results. This demonstrates that the change in costs of 'other' components, such as the bi-directional inverter and the converter, take up the largest proportion of the total costs in all cases. This is to be expected given these costs are assumed to be the same in 2030 as in 2020. In reality, these components may also undergo a slight reduction in costs between 2020 and 2030. One possibility to reduce the costs of the future scenarios would be to use a different system layout. In the current hybrid system, an AC micro-grid is used in the centralised location as it is the most common choice for such grids given the high costs of DC-DC converters. However, these costs are expected to reduce in the future. Thus, in the future, using a DC micro-grid could reduce costs by eliminating the need to purchase inverters and purchasing cheaper converters instead.

5.2.2 Electric demand

The system designed to meet the electric load in 2030 resulted in a 21% reduction of the LCOE, from 0.761 € /kWh in 2020 to 0.596€ /kWh in 2030. This change is in part caused by the increase in $E_{gen-load}$ from 3663MWh to 4006MWh, thus yielding a lower costs per kWh. In addition, the total costs also reduce from € 39.5 million to € 33.67 million, mostly caused by reduction in the costs of the PV system, the battery and the fuel cell. The contribution from the 'other' components has instead increased, due to the increase in the tank size and thus the size of the dryer.

5.2.3 Smart load management

When smart load management is implemented in people's houses, the LCOE reduced by 28% from 0.749 € /kWh in 2020 to 0.542 € /kWh in 2030. This change was mostly caused by the reduction in costs from € 36.8 million to € 25.9 million, as shown in Figure 5.9. This is caused by a reduction in costs of every component compared to the costs of 2020.

5.2.4 Electric and head demand

When the heat demand is added to the electric load, this results in the largest LCOE of all the load profile cases. Yet, the LCOE it still reduces by 21% from 1.038 € /kWh in 2020 to 0.815 € /kWh in 2030. Figure 5.9 indicates that this is caused by a drop in the costs of each of the components, causing the total costs to reduce significantly from € 81.8 million to € 55.2 million. In this case, the reduction in costs is not only caused by the future prices but also by a smaller system sizing. The heat demand in 2030 is lower due to an increase in external temperatures with insulation assumed to be the same, resulting in a smaller storage system being needed and so a reduction in the total costs.

Furthermore, this lower demand also means that $E_{gen-load}$ reduces from 5592MWh in 2020 to 4798MWh in 2030. In theory this should lead to a larger final LCOE. However, the LCOE has still reduced by a similar amount compared to other load profiles, demonstrating that the smaller system sizing (and so total costs) has a larger effect on the final LCOE than $E_{gen-load}$. Finally, it should be noted that the costs of the 'other' components has reduced more than in other cases due to the decrease in the price of the heat pumps.

5.2.5 Electric vehicles

The system designed to meet the electric load and provide for electric vehicles yields a reduction in the LCOE of 27% from 0.772€/kWh in 2020 to 0.566€/kWh in 2030. In this case, the $E_{gen-load}$ only sees a small increase thus the redcution in the LCOE is mostly caused by the reduction in the total costs from €57.0 million to €41.7 million. Figure 5.9 shows this reduction originates predominantly from the reduction in the costs for the PV system, electrolyser, fuel cell and the battery.

5.2.6 Load profiles

When comparing the results of the future scenario simulations for different load profiles, it is possible to see that the trends that were seen for 2020 simulations are also reflected in these results. Firstly, the LCOE for the SLM profile is lower than the base case (0.542 €/kWh compared to 0.596 €/kWh). Secondly, the LCOE of the EV load profile is once again similar to that of the base case scenario (0.566 €/kWh compared to 0.542 €/kWh respectively), indicating that $E_{gen-load}$ changes with the same ratio as the total costs for the EV scenario, as happened in the 2020 simulations.

6 CONCULSION

In this final chapter, a summary of the most interesting findings in this thesis is detailed. Thereupon, several recommendations are discussed, detailing where future research can be directed.

The aim of this research, as introduced in Chapter 1, follows the main objective to 'assess the feasibility of current and future grid-connected hybrid PV-Battery-Electrolyser-FC energy systems from a techno-economical point of view, based on the optimal system sizing for the neighbourhood of Ackerswoude.'

6.1 CONCLUSION

This master thesis research analyses the techno-economical feasibility of a grid connected PV-Battery-Electrolyser-FC hybrid energy system for a Dutch neighbourhood. The technical feasibility is based on the physical restrictions on the sizes at which the components can be purchased. The economic feasibility is based on optimising the system for minimum costs. The established energy system consists of: (1) PV modules, (2) a lithium ion battery or a lead-acid battery, (3) an alkaline electrolyser, (4) a PEM fuel cell, (5) a cylindrical storage tank, (6) a master controller and other components. The battery system is used as a short term energy storage method (on a daily basis) and the hydrogen as a long term storage method (on a seasonal basis). The chosen location is the neighbourhood of Ackerwoude in Zuid Holland, the Netherlands.

A simulation model of the PV-Battery-Electrolyser-FC energy system is developed in the TRNSYS environment. The theoretical models are developed for the different components. The electrical model for the PV modules is taken from Smets et al. [124], incorporating the dependence of temperature and irradiance on the efficiency of the PV module. The electrochemical model of the alkaline electrolyser is based on the empirically verified PHOEBUS electrolyser by Ulleberg and Meurer [141], [94]. A PEM fuel cell is chosen to convert hydrogen to electricity. The electrochemical model of the fuel cell is based on a study by Amphlett expanded to meet the requirements of a 500kW fuel cell [17]. For the lithium-ion battery and lead-acid battery, the model proposed by Raszmann et al. is used [109]. Any hydrogen produced is compressed and stored at 500 bar in a high pressure cylindrical tank. All of the components are controlled by a master controller to manage the energy flows between the PV generation, the load and the energy storage systems.

To find the optimal system size of the grid connected hybrid system, the PSO+Hookes-Jeeves optimisation method is chosen using a time step of 0.125 hours. Three different scenarios have been optimised: (1) the centralised scenario, (2) the de-centralised PV generation and (3) the de-centralised PV generation and battery storage. For each scenario, four case studies were analysed looking at different load profiles: (i) electrical demand, (ii) smart load management, (iii) combined electric and heat demand, (iv) electric vehicles. The smart load management assumes that some of the load is redistributed to when the PV generation is highest. The heat demand is either met with an old-fashioned gas boiler or heat pumps. For the electric vehicles case, the electrical demand of the electric vehicles is added to the original electric

demand. The load profiles cases for Scenario 1 were run 5 times to find the global optimum. For scenarios 2 and 3 they were run 3 times.

It was found that when comparing the LCOE of different scenarios and cases, Scenario 1, the most centralised scenario, always has the lowest LCOE, followed by Scenario 2 then Scenario 3. This is to be expected given the increase in the costs of the PV system in Scenarios 2 and 3. In addition, the restriction of the number of PV modules in scenarios 2 and 3 meant an increased reliance on the storage systems, also increasing the costs. The lowest LCOE came to 0.749 € /kWh with the smart load management load profile for Scenario 1.

Interestingly, the results indicate that using the lead acid battery technology in Scenario 3 may have resulted in additional unexpected costs. The smaller depth of discharge of the lead acid battery (50% instead of 75%) required a larger battery system size that in the end negated the effects of the significantly lower costs.

In terms of the load profile cases, a few conclusions can be drawn. Firstly, it should be noted that the LCOE of the smart load management was lower than the base case electricity profile for Scenarios 1 and 2. This is to be expected given that more of the electricity produced will be sent directly to meet the load demand, reducing the reliance on the expensive hydrogen storage system. However, in Scenario 3 this was not the case, possibly due to a problem in the optimisation process here.

Furthermore, the LCOE of the electric vehicles case in all scenarios has the tendency to be similar to the base case. The reason for this is found by breaking the LCOE into its components: the total costs of the system and generated energy delivered to the load. The total costs of system for the EV case is 45 % larger than the base case in Scenario 1 and 30% larger in Scenario 2. This is expected due to the increase in the system sizing needed to meet the larger load demand. However, at the same time the generated energy delivered to the load has increased by a similar proportion, resulting an LCOE comparable to the base case. In contrast to this, the LCOE of heat demand case increased significantly, caused by a larger increase in the total costs compared to the generated energy delivered to the load.

When supplying the heat and electricity demand for scenarios 2 and 3, a deficit in the final energy is seen at the end of the year. This indicates that the maximum PV generation sizing was not enough to meet this load demand and also keep the SSR at 1%.

Finally, to predict the costs of different components in 2030, a literature review of the learning curves for each component is conducted. An average, upper bound and lower bound cost for 2030 is found for: (1) utility scale PV system, (2) residential PV system, (3) lithium ion battery, (4) alkaline electrolyser, (5) PEM fuel cell, (6) heat pumps and (7) hydrogen boilers. This is intended to be used to predict the future costs of the different PV-battery-electrolyser-FC energy systems in 2030.

Prelimery results for the future scenarios were found by running simulations from Scenario 1. As expected, the LCOE of every case decreased by 21 - 28 %. The results from these simulations demonstrate similar trends between the different load profile, suggesting these trends will remain even in future scenarios. Further research is needed to draw full conclusions from this work.

6.2 FUTURE RECOMMENDATIONS

Given the conclusions found in this thesis study, the following recommendations can be made for future research on this topic: finishing the optimisation of the system sizing in 2030, replacing gas heating with hydrogen heating in 2030, checking the sensitivity of the obtained metrics as a function of the SSR, exploring possible

different system layouts, changing the behaviour of the electrolyser and comparing the results found in this study to those in different locations.

By analysing the learning curves of the different components of the energy system, their costs in 2030 have been predicted. In this study, only preliminary results of the system sizing for the future scenarios were presented. In future work, it will be possible to complete the optimisation process for all scenarios and cases as if they were built in 2030. This would enable the prediction of when such a system would become economically viable for a neighbourhood in the Netherlands.

Next, it would be interesting to study different cases for load profiles that would be applicable in 2030 but not today. One such example is hydrogen heating. Hydrogen can be used to replace natural-gas heating in the Netherlands. Already the Netherlands has proposed an investment plan to deliver commercially available hydrogen within the next decades [98]. Replacing natural gas boilers with hydrogen heating systems would be a logical step to make and would significantly reduce national CO_2 emissions. By using predicted prices for hydrogen boilers, it would be possible to analyse the economic feasibility of different scenarios in 2030 when all heating is supplied by hydrogen gas.

For both the current and future scenarios, it would also provide insight to repeat simulations with differing values for the SSR. This would check the sensitivity of the final output metrics to the SSR, something that was not possible in this study due to lack of time.

In addition, it could be valuable to analyse the effects of changing the layout of the system designed to further reduce the costs. This could include using the lithium ion battery technology in place of the lead acid battery in the de-centralised scenario, providing insight into whether changing the technology was the sole cause of the increase in LCOE in the fully de-centralised scenario. Another possible layout could involve implementing a DC micro grid instead of an AC micro grid and testing if this could reduce costs in current and future scenarios.

Next, it could be interesting to study the implementation of a different energy management strategy that prioritises running the electrolyser. The lifetime electrolyser is significantly reduced by the need to constantly turn it on and off whenever hydrogen needs to be generated. It may be possible to use the batteries not only as short term storage but also to power the electrolyser during the night. This would extend the lifetime of the electrolyser, thus reducing the number of times it needs to be replaced during the project lifetime and ultimately reducing the LCOE of the project.

Finally, it may also be possible to perform the optimisation of the system sizing for different locations outside the Netherlands. By changing the solar irradiation and the load demand, it will be possible to test whether such a system would be economically viable in other locations and compare the results and conclusions with those found in this study.

BIBLIOGRAPHY

[1] (2018). *HydroGEM: Hydrogen-powered catalytic boiler*. Giacomini.

[2] (2019a). Accessed 21-01-2020. URL: https://www.rixindustries.com/.

[3] (2019). Dc/dc-omzetters. Accessed 2020-01-02. URL: https://nl.mouser.com/Power/DC-DC-Converters/_/N-brvxe.

[4] (2019a). Demineralised water. Accessed 06-01-2020. URL: https://www.thedistilledwatercompany.com/buy-demineralised-deionised.

[5] (2019a). Drierite. Accessed 06-01-2020. URL: https://secure.drierite.com/catalog3/default_home.cfm.

[6] (2019b). Drierite storage tank vent drier performance data. Accessed 06-01-2020. URL: https://secure.drierite.com/catalog3/Storage_Vent_Drier_Performance_Data.pdf.

[7] (2019b). *Rix 4VX Industrial Gas/Air Compressor*. Rix Industries.

[8] (2019b). Statistics and market data on demographics. Accessed 12-01-2020. URL: https://www.statista.com/markets/411/topic/446/demographics/.

[9] (2020). Dab nova up 180 m-na. Accessed 08-01-2020. URL: https://www.waterpompshop.nl/dab-nova-up-180-m-na-vlakzuiger-dompelpomp#prod-ups.

[10] (2020). Introduction to the air compressor buying process. Accessed 01-02-2020. URL: https://www.purchasing.com/construction-equipment/air-compressors/purchasing-guide/.

[11] (2020). *Panasonic HIT Catalogue*. Panasonic. Accessed 25-02-2020. URL: https://eu-solar.panasonic.net/cps/rde/xbcr/solar_en/Panasonic_HIT_Catalogue_EN.pdf.

[12] A1 Well Drilling (2017). What determines the lifespan of a well pump? Accessed 08-01-2020. URL: https://a1welldrilling.com/lifespan-well-pump/.

[13] Agency, D. E. and Energinet (2016). Technology data catalogue for individual heating installations. Technical report, Danish Energy Agency.

[14] Agreement, P. (2015). Paris agreement. In *Report of the Conference of the Parties to the United Nations Framework Convention on Climate Change (21st Session, 2015: Paris). Retrived December*, volume 4, page 2017. HeinOnline.

[15] Ammermann, H., Hoff, P., Atanasiu, M., Aylor, J., Kaufmann, M., and Tisler, O. (2015). Advancing europe's energy systems: Stationary fuel cells in distributed generation. *Fuel Cells And Hydrogen Joint Undertaking (FCH JU) & Roland Berger*.

[16] Amores, E., Rodríguez, J., Oviedo, J., and de Lucas-Consuegra, A. (2017). Development of an operation strategy for hydrogen production using solar pv energy based on fluid dynamic aspects. *Open Engineering*, 7(1):141–152.

[17] Amphlett, J. C., Baumert, R. M., Mann, R. F., Peppley, B. A., Roberge, P. R., and Harris, T. J. (1995). Performance modeling of the ballard mark iv solid polymer electrolyte fuel cell i. mechanistic model development. *Journal of the Electrochemical Society*, 142(1):1–8.

[18] Anuphappharadorn, S., Sukchai, S., Sirisamphanwong, C., and Ketjoy, N. (2014). Comparison the economic analysis of the battery between lithium-ion and lead-acid in pv stand-alone application. *Energy Procedia*, 56:352–358.

[19] Attema, J., Bakker, A., Beersma, J., Bessembinder, J., Boers, R., Brandsma, T., van den Brink, H., Drijfhout, S., Eskes, H., Haarsma, R., et al. (2014). Knmi'14: Climate change scenarios for the 21st century—a netherlands perspective. *KNMI: De Bilt, The Netherlands*.

[20] Bahadori, A. (2014). *Natural gas processing: technology and engineering design*. Gulf Professional Publishing.

[21] battery, F. (2010). Fullreiver battery charging instructions. Accessed 16-01-2020. URL: https://www.i-b-s.org/uploads/media/Fullriver_Lade-Anweisung_01.pdf.

[22] Bertuccioli, L., Chan, A., Hart, D., Lehner, F., Madden, B., and Standen, E. (2014). Development of water electrolysis in the european union, fuel cells and hydrogen joint undertaking. *Final Report*, pages 1–42.

[23] Bissey, S., Jacques, S., Reymond, C., and Le Bunetel, J.-C. (2018). An innovative bidirectional dc-ac converter to improve power quality in a grid-connected microgrid.

[24] Bizon, N. and Tabatabaei, N. M. (2013). *Advances in Energy Research: Energy and Power Engineering*. Nova Publishers, Incorporated.

[25] Blomen, L. J. and Mugerwa, M. N. (2013). *Fuel cell systems*. Springer Science & Business Media.

[26] Bocklisch, T., Böttiger, M., and Paulitschke, M. (2014). Multi-storage hybrid system approach and experimental investigations. *Energy Procedia*, 46:186–193.

[27] Bouwkracht, A. (2019). Ackerswoude inrichtingsplan. Accessed 19-12-2019. URL: https://www.ackerswoude.nl/ackerswoude/plan/.

[28] Boye, B. A., Falconer, R. A., and Akande, K. (2013). Integrated water management solutions from cloud to coast: application to ribble basin. In *Proceedings of the 35th IAHR World Congress*, volume 4, page 1e12. IAHR Chengdu, China.

[29] CBS (2020). Natural gas and electricity, average prices of end users. Accessed 26-02-2020. URL: https://opendata.cbs.nl/statline/#/CBS/nl/dataset/81309NED/table?fromstatweb.

[30] Daware, K. (2010). Transformer - losses and efficiency. Accessed 21-01-2020. URL: https://www.electricaleasy.com/2014/04/transformer-losses-and-efficiency.html.

[31] Deign, J. (2018). Why pv costs have fallen so far—and will fall further. Accessed 08-04-2020. URL: https://www.greentechmedia.com/articles/read/why-pv-costs-have-fallen-so-far-and-will-fall-further.

[32] DiOrio, N., Dobos, A., Janzou, S., Nelson, A., and Lundstrom, B. (2015). Technoeconomic modeling of battery energy storage in sam. Technical report, National Renewable Energy Lab.(NREL), Golden, CO (United States).

[33] Diouf, B. and Pode, R. (2015). Potential of lithium-ion batteries in renewable energy. *Renewable Energy*, 76:375–380.

[34] Eberhart, R. C., Shi, Y., and Kennedy, J. (2001). *Swarm intelligence*. Elsevier.

[35] Elshof, P. (2016). Changing energy demand in the residential sector due to decentralized generators and the electrification of heating and driving. Master's thesis.

[36] Enbar, N., Weng, D., and Klise, G. T. (2016). Budgeting for solar pv plant operations & maintenance: Practices and pricing. Technical report, Sandia National Lab.(SNL-NM), Albuquerque, NM (United States).

[37] Energiewende, A., Mayer, J. N., Philipps, S., Saad, N., Hussein, D., Schlegl, T., and Senkpiel, C. (2015). Current and future cost of photovoltaics. *Long-term Scenarios for*.

[38] Engineering ToolBox (2018). Ratios of specific heat of gases. Accessed 03-02-2020. URL: https://www.engineeringtoolbox.com/specific-heat-ratio-d_608.html.

[39] Erdinc, O. and Uzunoglu, M. (2012). Optimum design of hybrid renewable energy systems: Overview of different approaches. *Renewable and Sustainable Energy Reviews*, 16(3):1412–1425.

[40] Evides Waterbedrijf (2019). Evides annual report 2018. Technical report, Evides Waterbedrijf.

[Fell] Fell, H.-J. Policy framework to achieve 100% renewable energy.

[42] Finance, B. N. E. (2017). Lithium-ion battery costs and market. *Online verfügbar unter https://data. bloomberglp. com/bnef/sites/14/2017/07/BNEF-Lithium-ion-battery-costs-and-market. pdf, zuletzt geprüft am*, 28:2017.

[43] Folkson, R. (2014). *Alternative fuels and advanced vehicle technologies for improved environmental performance: towards zero carbon transportation*. Elsevier.

[44] for Solar Energy Systems, I. F. I. (2019). Photovoltaics report. Technical report, Fraunhofer ISE.

[45] Foray, J. (2014). Energy efficiency considerations in pumps and pump stations. Accessed 03-02-2020. URL: http://www.energy.wsu.edu/LinkClick.aspx?fileticket=t3ubiA8D8A4%3D&tabid=692&mid=1345.

[46] Foster, S., Lyons, S., and Walker, I. (2017). Hybrid heat pumps final report for department for business, energy industrial strategy. Technical report, Element Energy Limited.

[47] from Economic Affairs, M. (2016). Energy agenda: Towards a low-co2 energy supply. *Central Government. The Hague*.

[48] Fthenakis, V., Betita, R., Shields, M., Vinje, R., and Blunden, J. (2012). Life cycle analysis of high-performance monocrystalline silicon photovoltaic systems: energy payback times and net energy production value. In *27th European Photovoltaic Solar Energy Conference and Exhibition*, pages 4667–4672.

[49] Germarel (2020). Rec-ger series electrolysis rectifier. Accessed 17-02-2020. URL: https://www.germarel-platingrectifier.de/.

[50] Ghenai, C. and Bettayeb, M. (2019). Grid-tied solar pv/fuel cell hybrid power system for university building. *Energy Procedia*, 159:96–103.

[51] Glenk, G. and Reichelstein, S. (2019). Economics of converting renewable power to hydrogen. *Nature Energy*, 4(3):216–222.

[52] Global Petrol Prices (2020). Netherlands natural gas prices. Accessed 27-08-2020. URL: https://www.globalpetrolprices.com/Netherlands/natural_gas_prices/.

[53] Goetzberger, A., Bopp, G., Griesshaber, W., and Stahl, W. (1993). The pv/hydrogen/oxygen-system of the self-sufficient solar house freiburg. In *Conference Record of the Twenty Third IEEE Photovoltaic Specialists Conference-1993 (Cat. No. 93CH3283-9)*, pages 1152–1158. IEEE.

[54] Goodall, C. (2014). Reasons for optimism: 'grid parity' for renewable energy sources.

[55] GreenHydrogen.dk (2017). Hyprovide large-scale alkaline electrolyser (mw). Technical report, Energy Technology Development and Demonstration Program (EUDP).

[56] Greening, B. and Azapagic, A. (2012). Domestic heat pumps: Life cycle environmental impacts and potential implications for the uk. *Energy*, 39(1):205–217.

[57] Hagerman, S., Jaramillo, P., and Morgan, M. G. (2016). Is rooftop solar pv at socket parity without subsidies? *Energy Policy*, 89:84–94.

[58] Hay, J. E. (1993). Calculating solar radiation for inclined surfaces: Practical approaches. *Renewable energy*, 3(4-5):373–380.

[59] Hekkenberg, M. (2014). en m. verdonk, 2014, nationale energieverkenning 2014. Technical report, ECN-O–14-036, oktober.

[60] Hernández, J., Sanchez-Sutil, F., and Muñoz-Rodríguez, F. (2019). Design criteria for the optimal sizing of a hybrid energy storage system in pv household-prosumers to maximize self-consumption and self-sufficiency. *Energy*, 186:115827.

[61] Hesse, H. C., Schimpe, M., Kucevic, D., and Jossen, A. (2017). Lithium-ion battery storage for the grid—a review of stationary battery storage system design tailored for applications in modern power grids. *Energies*, 10(12):2107.

[Hofmeijer] Hofmeijer, I. Global risks report 2020.

[63] Hooke, R. and Jeeves, T. A. (1961). "direct search"solution of numerical and statistical problems. *Journal of the ACM (JACM)*, 8(2):212–229.

[64] Hydrogenics: Advanced Hydrogen Solutions (2017). Hypm-xr power modules: For reliable backup and standby power. Accessed 25-02-2020. URL: hydrogenics.com/wp-content/uploads/HyPM-XR-Brochure-1.pdf.

[65] Hydrogenics: Advanced Hydrogen Solutions (2019). Hystat® hydrogen generators. Accessed 25-02-2020. URL: https://www.hydrogenics.com/wp-content/uploads/2-1-1-industrial-brochure_english.pdf?sfvrsn=2.

[66] IEA, I. (2019). World energy statistics and balances, iea.

[67] Institute, B. M. (2017). Manufacturing cost analysis of 100 and 250 kw fuel cell systems for primary power and combined heat and power applications. Technical report, U.S. Department of Energy.

[68] IRENA (2019). Utility-scale batteries – innovation landscape brief. Technical report, International Renewable Energy Agency, Abu Dhabi.

[69] IRENA, C. (2017). competitiveness indicators: Rooftop solar pv. Technical report, Tech. rep., International Renewable Energy Agency.

[70] Isa, N. M., Das, H. S., Tan, C. W., Yatim, A., and Lau, K. Y. (2016). A techno-economic assessment of a combined heat and power photovoltaic/fuel cell/battery energy system in malaysia hospital. *Energy*, 112:75–90.

[71] ISE, D. S. P. F. and AG, W. W. P. (2019). © fraunhofer ise: Photovoltaics report. *I: PHOTOVOLTAICS REPORT (nov. 2016). url: https://www. ise. fraunhofer. de/content/dam/ise/de/documents/publications/studies/Photovoltaics-Report. pdf*.

[72] Ito, M. (2011). Life cycle assessment of pv systems. In *Crystalline Silicon-Properties and Uses*. InTechopen.

[73] James, B. D. and DeSantis, D. A. (2015). Manufacturing cost and installed price analysis of stationary fuel cell systems. *Strategic Analysis Inc*.

[74] Jäger-Waldau, A. (2019). *PV Status Report 2019*. JRC118058. Publications Office of the European Union, Luxembourg.

[75] Kairies, K.-P. (2017). Battery storage technology improvements and cost reductions to 2030: A deep dive. *Int. Renew. Energy Agency Work*, 2017.

[76] Kennedy, J. and Eberhart, R. (1995). Particle swarm optimization. In *Proceedings of ICNN'95-International Conference on Neural Networks*, volume 4, pages 1942–1948. IEEE.

[77] Keshan, H., Thornburg, J., and Ustun, T. S. (2016). Comparison of lead-acid and lithium ion batteries for stationary storage in off-grid energy systems.

[78] Khatib, T. and Elmenreich, W. (2016). *Modeling of Photovoltaic Systems Using MATLAB: Simplified Green Codes*. John Wiley & Sons.

[79] King, D. L., Gonzalez, S., Galbraith, G. M., and Boyson, W. E. (2007). Performance model for grid-connected photovoltaic inverters. *Sandia National Laboratories SAND2007-5036*.

[80] Kiss, B., Neij, L., Jakob, M., Grubler, A., and Wilson, C. (2012). Heat pumps: A comparative assessment of innovation and diffusion policies in sweden and switzerland. *Energy technology innovation: Learning from historical successes and failures*.

[81] Kotowicz, J., Jurczyk, M., Wecel, D., and Ogulewicz, W. (2016). Analysis of hydrogen production in alkaline electrolyzers. *Journal of Power Technologies*, 96(3):149–156.

[82] Krishna, R., Titus, E., Salimian, M., Okhay, O., Rajendran, S., Rajkumar, A., Sousa, J., Ferreira, A., Gil, J. C., and Gracio, J. (2012). Hydrogen storage for energy application. In *Hydrogen storage*. IntechOpen.

[83] Kuo, T.-J. (2019). Development of a comprehensive model for the coulombic efficiency and capacity fade of lifepo4 batteries under different aging conditions. *Applied Sciences*, 9(21):4572.

[84] Kurland, S. D. and Benson, S. M. (2019). The energetic implications of introducing lithium-ion batteries into distributed photovoltaic systems. *Sustainable Energy & Fuels*, 3(5):1182–1190.

[85] Lagorse, J., Simoes, M. G., Miraoui, A., and Costerg, P. (2008). Energy cost analysis of a solar-hydrogen hybrid energy system for stand-alone applications. *International journal of hydrogen energy*, 33(12):2871–2879.

[86] Lewis, B. and Von Elbe, G. (2012). *Combustion, flames and explosions of gases*. Elsevier.

[87] Ludin, N. A., Mustafa, N. I., Hanafiah, M. M., Ibrahim, M. A., Teridi, M. A. M., Sepeai, S., Zaharim, A., and Sopian, K. (2018). Prospects of life cycle assessment of renewable energy from solar photovoltaic technologies: a review. *Renewable and Sustainable Energy Reviews*, 96:11–28.

[88] Mackenzie, W. (2019). Report: European pv system pricing 2019. *Wood Mackenzie (April 2019). url: https://www.greentechmedia.com/articles/read/europes-solar-renaissance-is-on-the-horizon*.

[89] Mahendru, K. (2020). A detailed guide to 7 loss functions for machine learning algorithms with python code. Accessed 15-08-2020. URL: https://www.analyticsvidhya.com/blog/2019/08/detailed-guide-7-loss-functions-machine-learning-python-code/.

[90] Majcen, D. (2016). Predicting energy consumption and savings in the housing stock. *A+ BE— Architecture and the Built Environment*, (4):1–224.

[91] Mathis, W. and Thornhill, J. (2019). Hydrogen's plunging price boosts role as climate solution. *BloomburgNEF (August 2019). url: https://www.bloomberg.com/news/articles/2019-08-21/cost-of-hydrogen-from-renewables-to-plummet-next-decade-bnef*.

[92] Matute, G., Yusta, J., and Correas, L. (2019). Techno-economic modelling of water electrolysers in the range of several mw to provide grid services while generating hydrogen for different applications: A case study in spain applied to mobility with fcevs. *International Journal of Hydrogen Energy*.

[93] Maxim Integrated Products, Inc (2004). Source resistance: The efficiency killer in dc-dc converter circuits. Accessed 20-01-2020. URL: https://www.maximintegrated.com/en/design/technical-documents/app-notes/3/3166.html.

[94] Meurer, C., Barthels, H., Brocke, W., Emonts, B., and Groehn, H. (1999). Phoebus—an autonomous supply system with renewable energy: six years of operational experience and advanced concepts. *Solar energy*, 67(1-3):131–138.

[95] Mondal, P. and Ghosh, S. (2016). Externally fired biomass gasification-based combined cycle plant: exergo-economic analysis. *International Journal of Exergy*, 20(4):496–516.

[96] Mongird, K., Viswanathan, V. V., Balducci, P. J., Alam, M. J. E., Fotedar, V., Koritarov, V. S., and Hadjerioua, B. (2019). Energy storage technology and cost characterization report. Technical report, Pacific Northwest National Lab.(PNNL), Richland, WA (United States).

[97] Moseley, P. T. and Garche, J. (2014). *Electrochemical energy storage for renewable sources and grid balancing*. Newnes.

[98] Netherlands, S. I. A. H. N. (2019). Heading for emission-free hydrogen at commercial scale 2019.

[99] Nijs, W. and van Wortswinkel, L. (2010). Industrial combustion boilers. Technical report, IEA Energy Technology Systems Analysis Programme.

[100] Noah Pflugradt (2017). Load profile generator. Accessed 12-01-2020. URL: https://www.loadprofilegenerator.de/.

[101] NPROXX (2019). Stationary hydrogen storage applications. Accessed 06-01-2020. URL: https://www.nproxx.com/hydrogen-storage/stationary-applications/.

[102] Nyholm, E., Goop, J., Odenberger, M., and Johnsson, F. (2016). Solar photovoltaic-battery systems in swedish households–self-consumption and self-sufficiency. *Applied energy*, 183:148–159.

[103] Pellow, M. A., Emmott, C. J., Barnhart, C. J., and Benson, S. M. (2015). Hydrogen or batteries for grid storage? a net energy analysis. *Energy & Environmental Science*, 8(7):1938–1952.

[104] Pernetti, R. (2019). Cravezero: Life cycle cost reduction and market acceleration for new nearly zero-energy buildings.

[105] PowerStream Technology (2019). Sealed lead acid battery size chart. Accessed 10-03-2020. URL: https://www.powerstream.com/Size_SLA.htm.

[106] PSE, A. (2019). Fraunhofer institute for solar energy systems ise. *Photovoltaics report*.

[107] Ralon, P., Taylor, M., Ilas, A., Diaz-Bone, H., and Kairies, K. (2017). Electricity storage and renewables: Costs and markets to 2030. *International Renewable Energy Agency: Abu Dhabi, United Arab Emirates*.

[108] Ram, M., Bogdanov, D., Aghahosseini, A., Oyewo, S., Gulagi, A., Child, M., Fell, H.-J., and Breyer, C. (2017). Global energy system based on 100% renewable energy—power sector. *Lappeenranta University of Technology and Energy Watch Group: Lappeenranta, Finland*.

[109] Raszmann, E., Baker, K., Shi, Y., and Christensen, D. (2017). Modeling stationary lithium-ion batteries for optimization and predictive control. In *2017 IEEE Power and Energy Conference at Illinois (PECI)*, pages 1–7. IEEE.

[110] Reijn, G. (2018). Het doodsvonnis van de cv-ketel is geveld: over drie jaar praktisch verboden. *De Volkstrant (March 2018). url: https://www.volkskrant.nl/nieuws-achtergrond/het-doodsvonnis-van-de-cv-ketel-is-geveld-over-drie-jaar-praktisch-verboden bad59232/*.

[111] Rijksoverheid (2020). Overheid bevordert groei zonne-energie. Accessed 11-08-2020. URL: https://www.rijksoverheid.nl/onderwerpen/duurzame-energie/zonne-energie.

[112] RIVM (2019). Klimaatakkoord. *www.nlimaatakkoord.nl*.

[113] Rutte, M., van Haersma Buma, S., Pechtold, A., and Segers, G. (2017). Vertrouwen in de toekomst. *Regeerakkoord*, 2021:2017.

[114] Ryan Austin, Understand Solar (2017). Solar inverter costs and how to choose the right one. Accessed 01-02-2020. URL: https://understandsolar.com/solar-inverter-costs/.

[115] Saba, S. M., Müller, M., Robinius, M., and Stolten, D. (2018). The investment costs of electrolysis–a comparison of cost studies from the past 30 years. *International Journal of Hydrogen Energy*, 43(3):1209–1223.

[116] Salameh, Z. (2014). *Renewable energy system design*. Academic Press.

[117] Sangwongwanich, A., Yang, Y., Sera, D., and Blaabjerg, F. (2017). Lifetime evaluation of grid-connected pv inverters considering panel degradation rates and installation sites. *IEEE Transactions on Power Electronics*, 33(2):1225–1236.

[118] Schleussner, C.-F., Lissner, T., Fischer, E. M., Wohland, J., Perrette, M., Golly, A., Rogelj, J., Childers, K., Schewe, J., Frieler, K., et al. (2015). Differential climate impacts for policy-relevant limits to global warming: the case of 1.5 c and 2 c. *Earth System Dynamics Discussions*, 6(2).

[119] Schmidt, O., Gambhir, A., Staffell, I., Hawkes, A., Nelson, J., and Few, S. (2017a). Future cost and performance of water electrolysis: An expert elicitation study. *International Journal of Hydrogen Energy*, 42(52):30470–30492.

[120] Schmidt, O., Hawkes, A., Gambhir, A., and Staffell, I. (2017b). The future cost of electrical energy storage based on experience rates. *Nature Energy*, 2(8):1–8.

[121] Schneeweiss, Z. (2017). German, dutch working mothers mostly employed part time: Chart. Accessed 12-01-2020. URL: https://www.bloomberg.com/news/articles/2017-03-08/german-dutch-working-mothers-mostly-employed-part-time-chart.

[122] Schoots, K. and Hammingh, P. (2015). Nationale energieverkenning 2015, ecn-o–15-033.

[123] Schoots, K. and Hammingh, P. (2019). Klimaat-en energieverkenning 2019. *Den Haag: Planbureau voor de Leefomgeving*.

[124] Smets, A. H., Jäger, K., Isabella, O., Swaaij, R. A., and Zeman, M. (2015). *Solar Energy: The physics and engineering of photovoltaic conversion, technologies and systems*. UIT Cambridge.

[125] Smit, M. (2014). Towards 40 000 hours of operation for nedstack's fcs xxl pem fuel cell stacks. *Fuel Cells Bulletin*, 2014(8):12–15.

[126] Solar Energy International (2012). *Solar Electric Handbook: Photovoltaic Fundamentals and Applications*. Pearson.

[127] Spirit Energy (2015). Understanding batteries. Accessed 16-01-2020. URL: https://www.spiritenergy.co.uk/kb-batteries-understanding-batteries#.

[128] Spirit Energy (2019). Tesla powerpack. Accessed 25-02-2020. URL: https://www.spiritenergy.co.uk/kb-batteries-tesla-powerpack#.

[129] Staffell, I. and Green, R. (2009). Estimating future prices for stationary fuel cells with empirically derived experience curves. *International Journal of Hydrogen Energy*, 34(14):5617–5628.

[130] Staffell, I., Scamman, D., Abad, A. V., Balcombe, P., Dodds, P. E., Ekins, P., Shah, N., and Ward, K. R. (2019). The role of hydrogen and fuel cells in the global energy system. *Energy & Environmental Science*, 12(2):463–491.

[131] Stamp, S., Altamirano-Medina, H., and Lowe, R. (2017). Measuring and accounting for solar gains in steady state whole building heat loss measurements. *Energy and Buildings*, 153:168–178.

[132] Statista (2019). Photovoltaic capacity installed and connected in the netherlands 2013-2018. Accessed 21-02-2020. URL: statista.com/statistics/497350/installed-photovoltaic-capacity-netherlands/.

[133] Stedin Holding N.V (2019). Annual report 2018 stedin group. Technical report, Stedin Holding N.V.

[134] Tamarzians, M. (2019). Future city hydrogen: Reality or utopia?: A techno-economical feasibility study of an optimal stand-alone solar-electrolyzer-battery-fuelcell system for residential utilization.

[135] Tariq, J. (2019). Incorporating lca in solar pv design and planning for sustainability optimization.

[136] Tsiropoulos, I., Tarvydas, D., and Lebedeva, N. (2018a). Li-ion batteries for mobility and stationary storage applications scenarios for costs and market growth. *Publications Office of the European Union: Luxembourg*.

[137] Tsiropoulos, I., Tarvydas, D., and Zucker, A. (2018b). Cost development of low carbon energy technologies-scenario-based cost trajectories to 2050, 2017 edition. *Publications Office of the European Union, Luxemburgo*.

[138] Türkay, B. E. and Telli, A. Y. (2011). Economic analysis of standalone and grid connected hybrid energy systems. *Renewable energy*, 36(7):1931–1943.

[139] Ulleberg, O. (1998). Stand-alone power systems for the future: optimal design, operation & control of solar-hydrogen energy systems. *NTNU, Trondheim, Norvège*, page 225.

[140] Ulleberg, Ø. (2001). Evaluation of ife's 100 w pem fuel cell stack performance. Technical report, Internal report, Institute for Energy Technology.

[141] Ulleberg, Ø. (2003). Modeling of advanced alkaline electrolyzers: a system simulation approach. *International journal of hydrogen energy*, 28(1):21–33.

[142] UN (2015). Adoption of the Paris Agreement. *21st Conference of the Parties, Paris: United Nations*.

[143] University of Wisconsin–Madison. Solar Energy Laboratory. (1975). Trnsys, a transient simulation program. Accessed 24-02-2020. URL: .http://sel.me.wisc.edu/trnsys/index.html.

[144] Ursua, A., Gandia, L. M., and Sanchis, P. (2011). Hydrogen production from water electrolysis: current status and future trends. *Proceedings of the IEEE*, 100(2):410–426.

[145] Varro, L. and Ha, J. (2015). Projected costs of generating electricity–2015 edition. *Paris, France*.

[146] Vartiainen, E., Masson, G., Breyer, C., Moser, D., and Román Medina, E. (2019). Impact of weighted average cost of capital, capital expenditure, and other parameters on future utility-scale pv levelised cost of electricity. *Progress in Photovoltaics: Research and Applications*.

[147] Version, M. (2020). 7, software version 7.3.4 of march 2020. *Meteotest, Switzerland*.

[148] Viktorsson, L., Heinonen, J., Skulason, J., and Unnthorsson, R. (2017). A step towards the hydrogen economy—a life cycle cost analysis of a hydrogen refueling station. *Energies*, 10(6):763.

[149] Vismara, R. (2014). Optical characterization of photovoltaic materials and structures for thin-film solar cells based on advanced texturization. Master's thesis, TU Delft, The Netherlands.

[150] Walker, I., Madden, B., and Tahir, F. (2018). Hydrogen supply chain evidence base.

[151] Wallace, J. and Ward, C. (1983). Hydrogen as a fuel. *International Journal of Hydrogen Energy*, 8(4):255–268.

[152] Wang, J., Wang, H., and Fan, Y. (2018). Techno-economic challenges of fuel cell commercialization. *Engineering*, 4(3):352–360.

[153] Weiss, M., Junginger, H. M., and Patel, M. K. (2008). Learning energy efficiency: experience curves for household appliances and space heating, cooling, and lighting technologies.

[154] Wetter, M. (2009). Generic optimization program user manual version 3.0. 0. Technical report, Lawrence Berkeley National Lab.(LBNL), Berkeley, CA (United States).

[155] Yilanci, A., Dincer, I., and Ozturk, H. K. (2009). A review on solar-hydrogen/fuel cell hybrid energy systems for stationary applications. *Progress in energy and combustion science*, 35(3):231–244.

[156] Zhang, Y., Campana, P. E., Lundblad, A., and Yan, J. (2017). Comparative study of hydrogen storage and battery storage in grid connected photovoltaic system: Storage sizing and rule-based operation. *Applied energy*, 201:397–411.

[157] Zhang, Y., Lundblad, A., Campana, P. E., and Yan, J. (2016). Employing battery storage to increase photovoltaic self-sufficiency in a residential building of sweden. *Energy Procedia*, 88:455–461.

[158] Zhou, Y. and Gu, A. (2019). Learning curve analysis of wind power and photovoltaics technology in us: Cost reduction and the importance of research, development and demonstration. *Sustainability*, 11(8):2310.

[159] Züttel, A. (2003). Materials for hydrogen storage. *Materials today*, 6(9):24–33.

A MATHEMATICAL REFERENCE FOR COMPONENTS

This appendix details the mathematical equations used while modelling various components.

A.1 V_{oc} AND I_{sc} DEPENDENCE ON IRRADIANCE

The effects of irradiance on the efficiency of the module can be found as a function of the incident irradiance (G_{POA}) over the irradiance at standard test conditions (G_{STC}). The I_{sc} depends on this linearly, according to Equation A.1.

$$I_{sc} = \frac{I_{ref} \cdot G_{POA}}{G_{STC}} \tag{A.1}$$

where

- I_{sc} is the short circuit current
- I_{ref} is the short circuit current at standard test conditions
- G_{POA} is the plane of array irradiance on the module
- G_{STC} is the plane of array irradiance on the module at STC

The V_{oc} depends on the incident irrandiance logarithmically according to Equation A.2.

$$V_{oc} = V_{ref} + \frac{nk_BT}{q} ln(\frac{G_{POA}}{G_{STC}}) \tag{A.2}$$

where

- V_{oc} is the open circuit voltage
- V_{ref} is the open circuit voltage at standard test conditions

A.2 ALKALINE ELECTROLYSER ELECTRICAL MODEL

The cell voltage of an electrolyser (V_{cell}) is found using the thermoneatral voltage potential and taking away the irreversible losses, namely: the concentration overpotential (V_{con}), the ohmic overpotential (V_{ohm}) and the activation overpotential (V_{act}).

The concentration overpotential originates from limitations in the diffusion and convection of ions/electrons, otherwise known as mass transport. This limitation occurs at the interfaces between the electrolyte, where the charge carrier concentration varies throughout the electrolysis process, and the electrodes [144]. Ohmic losses are the cause of the ohmic overpotential, for example the electrical resistance of the current collectors, electrode and other interconnections. Other contributors can

be gas bubbles forming on the surface of the electrodes, membrane resistivity and transfer of ions in the electrolyte. Finally, the activation overpotential originates from the activation energies needed to form hydrogen and oxygen at the electrode surfaces. Here, ionic charge carriers must surpass an energy barrier to transfer from the electrolyte to the electrodes and back. This process is greatly dependant on the catalytic properties of the electrodes. The increased practical cell voltage caused by these overpotentials manifests as waste heat.

The reversible voltage and the effect of the overpotential terms on the on the voltage is demonstrated in Figure 2.2 as a function of current density. With increasing current density, the ohmic overpotential increases linearly and the concentration overpoential has parabolic tendency. The activation overpotential, however, increases logarithmically. Furthermore, an increase in the temperature decreases the reversible voltage and the overpotentials. Increasing the pressure, however, does not effect the overpotentials nor reversible voltage to great extent. Please note, a more detailed understanding of the current density-overpotentials relationship is not further discussed here as it is out of the scope of this study.

In Ulleburg's model, V_{cell} is determined empirically, with the current given to the electrolyser as the only external variable [141]. This is defined in Equation A.3.

$$V_{cell} = V_{tn} + \frac{[r_1 + r_2.T_{ely}].I_{ely}}{A_{cell}} + s_1.log[\frac{(t_1 + \frac{t_2}{T_{ely}} + \frac{t_3}{T_{ely}^2})}{A_{cell}} + 1] \tag{A.3}$$

where r_1 and r_2 are ohmic resistance coefficients and s_1, t_1, t_2 and t_3 are the overvoltage coefficients on the electrodes. Table A.1 lists empirically derived values for the the coefficients used by by Ulleberg for the alkaline electrolyser from the PHOEBUS system.

Coefficient	Value	Description
r_1	$8.05e^{-5}\Omega m^2$	Ohmic resistance
r_2	$-2.50e^{-7}\Omega m^2/^{circ}C$	Ohmic resistance
s_1	0.185V	Overvoltage on electrodes
t_1	$-0.10m^2/A$	Overvoltage on electrodes
t_2	$8.42m^{2\circ}C/A$	Overvoltage on electrodes
t_3	$247.27m^{2\circ}C^2/A$	Overvoltage on electrodes
A_{cell}	$3000cm^2$	Electrode area
T_{ely}	80°C	Maximum electrolyser temperature
n_s	98	Number of cells

Table A.1: Characteristics of the alkaline electrolyzer from the HyProvide Large-Scale Alkaline Electrolyser Project by GreenHydrogen and empirically derived coefficients by Ulleberg [141], [55]

A.3 ALKALINE ELECTROLYSER THERMAL MODEL

The temperature of the electrolyser is established using a quasi-static thermal model incorporating the PHOEBUS electrolyzer's thermal capacitance.

$$\frac{\partial T}{\partial t} = \frac{\dot{Q_{net}}}{C_{t_{ely}}} \tag{A.4}$$

where $C_{t_{ely}}$ the thermal capacitance of the electrolyser. $\dot{Q_{net}}$ is the net difference of the generated heat, defined as:

$$\begin{aligned} \dot{Q}_{net} &= \dot{Q}_{gen} - \dot{Q}_{loss} - \dot{Q}_{cool} \\ \dot{Q}_{gen} &= n_s \cdot I_{ely}(V_{cell} - V_{tn}) \\ \dot{Q}_{loss} &= \frac{T_{ely} - T_{amb}}{R_t} \\ \phi_{m_{H20}} &= \frac{\dot{Q}_{cool}}{C_{\rho_{H20}}(T_{w_{out}} - T_{w_{in}})} \end{aligned} \tag{A.5}$$

where:

- $\dot{Q}_{net}$ is net heat difference
- $\dot{Q}_{gen}$ is the generated heat
- $\dot{Q}_{loss}$ is the natural heat loss to the ambient
- $\dot{Q}_{cool}$ is the auxiliary cooling
- T_{amb} is the ambient temperature
- C_t is the thermal capacitance of the electrolyser [$650 \cdot 10^3 Jk^{-1}$]
- R_t is the thermal resistance of the electrolyser [$0.167\ KW^{-1}$]
- $C_{\rho_{H20}}$ is the heat capacity of water
- $T_{w_{out}}$ is the temperature of the cooling water entering the electrolsyer
- $T_{w_{in}}$ is the temperature of the cooling water leaving the electrolsyer

A.4 PEM FUEL CELL ELECTRICAL MODEL

Amphlett [17] defines the fuel cell's output voltage as:

$$V_{cell_{fc}} = V_{rev} - V_{ohmic} - V_{act} \tag{A.6}$$

The reversible voltage can be found using the Nernst equation. The ohmic voltage, related to the internal resistance losses in the fuel cell, is empirically defined by Amplett. The activation losses are based on theoretical equations for the fundamentals of thermodynamics, kinetics and electrochemistry. The mass transport losses are integrated into the proceeding terms and thus are not included separately. Due to the relatively constant pressure levels of hydrogen and oxygen in a PEM fuel cell, only the temperature effects are taken into account in these equations. The equations for the activation and ohmic voltage losses are defined by Amphlett as:

$$V_{ohm} = (\frac{I_{fc}.t_{temb}}{A_{PEM}}).\frac{8}{exp[3.6.\frac{(T_{fc}+273)-353}{(T_{fc}+273)}.[1 + (1.64.\frac{I_{fc}}{A_{PEM}}) + (\beta.(\frac{I_{fc}}{A_{PEM}})^3)]} \tag{A.7}$$

$$\begin{aligned} V_{act} = 0.95 &- [0.00243(T_{fc}+273)] - [0.000192(T_{fc}+273)ln(A_{PEM})] \\ &+ [0.000192.(T_{fc}+273).ln(I_{fc})][0.000076.(T_{fc}+273).ln(C_{O_2})] \end{aligned}$$

In this model, the stochiometric efficiency of hydrogen and oxygen are determined by the authors. Typically, both gases required an excess of 15% to allow for a

complete reaction [140]. Therefore, a constant stochiometric efficiency (η_{stoch}) can be assumed of 87% for both the hydrogen and oxygen inlets.

This final PEM fuel cell has 10 stacks in parallel, each with 283 cells and an electrode area of $780cm^2$. The same membrane thickness and maximum temperature set point has been used, see Table A.2.

Parameter	Value	Description
A_{pm}	$780cm^2$	Fuel cell electrode area
T_{fc}	80°C	Maximum fuel cell temperature
β	0	Well hydrated PEM
β	1.2	Water deficient PEM
n_s	283	Number of cells in series
n_p	10	Number of stack in paralel
t_{memb}	0.000118 m	PEM thickness

Table A.2: The characteristics of the adopted model for the PEM fuel cell based on Amphlett et al and a theoretical 500kW fuel cell [17].

A.5 PEM FUEL CELL THERMAL MODEL

The temperature of the fuel cell is established using a quasi-static thermal model for the thermal capacitance of a PEM fuel cell.

$$\frac{\partial T}{\partial t} = \frac{\dot{Q_{rest}}}{C_{t_{fc}}} \tag{A.8}$$

where $C_{t_{fc}}$ the thermal capacitance of the fuel cell. $\dot{Q_{rest}}$ is the net difference of the generated heat, defined using:

$$\begin{aligned} \dot{Q}_{rest} &= \dot{Q}_{gen} - \dot{Q}_{loss} - \dot{Q}_{cool} - \dot{Q}_{evap} \\ \dot{Q}_{gen} &= n_s \cdot I_{fc}(V_{cell} - V_{tn}) \\ \dot{Q}_{loss} &= \frac{T_{ely} - T_{amb}}{R_{t_{fc}}} \\ \dot{Q}_{evap} &= x_{evap} \cdot h_{fg} \cdot \phi_{m_{DEMI}} \\ \phi_{m_{H20}} &= \frac{\dot{Q}_{cool}}{C_{\rho_{H20}}(T_{w_{out}} - T_{w_{in}})} \end{aligned} \tag{A.9}$$

where:

- $\dot{Q}_{rest}$ is net heat difference
- $\dot{Q}_{gen}$ is the generated heat
- $\dot{Q}_{loss}$ is the natural heat loss to the ambient
- $\dot{Q}_{cool}$ is the auxiliary cooling
- $\dot{Q}_{evap}$ is the heat lost by the evaporation of water at the cathode
- T_{amb} is the ambient temperature
- C_t is the thermal capacitance of the fuel cell
- R_t is the thermal resistance of the fuel cell

Coefficient	Value	Description
n_s	283	number of cells in a single fuel cell stack
h_{fg}	0.25	Fraction of demi water that is vaporised
L_{frame}	0.029 m	Average distance between PEM fuel cell and air
A_{fc}	0.17 m^3	Total surface fuel cell
k_{fc}	14.1 W/(m K)	Thermal conductivity fuel cell material
t_{plate}	0.02 m	Thickness end plate
w_{plate}	0.231 m	Width end plate
h_{plate}	0.231 m	Height end plate
t_{pfc}	0.005 m	Thickness cell
w_{fc}	0.21 m	Width cell
h_{fc}	0.21 m	Height cell
ρ_{plate}	$7850 kg/m^3$	Density end plate material
ρ_{fc}	$2250 kg/m^3$	Density fuel cell material
$c_{p-plate}$	450 J/(kg K)	Heat capacity end plate material
c_{p-fc}	710 J/(kg K)	Heat capacity fuel cell material

Table A.3: Characterisations of the adopted PEM fuel cell model [140].

- $C_{\rho_{H20}}$ is the heat capacity of water
- x_{evap} is the enthalpy of water at vaporization
- h_{fg} is the fraction of demi-water vaporised
- $\phi_{m_{DEMI}}$ is the flow rate of demi-water
- $T_{w_{out}}$ is the temperature of the cooling water entering the fuel cell
- $T_{w_{in}}$ is the temperature of the cooling water leaving the fuel cell

The thermal resistance and the thermal capacitance depend on the of the geometry of the fuel cell. They can be found using the following equations. The constant used in the equations in this section can be found in Table A.3.

$$R_{t_{fc}} = \frac{L_{frame}}{k_{fc} \cdot A_{fc}} + \frac{1}{h_{air} \cdot A_{fc}} \tag{A.10}$$

$$C_{t_{fc}} = (c_{p-fc} \cdot \rho_{fc} \cdot n_s \cdot h_{fc} \cdot w_{fc} \cdot t_{fc}) + (2c_{p-plate} \cdot \rho_{plate} \cdot h_{plate} \cdot w_{plate} \cdot t_{plate}) \tag{A.11}$$

A.6 COMPRESSOR

The required work for compression, according to Bahadori et al., depends on whether the process is adiabatic, isothermic or polytropic [20]. An adiabtic process ensures that there is no heat exchanged with the surroundings. An isothermic process occurs at a constant gas temperature. A polytropic process combines both these processes. Most compression processes in practise are polytropic. This study adopts the compressor model from the TRNSYS standard library, a model based on an ideal gas in quasi-equilibrium compression for an isothermic and adiabatic process. To model slightly more realistic behaviour, the standard model has been modified

to reflect polytropic compression. Bahadori et al. defined the required work for polytropic compression as:

$$P_{comp} = \frac{\phi_m}{\eta_{poly}}.[\frac{N.R.(T_{in}+273)}{N-1}].[1-\frac{p_{out}}{p_{in}}^{(\frac{N-1}{N})}] \tag{A.12a}$$

$$\eta_{poly} = \frac{\frac{N}{N-1}}{\frac{k_{isen}}{k_{isen}-1}} \tag{A.12b}$$

$$k_{isen} = \frac{C_p}{C_v} \tag{A.12c}$$

The heat produced during polytropic compression is given by [20]:

$$T_{out} = ((T_{in}+273).[\frac{p_{out}}{p_{in}}^{\frac{N-1}{N}}]) - 273 \tag{A.13a}$$

$$Q_{comp} = \phi_m.C_p.\Delta T \tag{A.13b}$$

where:

- P_{comp} is the required compressor power
- Q_{comp} is the heat produced by compression
- η_{poly} is the polytropic efficiency
- ϕ_m is the mass flow
- N is the polytropic constant, dependent on the compressor type
- T_{in} is the inlet temperature gas
- T_{out} is the outlet temperature gas
- R is the ideal gas constant
- p_{in} is the inlet gas pressure
- p_{out} is the outlet gas pressure
- k_{isen} is the isentropic constant, dependent on gas type
- C_p is the specific heat capacity of a gas at constant pressure
- C_p is the specific heat capacity of a gas at constant volume

Assuming there is no mass flow loss, the mass flow into the compressor is equal to the mass flow out. k_{isen} for hydrogen gas is equal to 1.41 at 25° when it behaves as an ideal gas [38]. The polytropic exponent is determined experimentally for a given type of compression process, ranging between 1.0 and 1.4. As the polytropic exponent can change during the compression process, an average value of 1.2 is taken for this simulation model. Assuming this as a constant value yields a polytropic efficiency of 58%.

When compressing a gas to high pressures of 500 bar, multi-stage compression is required. 2 stages of compression are used in the reference compressor, with a maximum flow of 170 m^3/h [7]. The output pressure is defined by the pressure level of the hydrogen gas currently in the storage tank. It is assumed that no external cooling is required as all heat produced will be lost of the environment.

A.7 STORAGE TANK

The model performs a mass balance for the hydrogen entering the tank from the compressor, the gas leaving the tank to supply the fuel cell and the dumping if the tank is full. The volume of gas in the tank is defined by the remaining hydrogen. In addition, the inflow and outflow of the hydrogen gas is assumed to occur through an isothermal process. The occupied level in the tank is is then expressed as:

$$\phi_m(t) = \phi_{m_{in}}(t) - \phi_{m_{out}}(t) - \phi_{m_{dump}}(t) \tag{A.14a}$$

$$V_{gas}(t) = V_{gas}(t-1) \pm [\frac{\phi_m(t)}{\rho_{H2_{500bar,25C}}}.\Delta t] \tag{A.14b}$$

$$SOC_{tank}(t) = \frac{V_{gas}(t)}{V_{tank}} \tag{A.14c}$$

where:

- $SOC_{tank}(t)$ is the state of charge hydrogen tank at time t
- $V_{gas}(t)$ is the stored volume of hydrogen gas at time t
- $V_{gas}(t-1)$ is the stored volume of hydrogen gas at time t -1
- $\phi_{m_{in}}(t)$ is the mass flow in at time t
- $\phi_{m_{out}}(t)$ is the mass flow out at time t
- $\phi_{m_{dump}}(t)$ is the dumped mass flow at time t
- V_{tank} is the storage tank volume

B CHARACTERISTICS OF AEC AND PEMFC

	AEC	**PEMFC**
Anode Reaction	$4OH^-(aq) \rightarrow 2H_2O(l) + 4e^- + O_2(g)$	$2H_2(g) \rightarrow 4H^+(aq) + 4e^-$
Cathode Reaction	$4H_2O(l) + 2e^- \rightarrow 4OH^-(l) + 2H_2(g)$	$4H^+(aq) + O_2(g) \rightarrow 2H_2O(l)$
Charge Carrier	OH-	H+
Electrolyte	Aqueous solution of KOH	Solid Nafion membrane
Operating Temperature Range	80°C to 90°C	60°C to 80°C
Efficiency	65-75%	40-50%
Produced Hydrogen Purity	99.5-99.9998%	99.9-99.9999%
Stack size	1kW-100kW	5W-250kW
Stack lifetime	60000-90000 hours	20000-40000 hours
Initial Cost	1000-1200 €/kW	2300-4000 €/kW
Applications	Stand-alone systems, MW installation	Transport,stationary and distribution

Table B.1: Overview of the details of an Alkaline Electrolyser Cell (AEC) and Proton Exchange Membrane Fuel Cell (PEMFC) [134].

C OPERATION MODES

This section details the mathematical equations used for the master controller of the hybrid PV-Battery-Electrolyser-FC system

C.1 WITHOUT ELECTROLYSER MANAGEMENT

Operation Mode 1

The mathematical equations for this operation mode are:

$$P_{net} = P_{pv} - P_{load}$$
$$P_{exc} = P_{net} - P_{batt}$$
$$P_{aux} = P_{pump} + P_{conv_{inv}} + P_{comp}$$
$$P_{ely} = P_{pv} - P_{load} - P_{batt} - P_{aux}$$
$$P_{tank} = P_{ely} + P_{aux}$$
$$P_{sys} = P_{load} + P_{batt} + P_{tank}$$
$$P_{to_grid} = |P_{exc} - P_{tank}|$$

Operation Mode 2

The mathematical equations for this operation mode are:

$$P_{net} = P_{pv} - P_{load}$$
$$P_{short} - P_{net} - P_{batt}$$
$$P_{aux} = P_{pump} + P_{conv_{inv}}$$
$$P_{fc} = P_{load} + P_{batt} - P_{pv} + P_{aux}$$
$$P_{tank} = -P_{fc} - P_{aux}$$
$$P_{sys} = P_{load} - P_{batt} - P_{tank}$$
$$P_{from_grid} = |P_{short} - P_{tank}|$$

Operation Mode 3

All of the mathematical equations are the same as in *Operation Mode 2* with one additional equation:

$$P_{pv} = 0$$

D HEAT DEMAND EQUATIONS

The final equation used to determine the heat demand for each household can be found in Section 3.4.2. This appendix mathematically develops this equation further and details the assumptions made in these calculations.

$$Q_{conduction} = (\sum_{n=1}^{N} A_n.U_n).(t_{in} - t_{out}) \tag{D.1}$$

where:

- $Q_{conduction}$ is the heat loss through conduction
- A_n is the surface area of each surface of the house connected to the outside
- U is the heat transfer coefficient of each surface $[Wm^{-2}K^{-1}]$
- t_{in} is the thermostat setting
- t_{out} is the external air temperature

It is assumed that heat is lost through conduction through the four walls and the roof. In addition, 10% of the wall area is made up of glass windows and doors. The U-value for walls is taken as $0.18Wm^{-2}K^{-1}$, for windows it is $1.4Wm^{-2}K^{-1}$ and for the roof it is $0.13Wm^{-2}K^{-1}$ [131].

The equation for the heat loss through ventilation and infiltration ($Q_{ventilation}$) is:

$$Q_{ventilation} = \rho_{air}.C_p.q_{v,i}.(t_{in} - t_{out}) \tag{D.2}$$

where

- C_p is the specific heat capacity of air = 1005 $Jkg^{-1}K^{-1}$
- ρ is the density of air = $1.205kgm^{-3}$
- $q_{v,i}$ is air volume flow $[m^3]$

$q_{v,i}$ is given by Equation D.3. This is calculated using standard ventilation coefficients (f1, f2), which are greatly dependant on the infiltration rates and the ventilation type. In addition, the ventilation losses are relative to q_{ref} to account for the different floor areas etc. of each house in this study [90].

$$q_{v,i} = f_1.A_{floor} + f_2.q_{reference}.\frac{A_{floor}}{A_{reference}} \tag{D.3}$$

where

- f_1 = 0.47 for natural ventilation $[dm^3/s.m^2]$
- f_2 = 0.13 for natural ventilation $[dm^3/s.m^2]$
- $A_{reference}$ for a detached house = $120m^2$

- $q_{reference}$ for a detached house = $0.31m^2$

$Q_{internal}$ is the internal gains from objects that emit heat within the house. These are assumed to $6W/m^2$ of floor area [90].

E | ENERGY FLOWS

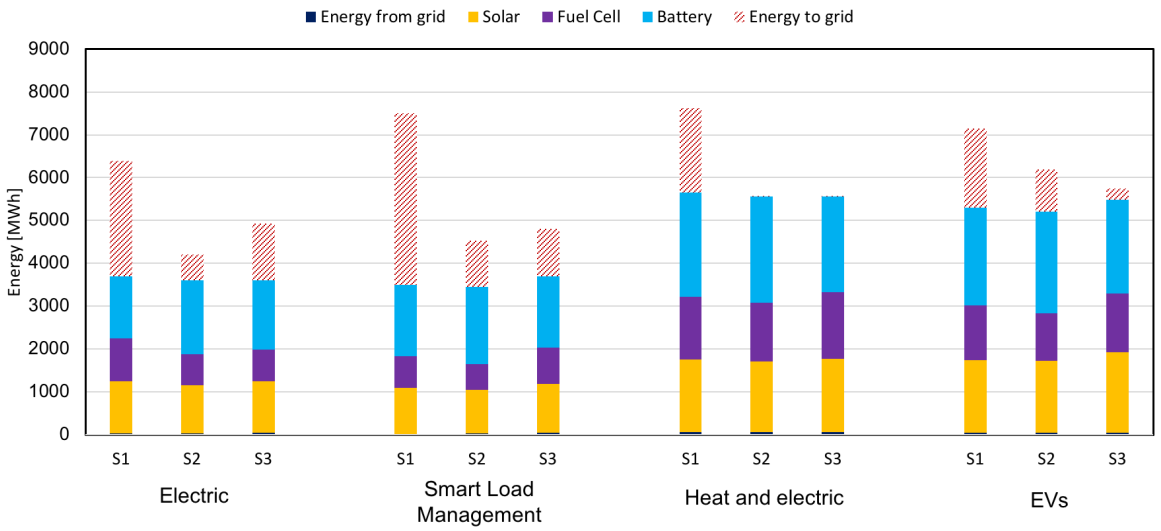

Figure E.1: The energy sent to the system for each scenario when providing for each load demand. The different colours represent what percentage of the energy was met by the PV generation, battery storage, the fuel cell or the grid. The dashed section represents the excess generated energy that was sent to the grid.

F LEARNING CURVES

This appendix details the starting year, starting price and learning rate of the different papers used to establish the learning curves of different technologies.

F.1 UTILITY-SCALE PV SYSTEM

Paper	Starting year	Starting Price [€/Wp]	Learning rate
Vartiainen et. al - Slow [146]	2019	0.71	20%
Vartiainen et. al - Moderate [146]	2019	0.71	30%
Vartiainen et. al - Fast [146]	2019	0.68	40%
Fraunhofer ISE - Slow [37]	2015	0.935	19%
Fraunhofer ISE - Moderate [37]	2015	0.995	20.9%
Fraunhofer ISE - Fast [37]	2015	1.055	23%
Zhou and Gu - Slow [158]	2019	0.88*	6.78%
Zhou and Gu - Fast [158]	2019	0.88*	6.78%
Goodall [54]	2019	0.88*	20%
Tsiropoulos et. al - Slow [137]	2017	1.02	10%
Tsiropoulos et. al - Moderate [137]	2017	1.02	20%
Tsiropoulos et. al - Fast [137]	2017	1.02	23%
Breyer [108]	2017	1.00	-

Table F.1: The starting year, starting price and learning rate of the different papers used to establish the learning curve for utility-scale PV systems. [*] means that the 2019 price given in this study was used as the starting price.

The trend line equations for the utility scale PV system are listed below. P_{low} represents the curve for the lower bound, P_{av} for the average price and P_{up} for the upper bound. x here represents the number of years since 2010

$$P_{low} = 13.424x^{-1.226} \tag{F.1a}$$

$$P_{av} = 1.923x^{-0.387} \tag{F.1b}$$

$$P_{up} = 1.1547x^{-0.12} \tag{F.1c}$$

F.2 RESIDENTIAL PV SYSTEM

Paper	Starting year	Starting Price [/Wp]	Learning rate
Fraunhofer ISE [106]	2019	1.3*	24%
Zhou and Gu - Slow [158]	2019	1.3*	10.86%
Zhou and Gu - Fast [158]	2019	1.3*	10.86%
Goodall [54]	2019	1.3*	20%
Tsiropoulos et. al - Slow [137]	2017	1.36	10%
Tsiropoulos et. al - Moderate [137]	2017	1.36	20%
Tsiropoulos et. al - Fast [137]	2017	1.36	23%
Breyer [108]	2017	1.36	-

Table F.2: The starting year, starting price and learning rate of the different papers used to establish the learning curve for residential PV systems. [*] means that the 2019 price given in this study was used as the starting price.

The trend line equations for the residential scale PV system are listed below. P_{low} represents the curve for the lower bound, P_{av} for the average price and P_{up} for the upper bound. x here represents the number of years since 2010

$$P_{low} = 5.5034x^{-0.836} \tag{F.2a}$$

$$P_{av} = 2.5085x^{-0.394} \tag{F.2b}$$

$$P_{up} = 1.9052x^{-0.21} \tag{F.2c}$$

F.3 LITHIUM-ION BATTERY SYSTEM

Paper	Starting year	Starting Price [/kWh]	Learning rate
Tsiropoulos et. al - Slow [136]	2017	500	12%
Tsiropoulos et. al - Moderate [136]	2017	500	16%
Tsiropoulos et. al - Fast [136]	2017	500	20%
Smchidt et. al - Slow [120]	2015	1320	9%
Smchidt et. al - Moderate [120]	2015	1320	12%
Smchidt et. al - Fast [120]	2015	1320	15%
BNEF [158]	2018	176	18%
Kohler et. al [104]	2018	863	15.8%
Breyer [108]	2015	600	-

Table F.3: The starting year, starting price and learning rate of the different papers used to establish the learning curve for lithium ion batteries

The trend line equations for the lithium ion battery are listed below. P_{low} represents the curve for the lower bound, P_{av} for the average price and P_{up} for the upper bound. x here represents the number of years since 2010

$$P_{low} = 254.82x^{-0.628} \tag{F.3a}$$

$$P_{av} = 762.79x^{-0.346} \tag{F.3b}$$

$$P_{up} = 1242.3x^{-0.269} \tag{F.3c}$$

F.4 ALKALINE ELECTROLYSER

The trend line equations for the alkaline electrolyser are listed below. P_{low} represents the curve for the lower bound, P_{av} for the average price and P_{up} for the upper bound. These prices are found in units of €/kW. x here represents the number of years since 2000.

$$P_{low} = 3934.1x^{-0.661} \tag{F.4a}$$

$$P_{av} = 3971.2x^{-0.529} \tag{F.4b}$$

$$P_{up} = 4444.8x^{-0.477} \tag{F.4c}$$

F.5 PEM FUEL CELL

The learning rate for PEM fuel cell systems is given in Table F.4. Given that these papers analysed residential fuel cell system, the price found for large scale fuel cell systems was used as the starting price from 2019.

Paper	**Learning rate**
Staffell et. al - Japan [130]	18%
Staffell et. al - Korea [130]	21%
Schmidt et al. - Fast [120]	20%
Schmidt et al. - Moderate [120]	18%
Schmidt et al. - Slow [120]	16%
Green and Staffell - Fast [129]	23.1%
Green and Staffell - Moderate 2 [129]	21.4%
Green and Staffell - Moderate 1 [129]	19.1%
Green and Staffell - Slow [129]	16.2%

Table F.4: The learning rate of the different papers used to establish the learning curve for fuel cells.

The trend line equations for the PEM fuel cell are listed below. P_{lav} represents the curve for the average price and P_{up} for the upper bound. x here represents the number of years since 2010

$$P_{av} = 82.039x^{-1.42} \tag{F.5a}$$

$$P_{up} = 167.81x^{-1.498} \tag{F.5b}$$

F.6 HEAT PUMP

Paper	Starting year	Starting Price [€/kW]	Learning rate
Kohler et. al [104]	2018	1285.7*	9.8%
EnergiNet [13]	2016	1200	-
Element Energy - Fast [46]	2017	1361	-
Element Energy - Moderate [46]	2017	1361	-
Element Energy - Slow [46]	2017	1361	-
Weiss et al [153]	2008	1285.7*	24.5%
Kiss et al [80]	2012	1285.7*	7.5%

Table F.5: The starting year, starting price and learning rate of the different papers used to establish the learning curve for heat pumps. [*] means that the 2019 price given in this study was used as the starting price.

The trend line equations for the residential scale PV system are listed below. P_{low} represents the curve for the lower bound and P_av for the average price. In this case, P_{up} did not have an equation as it was always the same value. These prices are found in units of € /kW. x here represents the number of years since 2015.

$$P_{av} = 1313.7x^{-0.081} \tag{F.6a}$$

$$P_{low} = -212.3 * ln(x) + 1412.6 \tag{F.6b}$$